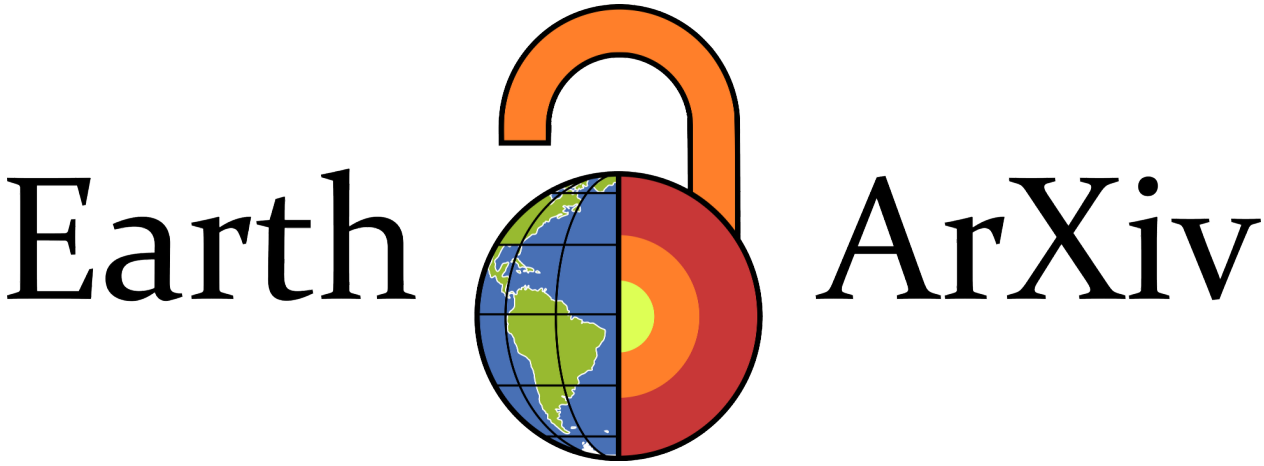


This is a non-peer-reviewed preprint submitted to EarthArXiv.

Please note the manuscript has yet to be formally accepted for publication. Subsequent versions of this manuscript may have slightly different content. Please feel free to contact any of the authors; we welcome feedback.

Earth Embeddings as the New Foundations for Geospatial Analysis: A Comprehensive Review

Yongchuan Cui[1], Keli Shi[2,3], Shunlin Liang[1*]

[1]Jockey Club STEM Lab of Quantitative Remote Sensing, Department of Geography, The University of Hong Kong, Hong Kong, China.
[2]Aerospace Information Research Institute, Chinese Academy of Sciences, Beijing, 100094, China.
[3]School of Electronic, Electrical and Communication Engineering, University of Chinese Academy of Sciences, Beijing, China.

*Corresponding author(s). E-mail(s): shunlin@hku.hk;

Abstract

The rapid growth of Earth observation data, particularly from satellite constellations, airborne sensors, in situ monitoring networks, and geospatial platforms, has created unprecedented opportunities for understanding the Earth system. However, transforming these massive, heterogeneous, multi-scale, and multi-temporal data streams into actionable geospatial intelligence remains challenging. Recently, Earth embeddings, such as AlphaEarth and TESSERA, have emerged as a promising approach to representing locations, pixels, image patches, objects, regions, trajectories, or spatiotemporal processes as learned vectors. These representations compress complex Earth data while preserving semantic, spatial, temporal, and relational information useful for downstream analysis. This review examines the emerging field of Earth embeddings through a Represent, Relate, and Reason framework. We first define Earth embeddings and explain their importance for integrating diverse Earth observation and geospatial data. We then review data modalities, embedding units, learning strategies, model architectures, existing embedding products, evaluation methods, and geospatial applications. Comparative experiments complement this review by examining embedding structure, predictive utility, and sensitivity to dimensionality. We also discuss key challenges and future directions concerning generalization across regions and time, interpretability, uncertainty, benchmark design, physical consistency, bias, and responsible use. This review provides readers with a structured understanding of what Earth embeddings are, how they are generated and evaluated, and how they can provide a reusable foundation for geospatial analysis and scientific inquiry.

Keywords: Earth observation, Foundation models, Global embeddings, Self-supervised learning, Remote sensing

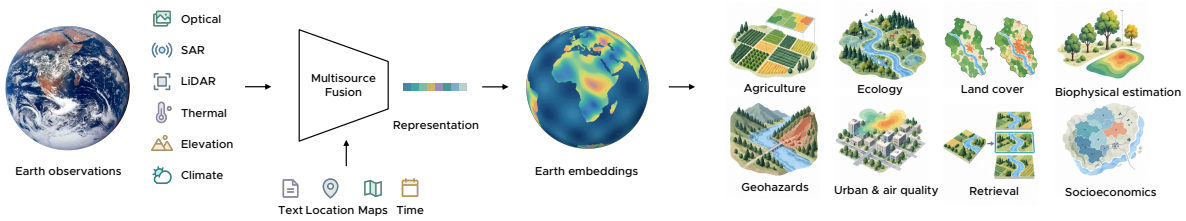
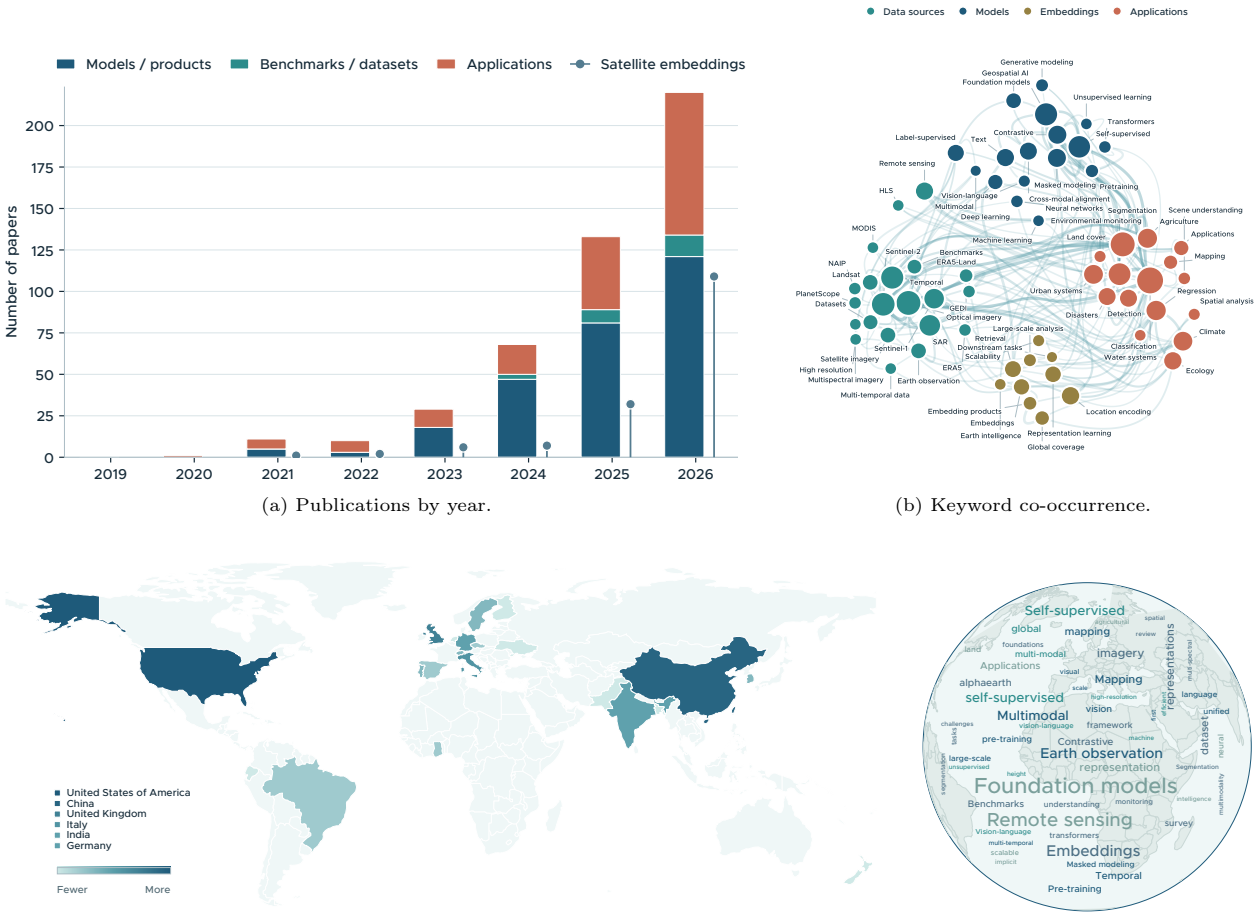


Fig. 1 Learning Earth embeddings from multisource inputs and using them for geospatial applications.



(a) Publications by year.

(b) Keyword co-occurrence.

(c) Affiliation distribution.

(d) Keyword cloud.

Fig. 2 Bibliometric overview of the literature considered in this review.

1 Introduction

Earth observation (EO) provides repeated measurements of the same world through different sensors, yet information learned for one analysis is not automatically available for another. Open archives have established the basis for sharing measurements: the Landsat archive extends back to 1972, complemented by openly distributed Sentinel data. NASA's Harmonized Landsat–Sentinel-2 (HLS) product harmonizes Landsat 8/9 observations from 2013 onward with Sentinel-2 observations from 2015 onward (Ju et al. 2025). These developments make observations accessible and comparable, but researchers often still construct features and train models for individual studies. This repeated effort is particularly demanding where labels are costly to collect and unevenly distributed across regions and dates (Tuia et al. 2021). Extending reuse from observations to the information learned from them would allow new analyses to build on existing features and focus local measurements on the question being investigated.

Pretraining supports this reuse by learning representations that can be adapted to different downstream tasks. Contrastive learning (Chen et al. 2020; He et al. 2020), masked image modeling (He et al. 2022), and self-distillation (Caron et al. 2021; Oquab et al. 2024) derive supervision from the observations themselves. Geospatial foundation models (GFMs) apply such objectives to satellite and related EO data, allowing their representations to be adapted to later tasks (Szwarcman et al. 2026; Reed et al. 2023; Xiong et al. 2024). Reusing a pretrained model still requires obtaining its weights, preparing sensor-specific input pipelines, and running inference over the study area. Precomputed products make the resulting representations directly available for analysis. The Google Satellite Embedding dataset, generated with AlphaEarth Foundations, releases learned vectors as openly distributed geospatial data (Brown et al. 2025). Users can fit lightweight predictors to these vectors without repeating large-scale encoding. New labels then connect reusable features to the target of interest, drawing on information learned from observations far beyond the labeled sample. Separating representation learning from individual applications reduces repeated processing and makes large-scale learning accessible without requiring every study to train or run a foundation model. Earth embeddings

thereby provide a new foundation for geospatial analysis: shared learned representations become the starting point for investigating new questions.

An Earth embedding is a learned numerical vector that encodes properties of a geographic location or spatial unit for reuse across tasks (Klemmer et al. 2026). Observations supply the measurements, an encoder transforms them into embeddings, and a downstream method uses the vectors to estimate a target or compare locations. The embedding is therefore distinct from both the original measurements and a particular prediction. Fig. 1 illustrates this connection through multisource learning and applications in mapping, estimation, and retrieval. Fig. 2 summarizes the growth of the research. Annual records retrieved through OpenAlex (Priem et al. 2022) and the satellite embedding literature both increase sharply after 2023. The keyword cloud emphasizes *foundation models*, *Earth observation*, *embeddings*, *multimodal*, and *self-supervised*. The co-occurrence network shows how these topics connect: its four groups distinguish data sources, models, embeddings, and applications, with links indicating terms occurring in the same study. Sources such as *Sentinel-2*, *SAR*, and *Landsat* connect to learning methods and applications in land cover, agriculture, environmental monitoring, and ecology. These links motivate comparison across applications, where similar methods may retain different information or serve different targets. The affiliation map shows substantial contributions from North America, Europe, and Asia. Together, the four panels show that Earth embedding research is growing rapidly across methods, applications, and regions.

1.1 Related Reviews and Our Contributions

Existing reviews approach geospatial representation learning from several directions. Reviews of remote sensing foundation models organize architectures, pretraining objectives, transfer methods, and downstream tasks (Xiao et al. 2025). Multimodal reviews focus on sensor fusion and cross-modal learning (Yang et al. 2025), while broader analyses discuss the opportunities and foundations of geospatial models (Mai et al. 2024; Zhu et al. 2026). Within the more recent embedding literature, Rolf et al. (2025) provide a concise perspective on reusable Earth representations, and Klemmer et al. (2026) define their principal functions and propose a research agenda. Fang et al. (2026) compare seven released products and implement common access through TorchGeo. Wang (2026) develops an embedding-centered taxonomy and evaluates 19 models on a regional benchmark in Wuhan. Gomes et al. (2025b) examine neural compression, storage, and machine-to-machine transfer, whereas Stewart et al. (2026) compare embedding types, coverage, resolution, storage, licensing, applications, and two practical workflows.

Limitations of existing reviews. These works differ in the questions they resolve. The foundation-model reviews emphasize pretraining and adaptation (Xiao et al. 2025; Mai et al. 2024; Zhu et al. 2026), while the conceptual embedding papers establish functions and research priorities (Rolf et al. 2025; Klemmer et al. 2026). The product-access study compares releases but leaves cross-product benchmarking for future work (Fang et al. 2026). The Wuhan study contributes a regional evaluation (Wang 2026), and the compression review examines storage and transmission (Gomes et al. 2025b). The practical chapter broadens guidance on obtaining and using embeddings without the globally distributed experimental comparison undertaken here (Stewart et al. 2026). These contributions provide complementary accounts, but the connection between representation design and performance across applications remains less developed.

Contributions of this review. We develop Represent, Relate, and Reason (3R) as a perspective for explaining how information learned from observations becomes useful across geospatial questions. Compared with the separate emphases of the reviews above, we connect learning methods, models and products, distribution platforms, software libraries, benchmarks, and applications. This coverage allows us to examine how supervision and fusion determine retained information, how spatial and temporal relationships support reuse, and when new measurements or domain knowledge remain necessary. We compare the conditions under which studies obtain useful results. Experiments on globally distributed samples complement this analysis through embedding structure, predictive performance, and dimension sensitivity. The review brings these findings together to inform representation design, evaluation, and future geospatial research.

1.2 Organization of This Review

Fig. 3 outlines the questions and comparisons developed in each chapter. Section 2 develops the Represent, Relate, and Reason perspective. Section 3 reviews the data, feature representations, and pretraining methods behind Earth embeddings, and Section 4 examines models, released products, design choices, distribution infrastructure, and evaluation benchmarks. Section 5 describes the evaluation data and analyzes representation geometry, downstream classification and regression, and sensitivity to embedding dimension. Section 6 reviews published applications, Section 7 discusses unresolved technical and scientific problems, and Section 8 concludes the review.

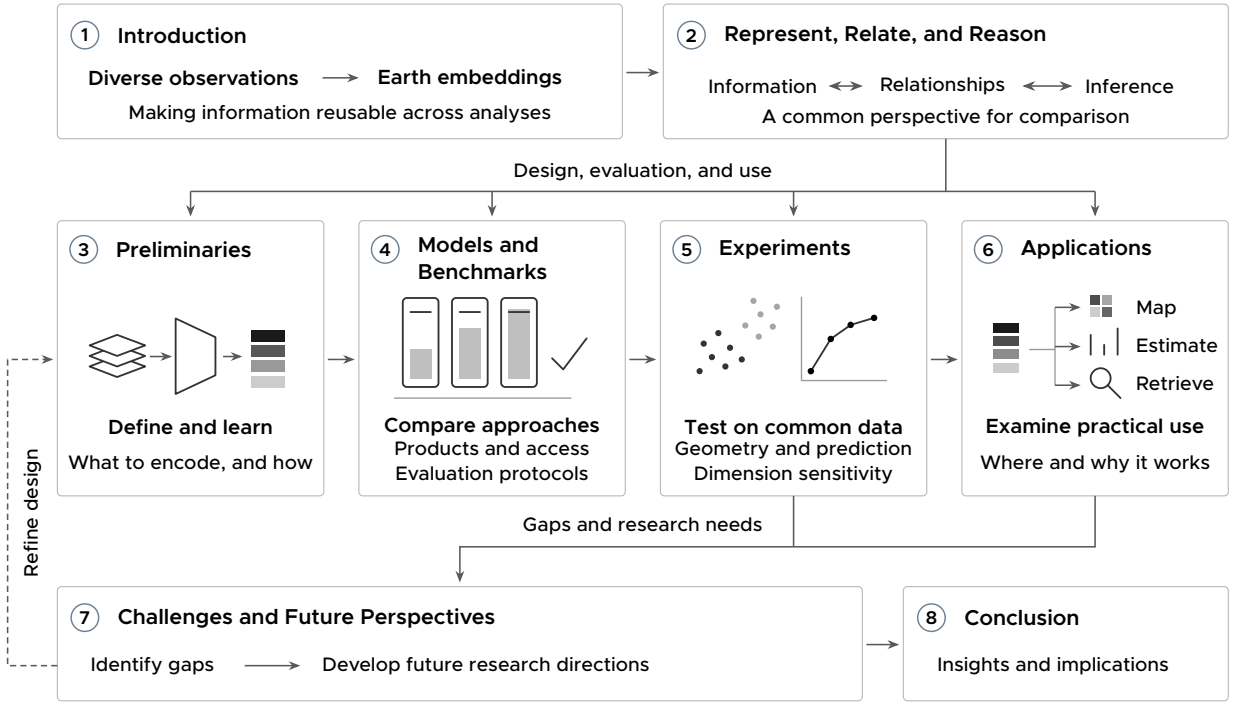


Fig. 3 Organization of the review and the questions addressed in each chapter.

2 Represent, Relate, and Reason

Geospatial analysis connects observations with knowledge of the Earth's properties, organization, and change. Earlier perspectives examine Earth embeddings as reusable descriptions and geospatial datasets (Klemmer et al. 2026; Fang et al. 2026). Reuse, however, raises questions that a model or product inventory alone cannot answer: which distinctions remain available, what relationships the vectors express, and how these support a particular inference. We examine these questions through *Represent*, *Relate*, and *Reason* (3R). They are interdependent aspects of analysis, not successive stages of development. Fig. 4 expresses their connections in three reciprocal pairs. Represent supplies a *structure* for comparing observations, while Relate brings spatial, temporal, and semantic *context* into representation learning. Represent provides *information* for inference, while Reason sets *requirements* for what the representation must preserve. Relate identifies *relations* that inform inference, while Reason formulates *hypotheses* that guide which relations to examine.

2.1 Represent

Information and abstraction. A representation makes selected properties accessible while suppressing other variation. This choice connects the observed signal with the phenomenon to be studied: appearance, environmental context, and a measured physical property are related but different descriptions. Change-aware contrastive learning encourages invariance to seasonal variation while retaining sensitivity to longer-term changes (Mall et al. 2023); temporal encoding in TESSERA uses within-year observations to retain information relevant to vegetation phenology (Feng et al. 2026a). Seasonal variation can obscure a persistent land-cover category yet help distinguish vegetation types. A useful representation must therefore combine stability to irrelevant differences with sensitivity to differences that matter. This tension connects learning objectives to temporal aggregation and compression: each can simplify analysis while making some distinctions less accessible.

Observation and prior knowledge. Different measurements provide partial descriptions of the same phenomenon, while maps, text, and training targets introduce previously interpreted information. CROMA learns radar, optical, and joint encodings, whereas AlphaEarth Foundations combines multiple observation and supervision sources (Fuller et al. 2023; Brown et al. 2025). What a vector contains consequently depends on both what was measured and what the model was asked to predict or align. A coordinate encoder illustrates the distinction: it can associate position with learned environmental characteristics without observing current conditions at query time (Klemmer et al. 2025). Such context is valuable for sparse-data inference, but newly observed events may require additional measurements. The relevant question is not whether the representation is purely observational, but which sources of information support its use for a particular target.

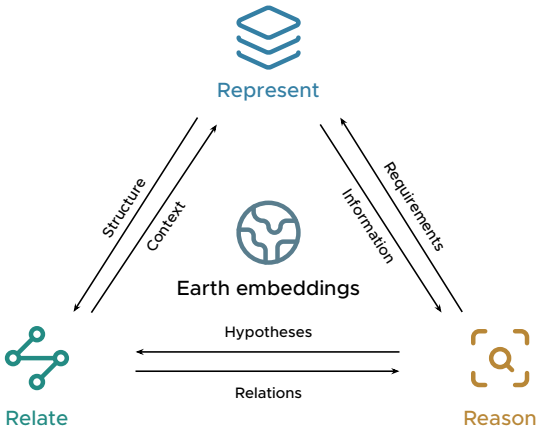


Fig. 4 Represent, Relate, and Reason as interdependent questions for Earth embedding research.

Representation reuse. Reuse changes how existing observations and new measurements contribute to analysis. The shared features of MOSAIKS and the released layers of AlphaEarth Foundations separate feature construction from fitting a predictor to a particular target (Rolf et al. 2021; Brown et al. 2025). This allows knowledge learned across a large observation collection to support questions with comparatively limited labels. Access to an encoder permits new inputs or adapted features, whereas a precomputed collection fixes earlier choices about observations, support, and aggregation. Keeping access to source measurements makes it possible to reconsider those choices when a new question requires different information. Reusability thus involves both efficient access to learned features and the ability to revise an inadequate description.

2.2 Relate

Similarity and dependence. Geographic properties are organized through proximity, boundaries, connections, and change. Spatial proximity can suggest shared conditions, but distant places can resemble one another and adjacent places can differ across a boundary. Major TOM supports imagery search through feature similarity, while SatCLIP associates coordinates with satellite-derived characteristics (Czerkawski et al. 2024; Klemmer et al. 2025). Embeddings therefore provide an additional basis for identifying comparable observations beyond distance alone. Their usefulness depends on the relation sought: similar appearance, comparable environmental conditions, and functional connection require different reference information. For example, vegetation similarity can identify candidate environmental analogues, while observations of connectivity or exchange are needed to study interaction.

Structure and composition. Relations can also be supplied explicitly rather than inferred from vector distance. Adjacency, containment, and network links describe how local units form a larger whole. OSMGraphCLIP uses typed map features and their relations to supervise location representations (Michail et al. 2026); graph-based poverty prediction instead combines previously computed satellite embeddings within a downstream graph model (Pettersson and Daoud 2025). These are different ways to use relational information. The former changes what is learned during encoding; the latter supplies connections when answering a target question. This distinction extends to human–environment interactions and hierarchical analysis: aggregating local attributes describes composition, whereas preserving their arrangement or connections may require an explicit relational model. Pooling studies provide an empirical starting point for examining what survives a change in analysis unit (Corley et al. 2026a).

Correspondence across observations. Different observations of the same place offer another kind of relation. Spatial registration identifies co-located measurements; learned correspondence connects their content, as in radar–optical learning with CROMA and image–location alignment with SatCLIP (Fuller et al. 2023; Klemmer et al. 2025). Agreement is useful, but not all useful information is shared. DeCUR explicitly separates common and modality-specific components (Wang et al. 2025a), illustrating why fusion should preserve complementary information as well as alignment. Temporal correspondence raises a related choice: repeated observations may describe a stable property, a recurring cycle, or an irreversible change. The appropriate matching rule depends on which of these the analysis seeks. Paired retrieval, observations of change, and tests with missing sources can assess different aspects of correspondence.

Transfer and complementarity. Transfer asks whether relationships learned under one set of conditions remain informative under another. Geographic adaptation with SatCLIP examines this question across regions (Klemmer et al. 2025). Collections from multiple encoders in Major TOM and common-access tools

make it possible to compare alternative descriptions of the same locations (Czerkawski et al. 2024; Fang et al. 2026). The comparison should distinguish a useful transferable association from a local association that must be recalibrated. A second embedding is valuable when it adds information relevant to the target, not merely when its geometry differs. Holding the target, available observations, and prediction method consistent helps test that contribution; testing another region or period then examines its persistence. Together, these comparisons connect relationships learned during pretraining with the conditions required for their later reuse.

2.3 Reason

Inference from shared descriptions. Geographic inference connects observations with quantities that have not been measured everywhere. Here, *Reason* denotes inference using embeddings, independent measurements, analytical methods, and domain knowledge. MOSAIKS uses common features for environmental and socioeconomic estimation, while TESSERA examines temporal features across classification and continuous-variable targets (Rolf et al. 2021; Feng et al. 2026a). These uses link widely available descriptions to more sparsely measured properties. Their scientific interpretation depends on whether the representation supplies direct target-related information, contextual associations, or information complementary to other predictors. Comparisons with expert variables and physical measurements can help distinguish these roles (Koch et al. 2026). The contribution of an embedding is consequently best understood relative to what the analysis already knows.

Scientific hypotheses. Representations can help organize comparisons that expose unresolved explanations. Similar vegetation embeddings paired with different biomass measurements, for example, could motivate tests of missing structural information or mismatched observation dates. Such a discrepancy can be investigated with independent observations. Hybrid modeling provides a way to connect learned information with process knowledge (Reichstein et al. 2019). Embeddings could describe spatially varying conditions, while a process model specifies how these conditions enter an explanation. Comparisons of resulting predictions and residuals could then identify where further measurements are needed. Testing causal explanations requires a research design that distinguishes competing causal accounts.

Cumulative geographic knowledge. Repeated analysis can establish which attributes remain accessible and where new observations would be useful. An embedding that supports land-cover mapping but misses a recorded disturbance motivates examination of temporal aggregation and sensitivity to change. If an environmental association fails in a new region, additional measurements may clarify whether the missing information concerns local conditions or the target itself. This feedback links the questions in Fig. 4. It also connects prediction with observation design: the next measurement can be chosen to resolve an uncertainty in the analysis, rather than simply enlarge the dataset.

3 Preliminaries

The content of an Earth embedding depends on what is observed, how measurements are grouped, and what the learning objective rewards. These choices connect the information-preservation question above to the data sources, feature representations, and pretraining objectives reviewed here. Fig. 5 places these components alongside models, access infrastructure, and applications; Section 4 examines their consequences for products and evaluation.

3.1 Earth Observation Data Sources

Earth observation sources enter representation learning in different roles: some are direct encoder inputs, some provide targets or auxiliary supervision during pretraining, and others are used only as downstream labels or covariates. Surface imagery from Sentinel-2, Landsat, HLS, and Sentinel-1 forms the main input to many of the models summarized here because these missions combine broad coverage with repeated observations (Drusch et al. 2012; Ju et al. 2025; Torres et al. 2012). ALOS-2 PALSAR-2 (Rosenqvist et al. 2014), GEDI (Dubayah et al. 2020), ERA5-Land (Muñoz Sabater et al. 2021), Copernicus GLO-30 DEM (and 2022), VIIRS, Sentinel-3, ICESat-2 ATL08 (Neuenschwander et al. 2025), Sentinel-5P, PlanetScope, and NAIP contribute structural, environmental, atmospheric, or higher-resolution information in selected models and benchmarks. Embedded Seamless Data (ESD) (Chen et al. 2026) is generated from the Global 30 m Seamless Data Cube of Land Surface Reflectance (SDC30) (Chen et al. 2024), which harmonizes Landsat 5, 7, 8, and 9 with MODIS Terra into a gap-filled daily reflectance record. Linked source names in Table 1 lead to the official instrument and product specifications.

Table 1 compares the listed sources and their use in geospatial representation learning. Sentinel-2 and Sentinel-1 appear most often in current GFM and embedding pipelines, while Landsat and HLS provide longer temporal coverage. GEDI and elevation products add information about vertical structure and terrain;

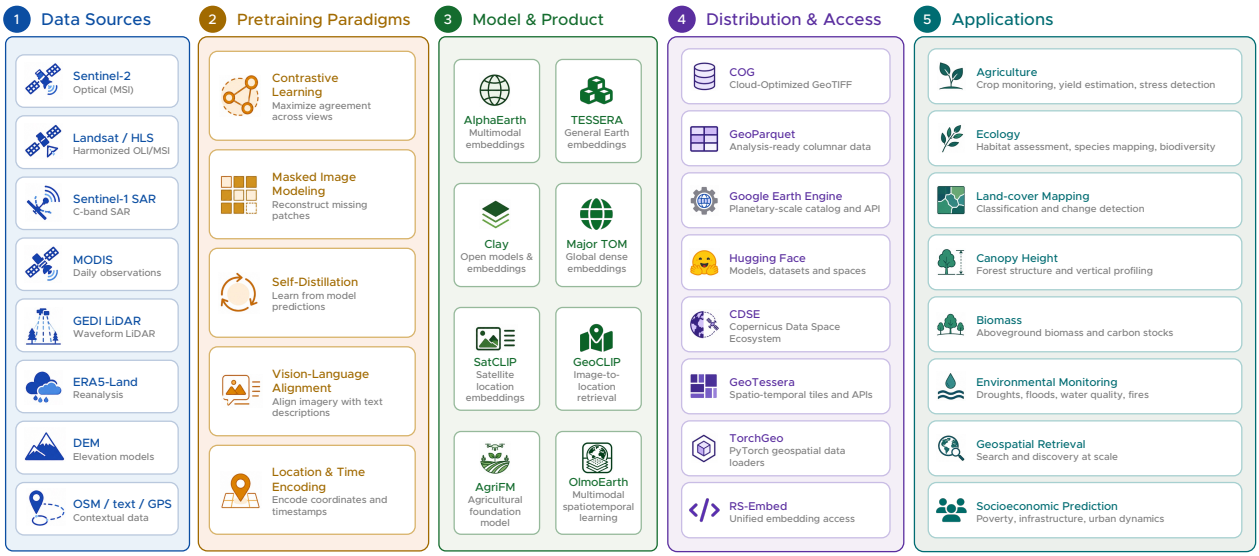


Fig. 5 Data sources, pretraining methods, models, access infrastructure, and applications covered in this review.

Table 1 Representative Earth observation data sources used in geospatial representation learning.

Source / Product	Modality	Time span	Resolution	Cadence	Representative uses
Sentinel-2 MSI	Optical multispectral (13 bands)	2015–	10–60 m	5 days	High (SatMAE; Copernicus-FM; AlphaEarth)
Landsat 8/9	Optical and thermal (11 bands)	2013/2021–	15/30/100 m	8 days	High (MOSAIKS; AlphaEarth)
HLS L30/S30	Optical and thermal (10/13 bands)	2013/2015–	30 m	1.4 days avg.	Medium (Prithvi-EO; GEO-Bench-2)
MODIS	Optical and thermal (36 bands)	2000–	250 m–1 km	1–2 days	Medium (ESD; SEN12MS)
VIIRS	Visible and infrared (22 bands)	2011–	375–750 m	daily	Low (few current foundation model examples)
Sentinel-3 (OLCI, SLSTR)	Optical and thermal (21 + 9 channels)	2016–	300 m–1 km	1–2 days	Low (Copernicus-FM / Copernicus-Bench)
Sentinel-1 SAR	C-band SAR	2014–	∼20×22 m (IW GRD)	6–12 days	High (CROMA; SoftCon; AlphaEarth)
ALOS-2 PALSAR-2	L-band SAR	2014–	10–100 m	14 days	Low (AlphaEarth; RingMoE)
GEDI	Waveform LiDAR	2019–	25 m footprints	irregular	Medium (AlphaEarth; MMEarth)
ICESat-2 ATL08	Photon LiDAR	2018–	100 m along-track	91 days	Low (few current foundation model examples)
Copernicus GLO-30 DEM	Digital elevation model	static	30 m	static	Low (AlphaEarth; Copernicus-FM)
SRTM	Digital elevation model	static	30 m	static	Low (Presto)
ASTER GDEM	Digital elevation model	static	30 m	static	Low (few current examples)
ERA5-Land	Reanalysis	1950–	∼9 km	hourly	Low (AlphaEarth)
ERA5	Reanalysis	1940–	∼31 km	hourly	Medium (Presto; Climplicit; MMEarth)
Sentinel-5P / TROPOMI	Atmosphere	2017–	5.5–7 km	daily	Low (Copernicus-FM / Copernicus-Bench)
PlanetScope	Commercial optical (4–8 bands)	2017–	3 m	near-daily	Medium (DynamicEarthNet; SpaceNet7; GEO-Bench-2)
NAIP	Aerial optical (4 bands)	2003– (U.S.)	0.6–1 m	2–3 years	Medium (Tile2Vec; SatlasPretrain; USat)

ERA5-Land, ERA5, and Sentinel-5P supply environmental variables at coarser resolution. PlanetScope, NAIP, VIIRS, Sentinel-3, and ICESat-2 are used more selectively. Their use depends on geographic coverage, co-registration, temporal alignment, access conditions, cost, and licensing as well as information content.

The representation unit determines how measurements enter an analysis. Sensor resolution describes the input measurements, spatial support identifies the ground footprint assigned to a vector, and the encoder's context determines which surrounding observations can influence that vector. A pixel-wise vector can incorporate neighboring context, whereas a pooled patch vector summarizes a larger footprint. Neither automatically matches the area represented by a field plot, parcel, or administrative label. The matching

rule is part of the scientific question: estimating an average property requires a different treatment of within-area variation from detecting a localized disturbance. Pooling evaluations illustrate how this choice changes what downstream prediction can recover (Corley et al. 2026a). Thus, resampling inputs to a common grid establishes correspondence without making their physical support or information content identical.

The sources used to teach an encoder may also differ from those available when it produces vectors. AlphaEarth Foundations uses several observation and supervision sources in training, while inference uses optical, thermal, and SAR observations from Sentinel-2, Landsat 8/9, and Sentinel-1 (Brown et al. 2025). In OlmoEarth, derived maps provide prediction targets during pretraining but are not encoded as inputs at inference (Herzog et al. 2026). Maps and text can consequently contribute interpreted knowledge without being required for each subsequent query. Their categories, coverage, and reference dates help determine what is learned. Independence from new task labels therefore does not imply independence from previously labeled or modeled information. Availability adds another constraint: clouds can obscure more than 50% of optical observations in tropical regions (Meraner et al. 2020), SAR contains speckle and layover artifacts, and acquisition times are irregular. Joint encoding must account for these differences in noise, availability, and geometry (Zhu et al. 2026; Bodnar et al. 2025).

Models differ in how they combine these inputs. AlphaEarth Foundations (Brown et al. 2025) uses source-specific encoders whose outputs feed a common spatiotemporal representation; missing frames or input sources can be accommodated at inference. TESSERA (Feng et al. 2026a) encodes optical and SAR time series separately, fuses their representations, and trains on independently sampled temporal views of each pixel. The Clay Foundation Model (Clay Foundation 2024) uses wavelength-conditioned patch embeddings in a Vision Transformer, with spatial-resolution, location, and time information. TerraMind (Jakubik et al. 2025) and TerraFlow (Puriy et al. 2026) quantize modalities into discrete tokens and predict target tokens from the available context. CROMA (Fuller et al. 2023) uses cross-attention to reconstruct one modality from masked observations of another. The choice depends on source availability, temporal alignment, and missing-input handling.

3.2 Feature Representations

Feature representations convert measurements into variables for subsequent analysis. Their content is selected through expert definitions, task labels, or supervision derived from observations. Precomputed products change access to learned features, rather than constitute a separate learning objective.

Hand-Crafted Descriptors. Hand-crafted indices and descriptors condense multi-band imagery into variables selected for a particular task. The normalized difference vegetation index (NDVI) (Tucker 1979), computed from red and near-infrared reflectance, remains a standard indicator of vegetation condition; related formulations target water bodies (NDWI (McFEETERS 1996)), built-up areas (NDBI (Zha et al. 2003)), and snow cover (NDSI (Hall et al. 2002)). Grey-level co-occurrence matrices (GLCM) (Haralick et al. 1973) and local binary patterns (LBP) (Ojala et al. 2002) describe texture and are commonly paired with random forest (RF) or support vector machine (SVM) classifiers (Breiman 2001; Cortes and Vapnik 1995; Gislason et al. 2006). Such features are interpretable and inexpensive, but their task-specific definitions retain only selected spectral and spatial information.

Label-Supervised Deep Representations. Label-supervised representations emphasize distinctions specified by scene labels, segmentation masks, or continuous targets. ImageNet pretraining (Deng et al. 2009) with VGG (Simonyan and Zisserman 2015) or ResNet (He et al. 2016) supplies hierarchical features for remote sensing classification and segmentation (Cheng et al. 2017; Volpi and Tuia 2017); long short-term memory networks (Hochreiter and Schmidhuber 1997) and Vision Transformers (Dosovitskiy et al. 2021) accommodate sequences and attention-based image encoding. Their learned content depends on both architecture and supervision. Transfer from natural imagery is limited where the target requires spectral or temporal information absent from the source data (Neumann et al. 2020; Mañas et al. 2021).

Self-Supervised EO Representations. Self-supervised EO methods derive supervision from the observations rather than task labels. Tile2Vec (Jean et al. 2019) uses spatial proximity, Seasonal Contrast (SeCo) (Mañas et al. 2021) uses multi-date observations of the same location, and SSL4EO-S12 (Wang et al. 2023) supplies Sentinel-1/2 data for comparing contrastive, distillation, and reconstruction objectives. RingMo (Sun et al. 2023), SatMAE (Cong et al. 2022), Scale-MAE (Reed et al. 2023), SkySense (Guo et al. 2024), and DINOv3 (Siméoni et al. 2025) extend self-supervised learning to multispectral, multimodal, or multitemporal inputs. These methods reduce dependence on downstream labels, but users must still obtain the model weights, reproduce the required preprocessing, and run the encoder over their study regions.

Embedding Products. Embedding products release precomputed vectors rather than requiring every user to run the encoder. MOSAIKS (Rolf et al. 2021) provided a shared global feature set for environmental and socioeconomic prediction, while Major TOM (Francis and Czerkawski 2024; Czerkawski et al. 2024) released

Table 2 Feature-representation families in Earth observation.

Feature Representation	Supervision	Representative examples	Output form	Characteristics
Hand-crafted descriptors	Expert-designed formulas and statistics	Spectral indices (NDVI, NDWI, NDBI, NDSI) Texture descriptors (GLCM, LBP) Classical ML (RF, SVM)	Scalars or low-dimensional descriptors	Interpretable and inexpensive, but task-specific and context-limited
Label-supervised deep representations	Human annotations such as class labels, masks, or target variables	CNN-based features (VGG, ResNet) RNN-based temporal encoders (LSTM) Transformer-based encoders (ViT)	Feature maps or latent vectors	Hierarchical and task-effective, but label-dependent and domain-sensitive
Self-supervised EO representations	Pretext tasks derived from unlabeled EO archives	Contrastive models (Tile2Vec, SeCo) Masked autoencoders (SatMAE, Scale-MAE) Self-distillation (SSL4EO-S12 DINO, DINOv3)	Latent features extracted by inference	Scalable and domain-adapted, but still largely model-centric
Embedding products	Inherited from pretrained encoders and released in precomputed form	Global feature collections (MOSAIKS, Major TOM) Dense embedding products (LGND, TESSERA, Google Satellite Embedding, ESD)	Precomputed vector fields or embedding layers	Directly reusable, but constrained by storage, interoperability, and update cycles

vectors from multiple frozen encoders over globally sampled satellite tiles. LGND distributes near-global chip embeddings generated with Clay (Clay Foundation 2024; LGND.ai 2026); TESSERA v1 and the Google Satellite Embedding dataset produced with AlphaEarth Foundations provide dense annual layers (Feng et al. 2026a; Brown et al. 2025); and ESD retains a temporally indexed record (Chen et al. 2026). TESSERA v2 extends the product design with distilled temporal encoders and selectable output dimensions (Feng et al. 2026c). Downstream analysis can begin with released vectors and a task-specific prediction model, while storage, access, updating, version compatibility, and interpretation remain product concerns.

3.3 Pretraining Paradigms

A pretraining objective specifies which comparisons or predictions the encoder is rewarded for supporting. Its meaning depends on how observations are paired, masked, or used as targets, not only on the algebraic form of the loss. Nearby patches may supply spatial context; repeated acquisitions may emphasize persistence or change; another modality may supply information unavailable in the encoded input. These choices introduce assumptions about which variation matters. These assumptions influence the information that the model learns to retain. Storage and distribution are considered in Section 4.

Contrastive Objectives. Contrastive objectives learn representations by bringing matched views closer in embedding space and pushing mismatched views apart. Given a positive pair (z_i, z_j) and a set of $2N$ augmented views within a mini-batch, the InfoNCE loss (Oord et al. 2018; Chen et al. 2020) is

$$\mathcal{L}_{\mathrm{CL}} = -\log \frac{\exp\big(\mathrm{sim}(z_i, z_j)/\tau\big)}{\sum_{k=1}^{2N} \mathbf{1}_{[k\neq i]} \exp\big(\mathrm{sim}(z_i, z_k)/\tau\big)}, \tag{1}$$

where $\mathrm{sim}(\cdot,\cdot)$ denotes cosine similarity and τ is a temperature parameter. In EO, the definition of positive and negative pairs is as important as the loss. SeCo (Mañas et al. 2021) treats observations of the same location in different seasons as positives, encouraging invariance to seasonal and atmospheric variation. CACo (Mall et al. 2023) modifies temporal pairing to distinguish short-term variation from persistent change. Tile2Vec (Jean et al. 2019) instead defines pairs through geographic proximity and uses a triplet objective adapted from distributional semantics:

$$\mathcal{L}_{\mathrm{triplet}} = \max\left(0,\, d(f(x_a), f(x_p)) - d(f(x_a), f(x_n)) + m\right), \tag{2}$$

where x_a, x_p, and x_n denote an anchor tile, a nearby tile, and a distant tile, respectively. SSL4EO-S12 (Wang et al. 2023) supplies Sentinel-1/2 data for comparing contrastive and alternative objectives at scale. Pairing policy specifies the desired invariance: seasonal pairs encourage temporal consistency, spatial pairs promote local similarity, and image–location pairs in SatCLIP and GeoCLIP (Klemmer et al. 2025; Vivanco Cepeda

et al. 2023) introduce geographic information. Their downstream value depends on whether the variation suppressed during learning is irrelevant to the target.

Reconstruction Objectives. Reconstruction objectives mask part of the input and train the model to recover the missing content, encouraging the encoder to preserve local structure and context. For masked autoencoders (He et al. 2022), the loss is

$$\mathcal{L}_{\text{MAE}} = \frac{1}{|\mathcal{M}|} \sum_{p \in \mathcal{M}} \|\mathbf{x}_p - \hat{\mathbf{x}}_p\|^2, \tag{3}$$

where $\mathcal{M}$ is the set of masked patches, $\mathbf{x}_p$ is the original content, and $\hat{\mathbf{x}}_p$ is its reconstruction. RingMo (Sun et al. 2023), SatMAE (Cong et al. 2022), Scale-MAE (Reed et al. 2023), SpectralGPT (Hong et al. 2024), Clay (Clay Foundation 2024), and Prithvi-EO-2.0 (Szwarcman et al. 2026) apply this objective to multispectral, multiscale, or multitemporal inputs, while Presto (Tseng et al. 2023) adapts reconstruction to multisensor pixel time series. Because the encoder must predict missing content, these objectives encourage retention of spatial, spectral, or temporal context. Benefits depend on the mask design, encoder output, and downstream adaptation.

Redundancy-Reduction Objectives. Some models aim not primarily to reconstruct the input, but to produce invariant embeddings with minimal redundancy across dimensions. The Barlow Twins criterion (Zbontar et al. 2021) operates on the cross-correlation matrix $\mathbf{C}$ between embeddings of two valid views:

$$\mathcal{L}_{\text{Barlow}} = \underbrace{\sum_i (1 - C_{ii})^2}_{\text{invariance}} + \lambda \underbrace{\sum_i \sum_{j \neq i} C_{ij}^2}_{\text{redundancy reduction}}, \tag{4}$$

where $C_{ij} = \sum_b z_{b,i}^A \, z_{b,j}^B / \sqrt{\sum_b (z_{b,i}^A)^2 \sum_b (z_{b,j}^B)^2}$ is the cross-correlation between dimensions i and j computed over a batch of augmented pairs (A, B) after centering each feature over the batch. TESSERA v1 (Feng et al. 2026a) applies this criterion to annual Sentinel-1/2 time series, and TESSERA v2 (Feng et al. 2026c) retains it while varying encoder capacity, training-data volume, and compute. DeCUR (Wang et al. 2025a) uses a related objective to separate common and modality-specific information. Decorrelation reduces redundancy but does not measure retained task information.

Distillation Objectives. Distillation objectives replace explicit pixel reconstruction with consistency between a student and a teacher or target encoder. DINO (Caron et al. 2021), DINOv2 (Oquab et al. 2024), and DINOv3 (Siméoni et al. 2025) provide frozen features learned through this strategy. Panopticon (Waldmann et al. 2025) adapts DINOv2 to sensor-variable EO observations through channel attention and cross-sensor views of the same footprint. I-JEPA (Assran et al. 2023) and AnySat (Astruc et al. 2025a) instead predict targets in representation space. TESSERA v2 (Feng et al. 2026c) distills a temporal teacher into compact student encoders whose 128-dimensional output can be shortened without retraining, while Major TOM (Francis and Czerkawski 2024; Czerkawski et al. 2024) distributes globally sampled vectors from frozen encoders in the DINOv2 family. Fair comparisons with reconstruction objectives require matched architectures, data, and evaluation protocols.

Alignment and Generative Objectives. Alignment objectives learn a shared space for paired modalities. CLIP (Radford et al. 2021) optimizes a symmetric image–text contrastive loss over a batch of N matched pairs:

$$\mathcal{L}_{\text{CLIP}} = -\frac{1}{2N} \sum_{i=1}^{N} \left[\log \frac{e^{\text{sim}(v_i, t_i)/\tau}}{\sum_j e^{\text{sim}(v_i, t_j)/\tau}} + \log \frac{e^{\text{sim}(t_i, v_i)/\tau}}{\sum_j e^{\text{sim}(t_i, v_j)/\tau}} \right] \tag{5}$$

where v_i and t_i are the image and text embeddings, respectively. In EO, the paired input may be text, coordinates, ground imagery, or another observation of the same place. RemoteCLIP (Liu et al. 2024), GRAFT (Mall et al. 2024), GeoCLIP (Vivanco Cepeda et al. 2023), SatCLIP (Klemmer et al. 2025), SoundingEarth (Heidler et al. 2023), and Sat2Cap (Dhakal et al. 2024) use different pairings to support retrieval, geolocalization, or cross-modal queries. The structure of the shared space consequently reflects both the data modality and the definition of matched locations.

Generative and predictive objectives infer a missing modality, timestamp, or token stream from the available context. TerraMind (Jakubik et al. 2025) tokenizes multiple geospatial modalities and predicts selected targets, and TerraFlow (Puriy et al. 2026) applies this formulation to temporal inputs. Copernicus-FM (Wang et al. 2025b) combines masked reconstruction with distillation from frozen teachers, whereas Galileo (Tseng et al. 2025) uses global and local contrastive masked modeling. AlphaEarth Foundations (Brown et al. 2025)

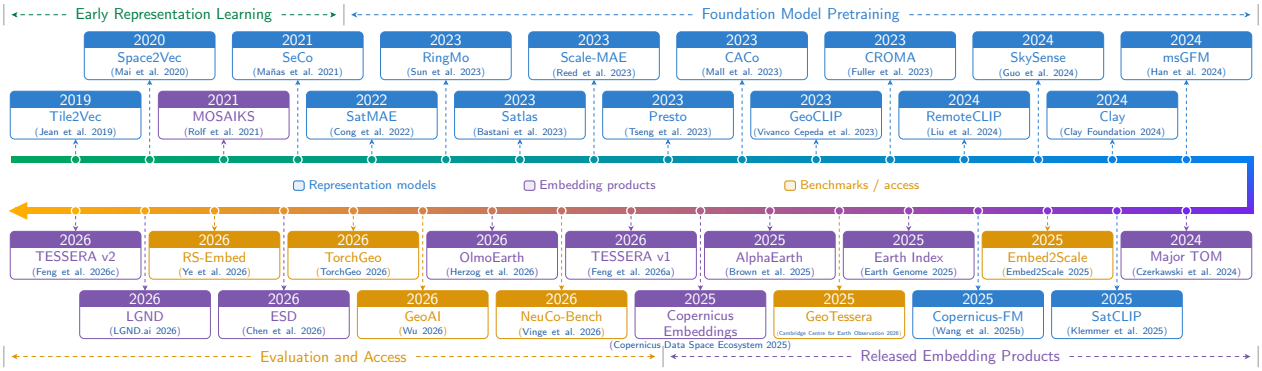


Fig. 6 Evolution of Earth embedding research from representation learning to products, evaluation, and access.

combines source-specific reconstruction, consistency constraints, and text alignment before releasing annual global embedding layers. Attributing a downstream property to one loss requires ablations that vary that loss while holding the other components fixed.

These objectives balance invariance against sufficiency: a representation should suppress irrelevant variation without losing information needed later. Contrastive and distillation objectives encourage consistency across selected views; reconstruction rewards prediction of missing content; multimodal learning links information across sources. The practical comparison is whether the resulting invariances match the intended analysis. This requires downstream evaluation, because an objective can reward successful pretraining without preserving every property of interest.

4 Models and Benchmarks

The preceding learning choices become constraints on subsequent analysis when weights or precomputed vectors are released. We compare what users can encode or obtain, which information the design preserves, and how that information is evaluated. Spatial support, temporal aggregation, compression, and access link the methods to practical use; architecture and pretraining alone do not determine suitability.

4.1 Models and Products

Fig. 6 outlines four stages in the development of Earth embeddings. Early studies learned reusable features from satellite imagery; later work increased model scale and incorporated additional sensors and supervision. The most recent stage centers on large embedding collections, benchmark-based evaluation, common access tools, and data standards.

Model capabilities and release conditions jointly determine how a representation can be reused. Foundation-model studies examine what can be learned through pretraining and adaptation; released embedding encoders permit feature extraction for new inputs; precomputed products make an existing spatial collection directly available. Recent embedding-centered reviews similarly distinguish model access from direct access to embeddings (Wang 2026; Fang et al. 2026). Table 3 compares representative models, embedding datasets, and released layers. Their practical difference is how much of the original description a user can change: a new prediction head changes how vectors are used, whereas new observations or an adapted encoder can change the information represented.

4.1.1 Geospatial Foundation Models

Geospatial foundation models learn transferable representations through pretraining on Earth observation data. Their objectives and treatment of spatial, spectral, and temporal variation determine the information available for subsequent analysis. Masked reconstruction and scale-aware learning, represented by SatMAE and Scale-MAE, emphasize information recoverable from incomplete observations and across resolutions (Cong et al. 2022; Reed et al. 2023). Learning across sensors additionally requires accommodating different spectral bands and observation conditions. DOFA, Panopticon, and RobSense address sensor-variable or incomplete inputs through different encoding designs (Xiong et al. 2024; Waldmann et al. 2025; Do et al. 2025).

Temporal and generative learning expand the information available beyond individual images. OmniSat combines heterogeneous observations, including image time series, while TerraMind and TerraFlow learn to predict target modalities or temporal inputs (Astruc et al. 2025b; Jakubik et al. 2025; Puriy et al. 2026). The key comparison is how these choices affect information retained for later use, rather than the number of

sensors alone. Table 3 summarizes representative releases; broader architectural comparisons are provided by existing reviews (Xiao et al. 2025; Yang et al. 2025).

The source of supervision also determines which geographic distinctions a model can learn. OpenStreetMap supervision and knowledge-guided pretraining supplement imagery with mapped or semantic information (Bai et al. 2025; Ravirathinam et al. 2026; Han et al. 2025). Multisensor learning is examined in TerraFM and SkySense V2 (Danish et al. 2026; Zhang et al. 2025b), while SpecAware addresses spectral variation in hyperspectral mapping and WV-Net specializes in SAR observations of the ocean (Ji et al. 2026; Glaser et al. 2025). These studies extend representation learning beyond a single optical sensor, but their specialization and downstream evaluation differ from those of globally released vector layers.

4.1.2 Released Embedding Products

A released embedding product fixes a spatial and temporal collection before downstream use. This differs from releasing methods for spatial and seasonal feature learning (Jean et al. 2019; Mañas et al. 2021; Ayush et al. 2021), pretrained image encoders (Wang et al. 2023; Cong et al. 2022; Reed et al. 2023), or coordinate encoders (Klemmer et al. 2025; Vivanco Cepeda et al. 2023): users receive vectors rather than only the means to generate them. Coverage and support then become essential comparison criteria. MOSAIKS provides global features (Rolf et al. 2021); Major TOM Embeddings covers globally sampled tiles using multiple encoders (Francis and Czerkawski 2024; Czerkawski et al. 2024); and Earth Index encodes billions of overlapping patches (Earth Genome 2025). The distinction also applies within a model family: Clay v1.5 supplies weights (Clay Foundation 2024), while LGND Clay Embeddings distributes a separate near-global dataset generated with that encoder (LGND.ai 2026).

Dense, temporally indexed releases include TESSERA v1 (Feng et al. 2026a), the Google Satellite Embedding dataset produced with AlphaEarth Foundations (Brown et al. 2025), and ESD, a record at 30 m resolution beginning in 2000 (Chen et al. 2026). TESSERA v2 studies distilled temporal encoders and selectable dimensions within the same product family (Feng et al. 2026c). The Copernicus Data Space distributes more than 60 TB of embeddings generated by several frozen encoders (Copernicus Data Space Ecosystem 2025), while Earth Embeddings as Products provides common loaders for accessing multiple releases (Fang et al. 2026).

Table 3 uses CL, MAE, SD, RCF, VLA, and FSQ for contrastive learning (Chen et al. 2020), masked autoencoding (He et al. 2022), self-distillation (Caron et al. 2021), random convolutional features (Rolf et al. 2021), vision–language alignment (Radford et al. 2021), and finite scalar quantization (Mentzer et al. 2024), respectively. The year is the formal publication year of the cited paper or, for dataset records without a paper, the first public-release year. *Res.* denotes the ground support of one vector; checkmarks under *Time* and *Global* indicate that one vector combines multiple dates and that a global or near-global collection is publicly available.

These collections support different analyses. Patch-level features facilitate regional prediction and retrieval (Rolf et al. 2021; Earth Genome 2025), while multi-encoder collections enable comparison on shared imagery (Czerkawski et al. 2024; Copernicus Data Space Ecosystem 2025). The LGND collection and Clay v1.5 weights distinguish access to existing vectors from encoding new observations (LGND.ai 2026; Clay Foundation 2024). Annual pixel-level layers retain finer spatial detail (Feng et al. 2026a; Brown et al. 2025), and the compressed 30-meter record in ESD supports comparison over approximately a quarter century (Chen et al. 2026). Selectable dimensions in TESSERA v2 introduce a further storage–performance choice (Feng et al. 2026c). The relevant distinction is the analysis each release permits without recovering or re-encoding its source observations.

4.1.3 Reusable Embedding Encoders

Publicly available pretrained weights allow users to generate embeddings for their own observations without repeating pretraining. The encoder can remain frozen while a downstream model is fitted to the extracted vectors. Image encoders such as Tile2Vec (Jean et al. 2019), SeCo (Mañas et al. 2021), and those pretrained on SSL4EO-S12 (Wang et al. 2023) provide satellite features, while DINOv2 (Oquab et al. 2024) and SigLIP (Zhai et al. 2023) offer general-purpose visual features. Reuse requires matching observations to the encoder's expected bands, normalization, spatial resolution, and temporal input. Multimodal encoders such as DeCUR (Wang et al. 2025a) and MMEarth (Nedungadi et al. 2025) extend the available inputs; Panopticon uses channel-level conditioning to apply one frozen encoder to optical, hyperspectral, and radar observations (Waldmann et al. 2025). The output also determines how the vectors can be used: spatial features can support local prediction, whereas pooled vectors summarize an image or region. Encoders trained to align imagery with text or co-located observations support comparisons across these inputs, as in RemoteCLIP (Liu

Table 3 Comparison of representative Earth embedding models and products.

Model / Product	Year	Architecture	Training objective	Dim.	Res.	Modalities	Time	Global	Format
Tile2Vec	2019	ResNet-18	Triplet CL	512	1.5 km	Optical			Weights
MOSAIKS	2021	Random conv.	RCF	8192/4000	1.1 km	Optical		✓	CSV / NPY
SeCo	2021	ResNet-50	MoCo-v2 CL	2048	2.65 km	Optical			Weights
CSP	2023	MLP + ResNet-50	CL	256	Coordinate	Optical + coord.			PyTorch weights
GeoCLIP	2023	Fourier features + MLP	Image–location CL	512	Coordinate	Image + coord.			PyTorch weights
Clay v1.5	2024	ViT	MAE + distillation	1024	–	MS + SAR			Weights
DINOv2	2024	ViT-L/14	SD	1024	2.24 km	Optical		✓	Parquet / HF
Major TOM Embeddings	2024	Multiple frozen encoders	Frozen inference	1024–2048	2.24–3.84 km	Optical + SAR		✓	Parquet / HF
SigLIP	2024	ViT-SO400M/14	VLA	1152	3.84 km	Optical + text		✓	Parquet / HF
SSL4EO-DINO	2024	ResNet-50	DINO (SD)	2048	2.24 km	Multispectral		✓	Parquet / HF
SSL4EO-MoCo	2024	ResNet-50	MoCo-v2 CL	2048	2.24 km	SAR		✓	Parquet / HF
Alphaearth embedding	2025	STP encoder	Reconstruction + CL + vMF	64	10 m	Optical + thermal + SAR	✓	✓	Earth Engine / COG
Copernicus Embeddings	2025	Multiple frozen encoders	Frozen inference	Varies	Varies	Optical + SAR		✓	GeoParquet / CDSE
Copernicus-Embed	2025	Copernicus-FM encoder	Frozen inference	768	0.25°	Multimodal EO + DEM	✓	✓	Parquet / NPZ / PT
Copernicus-FM	2025	ViT	MAE + distillation	768	–	Multimodal EO + DEM	✓		PyTorch weights
DeCUR	2025	ResNet-50	Redundancy reduction	2048	2.24 km	Multispectral + SAR		✓	GeoParquet / CDSE
Earth Index	2025	SoftCon ViT-S/14	Soft contrastive learning	384	320 m	Optical		✓	GeoParquet / Source Coop.
SatCLIP	2025	Spherical-harmonic MLP	Image–location CL	256	Coordinate	Optical + coord.			PyTorch weights
ESD	2026	Temporal CNN + FSQ	Reconstruction + supervised tasks	13	30 m	Optical + DEM	✓	✓	MGRS tiles
LGND Clay Embeddings	2026	Clay v1.5 encoder	MAE + distillation	256/1024	1.28/2.56 km	Optical	✓	✓	GeoParquet / Source Coop.
OlmoEarth	2026	ViT	Latent masked modeling + CL	128–1024	10–80 m	Optical + SAR + maps	✓		PyTorch weights
Prithvi-EO-2.0	2026	ViT-L / ViT-H	MAE	1024/1280	–	Multispectral	✓		HF / TerraTorch
TESSERA v1	2026	Transformer + GRU	Barlow Twins	128	10 m	Optical + SAR	✓	✓	NumPy / GeoTessera
TESSERA v2	2026	Dual-branch Transformer	Barlow Twins + distillation	16–128	10 m	Optical + SAR	✓	✓	–

et al. 2024), GeoRSCLIP (Zhang et al. 2024), GRAFT (Mall et al. 2024), SkyScript (Wang et al. 2024b), Sat2Cap (Dhakal et al. 2024), and SoundingEarth (Heidler et al. 2023). RS-Embed provides a common interface for extracting embeddings with selected pretrained encoders (Ye et al. 2026).

Reusable features can be learned for dense prediction, few-shot adaptation, or correspondence between observations. Contrastive pretraining for dense land-cover mapping and few-shot learning with global multimodal embeddings address the first two uses (Tarasiou and Zafeiriou 2022; Allen et al. 2023). Part-level consistency and region-level image–text alignment instead examine where correspondence is established within an image (Jha et al. 2025; Zhang et al. 2025a); VLM2GeoVec studies multimodal embeddings for remote sensing (Aimar et al. 2025). Raster–vector representations and location-tied contrastive learning further connect image features with mapped semantics or co-located observations (Knoblauch et al. 2026; Hecht et al. 2026). The representation must therefore be evaluated at the level where it is reused, rather than only through its pretraining objective.

4.1.4 Location Embeddings

Coordinate-based location encoders map geographic coordinates directly to vectors, without requiring imagery at query time. Table 4 compares their spatial representations and training information alongside related regional methods. Years refer to formal publication where available, otherwise to the preprint or model release. One group of methods determines how position is represented geometrically. Space2Vec uses multiscale periodic functions in planar coordinates (Mai et al. 2020), whereas Sphere2Vec and spherical-harmonic encoders operate on the Earth's surface to reduce projection distortion and represent several spatial scales (Mai et al. 2023b; Rußwurm et al. 2024). Localized Slepian encodings concentrate basis functions within a region of interest (Rao et al. 2026a). Continuous or adaptive representations instead learn spatial structure from observations: SINR learns a coordinate field for global species mapping (Cole et al. 2023), while Tessellating the Earth (TTE) replaces a fixed basis with learnable spherical Voronoi partitions and shared semantic tokens trained with satellite imagery (Cher et al. 2026).

The semantic content of a coordinate vector is determined by its supervision. Coordinate–image alignment is used by CSP and SatCLIP (Mai et al. 2023a; Klemmer et al. 2025), as well as GeoCLIP and SatCLE (Vivanco Cepeda et al. 2023; Hao et al. 2025), to associate locations with visual or image-derived semantics. Esri's Global Location Encoder (Sentinel-2) (GLE) applies the SatCLIP approach to globally sampled Sentinel-2 Level-2A imagery and is distributed as a pretrained model for generating location embeddings in ArcGIS (Esri 2026). OSMGraphCLIP instead aligns coordinates with OpenStreetMap graph features (Michail

Table 4 Location encoders and related regional representation methods.

Method	Year	Dim.	Training modalities	Spatial representation
Space2Vec	2020	Variable	Coordinates, point-of-interest categories, geotagged images	Multiscale periodic coordinate encoding
Sphere2Vec	2023	Variable	Coordinates and class labels; images for joint prediction	Multiscale spherical coordinate encoding
CSP	2023	64–1,024	Coordinates, natural and satellite images	Location encoder aligned with image features
GeoCLIP	2023	512	Coordinates and geotagged photographs	Multiscale coordinate encoder
SINR	2023	256	Coordinates and species occurrence records	Continuous coordinate-to-feature mapping
SIRENNET(SH)	2024	Variable	Coordinates, geographic labels, climate variables	Spherical harmonics with a sinusoidal network
SatCLIP	2025	256	Coordinates and Sentinel-2 imagery	Spherical-harmonic location encoder
SatCLE	2025	256	Coordinates and satellite imagery	Continuous location embedding
RANGE	2025	1,280	Coordinates and satellite-image features from pretrained encoders	Location vector augmented by retrieved features; no additional encoder training
Hybrid Slepian	2026	Variable	Coordinates and geographic measurements; image features in joint prediction	Localized Slepian basis combined with spherical harmonics
TTE	2026	512	Coordinates and satellite imagery	Learned spherical partitions and semantic tokens
Esri GLE	2026	256	Coordinates and Sentinel-2 Level-2A imagery	SatCLIP-based coordinate encoder
OSMGraphCLIP	2026	256	Coordinates and OpenStreetMap graphs	Location encoder aligned with graph features
UniGeoCLIP	2026	768	Coordinates, aerial and street-level images, elevation, text	Coordinate encoder in a multimodal embedding space
GAIR	2026	768	Coordinates, overhead and street-level imagery	Location encoding and geo-aligned image features
S2Vec	2026	256	Built-environment attributes: buildings, roads, points of interest	Rasterized attributes within S2 cells
MoRA	2026	128	Mobility, points of interest, imagery, demographics	Spatial tokens and mobility-graph representations

et al. 2026). Related regional representations retain information through different inputs: S2Vec encodes built-environment attributes rasterized within S2 cells, while MoRA learns from a mobility graph together with imagery, points of interest, and demographic information (Choudhury et al. 2026; Wen et al. 2026). UniGeoCLIP jointly aligns coordinates, aerial and street-level imagery, elevation, and text, while GAIR learns coordinate-level representations aligned with overhead and street-level imagery (Astruc et al. 2026; Liu et al. 2026c). The resulting proximity may therefore reflect physical distance, visual similarity, environmental conditions, or human activity.

Location encoders can also incorporate task-specific context rather than act as fixed geographic priors. RANGE augments coordinate embeddings with retrieved visual features (Dhakal et al. 2025), whereas proxy consistency loss (PCL) incorporates widely available geospatial proxy variables into a trainable location encoder for sparsely labeled prediction tasks (Wang et al. 2026b). A task-adapted location representation is not interchangeable with a frozen general-purpose encoder. TorchSpatial and LocBench compare 15 location encoders across classification and regression tasks and examine geographic bias (Wu et al. 2024). Unlike released raster layers, coordinate encoders can return a compact vector for an arbitrary coordinate, but its content depends on the training observations, spatial basis, and downstream adaptation protocol.

Reusable encoders address different aspects of reuse, including temporal prediction in EarthPT, cross-modal pixel representations in DUNIA, and image–text retrieval in RemoteCLIP (Smith et al. 2023; Fayad et al. 2025; Liu et al. 2024). Fixed-vector benchmarks and pooling studies examine how these representations support downstream prediction (Vinge et al. 2026; Corley et al. 2026a). Other comparisons investigate spatial semantics and the complementary information provided by different embeddings (Dalei et al. 2025; van der Plas et al. 2026).

4.2 Product Design Trade-offs

A design choice changes both the information available for inference and the cost of retaining it. Finer spatial support increases the number of vectors; temporal aggregation and fusion change what each vector describes; compression limits how that content is stored. These choices concern different forms of information loss. A shorter vector may preserve the attributes needed for a target, while an equally compact temporal average may remove the event of interest. Representation quality therefore depends on the properties recoverable after these design choices.

4.2.1 Embedding Space Properties

Embedding geometry and dimensionality affect similarity calculations, storage, and interpretation (Rolf et al. 2025). For released embeddings, the main questions are whether vectors are constrained to a particular space, how training controls information retention, and how nominal dimension relates to the variation present in the vectors.

Many released encoders produce vectors in $\mathbb{R}^d$ without an explicit norm constraint. Examples include Clay (Clay Foundation 2024), Prithvi-EO-2.0 (Szwarcman et al. 2026), SatMAE (Cong et al. 2022), TESSERA (Feng et al. 2026a), and the DINOv2-derived embeddings distributed by Major TOM (Czerkawski et al. 2024). Cosine similarity is commonly used to compare such vectors $\mathbf{u}$ and $\mathbf{v}$:

$$\mathrm{sim}(\mathbf{u}, \mathbf{v}) = \frac{\mathbf{u} \cdot \mathbf{v}}{\|\mathbf{u}\| \, \|\mathbf{v}\|}. \tag{6}$$

An unconstrained output can occupy a lower-dimensional subspace of the available coordinates, a behavior described as *dimensional collapse* (Jing et al. 2022). Cosine similarity also removes vector norm at evaluation time even when norm was unconstrained during training. Uniformity on the hypersphere has been associated with downstream performance in general representation learning (Wang and Isola 2020), although the relationship has not been established across Earth embedding products. AlphaEarth Foundations (Brown et al. 2025) explicitly places its output on the unit hypersphere $\mathbb{S}^{d-1}$ through a von Mises–Fisher (vMF) variational bottleneck. For $\mathbf{z} \in \mathbb{S}^{d-1}$, the distribution is parameterized by a mean direction $\boldsymbol{\mu} \in \mathbb{S}^{d-1}$ and concentration $\kappa \geq 0$:

$$p(\mathbf{z} \mid \boldsymbol{\mu}, \kappa) = C_d(\kappa) \, \exp\!\big(\kappa \, \boldsymbol{\mu}^\top \mathbf{z}\big), \tag{7}$$

where $C_d(\kappa)$ is a normalization constant. AlphaEarth combines this distribution with a batch-uniformity penalty that discourages concentration in a limited region of $\mathbb{S}^{63}$ (Brown et al. 2025). Unlike the embeddings above, AlphaEarth uses spherical geometry; its effect requires evaluation with the same data and tasks.

Cross-modal encoders introduce a second geometric issue. Separate encoders can occupy different regions of a nominally shared space, a phenomenon termed the *modality gap* (Liang et al. 2022). GeoCLIP (Vivanco Cepeda et al. 2023) aligns images and coordinates, whereas RemoteCLIP (Liu et al. 2024) aligns remote sensing imagery and text. Work on natural images links the gap to zero-shot performance and fairness differences (Liang et al. 2022), but few geospatial studies have measured it. Recent analyses use sparse concept decompositions and neuroscience-inspired probes to examine the information carried by location and Earth observation embeddings (Betti et al. 2026; van der Plas et al. 2025). Within- and cross-modal neighborhood analyses can complement downstream accuracy when these spaces are evaluated.

The information bottleneck provides a conceptual description of how an encoder can discard input variation while retaining information about a target. Let X denote the input, Z the embedding, and Y a downstream target. For a stochastic encoder $p(\mathbf{z} \mid \mathbf{x})$, the objective is

$$\min_{p(\mathbf{z}|\mathbf{x})} \; I(Z;\, X) - \beta \, I(Z;\, Y), \tag{8}$$

where $\beta > 0$ controls the balance between compression and target relevance. In self-supervised pretraining, the set of future targets Y is unknown, so this equation offers an interpretation rather than a directly optimized objective for most Earth embedding models. AlphaEarth fixes the vMF concentration at $\kappa = 8 \times 10^3$ (Brown et al. 2025); this controls distributional concentration but does not by itself provide a measured bound on $I(Z; X)$. TESSERA (Feng et al. 2026a) reduces cross-dimensional correlation with Barlow Twins (Zbontar et al. 2021), whereas masked-autoencoder models such as Clay (Clay Foundation 2024) rely primarily on architecture and output dimension to limit the code. Their relationship to mutual information has not been compared with matched EO data, architectures, and evaluation protocols (Zhu et al. 2026; Yang et al. 2025).

Reported full output dimensions range from 64 for AlphaEarth (Brown et al. 2025) to 8,192 for MOSAIKS (Rolf et al. 2021), while TESSERA v2 (Feng et al. 2026c) supports prefixes as short as 16 dimensions; Section 4 compares the associated storage costs. Nominal dimension does not reveal how many directions contain substantial variation. Participation ratio and effective rank summarize the spectrum of the embedding covariance matrix, whereas manifold estimators characterize nonlinear degrees of freedom. Rao et al. (2026b) estimate a manifold dimension of 2–10 for the geographic implicit neural representations studied in GeoINRID. That result applies to coordinate-based representations under the paper's data and estimator choices and should not be generalized to satellite embedding products. Effective dimension, compression loss, and downstream accuracy must be measured for each representation; principal component analysis (PCA) (Jolliffe and Cadima 2016) and product quantization (Jégou et al. 2011) provide possible reductions, but the attainable savings depend on the target and evaluation protocol. Product documentation should

therefore report the nominal dimension, numeric precision, normalization, recommended distance measure, and any empirical estimate of effective dimension.

4.2.2 Dimensionality and Compression

Embedding dimensionality affects storage and the degrees of freedom available to encode variation. MOSAIKS (Rolf et al. 2021) uses 8,192 random convolutional features, and Clay (Clay Foundation 2024) uses a 1,024-dimensional vector learned through masked autoencoding (He et al. 2022). Smaller vectors impose different constraints. AlphaEarth Foundations (Brown et al. 2025) maps observations to a 64-dimensional unit hypersphere, and the released Google Satellite Embedding dataset stores the resulting 64-dimensional vectors. TESSERA v1 (Feng et al. 2026a) uses Barlow Twins (Zbontar et al. 2021) to limit cross-dimensional redundancy in a 128-dimensional vector. TESSERA v2 (Feng et al. 2026c) orders a 128-dimensional student representation so that 64-, 32-, and 16-dimensional prefixes can be used directly; the 16-dimensional prefix retains approximately 92% of the reported full-vector aggregate performance with one eighth of the storage. The released ESD tiles provide 13 values per pixel-year (Chen et al. 2026). These dimensions are therefore not interchangeable measures of information content, and each must be evaluated on the intended downstream tasks.

Numeric precision provides a separate compression mechanism. Google Satellite Embedding stores 64 signed 8-bit values, or 64 bytes per vector, in Cloud-Optimized GeoTIFFs (Google Earth Engine 2026a; Brown et al. 2025). TESSERA v1 (Feng et al. 2026a) stores 128 signed 8-bit values and provides access through GeoTessera (Cambridge Centre for Earth Observation 2026). For a fixed dimension, either representation occupies one quarter of the value storage required by 32-bit floating point. Dimension and numeric precision should therefore be reported together.

Compression ratios depend on the reference data and the spatial and temporal support of one output. The 64-byte annual vectors in Google Satellite Embedding (Google Earth Engine 2026a; Brown et al. 2025) and the 128-byte annual vectors in TESSERA v1 (Feng et al. 2026a) summarize different input archives, so neither implies a unique reduction relative to raw observations. TESSERA v2 changes vector storage through its 16–128-dimensional prefixes (Feng et al. 2026c), whereas Clay's 1,024-dimensional 32-bit class token represents a 256×256-pixel scene (Clay Foundation 2024). ESD reports approximately $340\times$ compression specifically against its global daily Landsat–MODIS archive; the released annual product provides 13 values per pixel and occupies about 2.4 TB per year (Chen et al. 2026). NeuCo-Bench instead evaluates representation size jointly with downstream utility (Vinge et al. 2026), while model slimmability studies reduce encoder computation rather than the storage of a released embedding (Hackel et al. 2026). Compression claims are comparable only when the input baseline, output support, precision, and task protocol are stated.

Compression can also be learned explicitly for reuse across tasks, rather than imposed through a fixed output width (Gomes and Brunschwiler 2024). Application studies examine dimension selection for vegetation chemistry and feature selection for national biomass mapping (Alam and Simic Milas 2025; Watt et al. 2026), while embedding-only transmission for onboard retrieval introduces a communication constraint (Sim 2026). These are distinct questions: reducing stored values, selecting predictive features, and reducing transmitted information need not favor the same representation.

4.2.3 Temporal Representation

Temporal design determines whether a vector describes one acquisition, summarizes an interval, or preserves an ordered sequence. Tile2Vec (Jean et al. 2019), MOSAIKS (Rolf et al. 2021), and the DINOv2 (Oquab et al. 2024) features distributed by Major TOM (Czerkawski et al. 2024) encode individual images. SeCo uses observations from different seasons during pretraining, but its released image encoder still produces one vector from one image (Mañas et al. 2021); temporal supervision during training is therefore distinct from multi-date encoding at inference. Models that combine observations explicitly include AlphaEarth's time-conditioned annual summaries (Brown et al. 2025), SatMAE's temporal positional encoding (Cong et al. 2022), and Prithvi's three-dimensional patch embeddings (Szwarcman et al. 2026). TESSERA v1 samples annual optical and radar observations (Feng et al. 2026a), while TESSERA v2 uses day-of-year encoding, attention pooling, and adaptive use of valid observations at inference (Feng et al. 2026c). ESD preserves within-year temporal information for every annual record from 2000 onward (Chen et al. 2026). The appropriate design depends on whether the target follows phenology or rapid change (Lisaius et al. 2026; Ma et al. 2026), or is sufficiently stable to be represented by a single-date or annual summary.

Season-aware and time-series pretraining explicitly address temporal structure, as in SeaMo and TiMo (Li et al. 2026c; Qin et al. 2025). Irregular or unaligned acquisitions introduce a further problem beyond adding temporal position codes (Dumeur et al. 2025). Application-level comparisons of annual embeddings

with seasonal observations and tests of cross-year land-cover transfer assess whether the learned temporal information remains useful after encoding (Díaz-Ireland et al. 2026; Gbodjo and Ienco 2026). These tests distinguish representing a state from representing its evolution. Similar annual conditions can result from different sequences, and a brief event can be important despite contributing little to an interval summary. Temporal consistency is useful for persistent attributes, but excessive invariance would be undesirable for event detection. Which distinctions survive must be tested against dated observations, rather than inferred from the number of input acquisitions.

4.2.4 Multimodal Integration

Multimodal models differ in which sources they accept and where those sources interact. AlphaEarth is trained with optical, radar, LiDAR, environmental, topographic, and text observations; source-specific encoders feed a common spatiotemporal representation (Brown et al. 2025). TESSERA v1 processes Sentinel-1 and Sentinel-2 time series in separate Transformer–GRU branches before concatenation and multilayer-perceptron fusion (Feng et al. 2026a). TESSERA v2 replaces this stage with modality-specific temporal Transformers followed by a fusion Transformer (Feng et al. 2026c). Clay supports several image modalities but processes an input according to its modality and conditions the encoder on location and time metadata (Clay Foundation 2024); support for several modalities does not necessarily mean that they are fused in one vector. Fusion can encode complementary measurements, but it also introduces requirements for co-registration, temporal alignment, and missing-source handling.

Fusion can seek agreement between sources or preserve information that one source contributes uniquely. DeCUR separates shared and modality-specific content (Wang et al. 2025a), while OlmoEarth uses modality-aware masking to learn from partial observations (Herzog et al. 2026). These address different requirements: preserving complementarity and making useful predictions when some measurements are unavailable. Neither requirement is captured by counting input modalities. Comparing complete and missing-source conditions can reveal dependence on a particular sensor; comparing aligned and displaced acquisition periods can test whether a model relies on temporal correspondence. The useful degree of alignment depends on the analysis, since removing all source-specific variation could also remove the reason for including that source.

The stage at which information is combined determines which choices remain adjustable. Joint sensor embeddings have been investigated for lake-ice monitoring (Tom et al. 2022), and combining released AlphaEarth vectors with Sentinel-2 imagery has been studied for urban-water mapping (Yang et al. 2026a). RGB–infrared vision–language data and cross-modal predictive learning investigate correspondence during pretraining instead (Han et al. 2026; Hossain et al. 2026a,b). Fusion during encoding can learn interactions across observations; combination after release lets users introduce new information for a target without regenerating the original vectors. The latter can compensate for missing content only if the additional input contains it. Comparing the combined and individual inputs with the same predictor is more informative about complementarity than comparing their vector similarity alone.

4.2.5 Spatial Support and Release Form

Spatial support determines both the smallest resolvable target and the number of vectors that must be distributed. SatCLIP (Klemmer et al. 2025) and GeoCLIP (Vivanco Cepeda et al. 2023) return a vector for a coordinate without requiring a corresponding satellite image. MOSAIKS (Rolf et al. 2021), Clay (Clay Foundation 2024), and Major TOM Embeddings (Czerkawski et al. 2024) operate at scene or tile level. Google Satellite Embedding (Brown et al. 2025) and TESSERA v1 (Feng et al. 2026a) release pixel-wise embeddings at 10 m resolution; TESSERA v2 is evaluated at the same spatial support (Feng et al. 2026c), and ESD (Chen et al. 2026) operates at 30 m. A simple land-area calculation gives approximately 1.5×10^{12} cells for a global land grid at 10 m resolution. At 64 bytes per cell, this is about 96 TB before masking, tiling, compression, metadata, and projection overhead. Scene-level products require fewer vectors but cannot resolve variation within an input footprint. Parcel, administrative, and plot targets require aggregation chosen for their within-unit variation (Corley et al. 2026a).

The release format determines who performs the encoding. Precomputed layers from Google Satellite Embedding (Brown et al. 2025), TESSERA v1 (Feng et al. 2026a), and ESD (Chen et al. 2026) remove user-side global inference. Clay v1.5 releases weights for encoding new inputs when its preprocessing is reproduced (Clay Foundation 2024), while LGND distributes a separate vector collection generated with that encoder (LGND.ai 2026). Copernicus-FM similarly provides a model, whereas Copernicus-Embed-025deg provides 768-dimensional vectors on a global 0.25° grid (Wang et al. 2025b). Model weights permit new inputs and preprocessing choices but retain inference costs; released vectors are immediately usable but inherit the producer's input archive, masking, compositing, temporal definition, and encoder version. Additional dates and modalities offer more information to learn from, but their inclusion does not establish how much survives

encoding. Product choice should follow target scale, temporal sensitivity, source availability, and acceptable compression loss. An annual collection can be convenient for recurring estimates, whereas an event-centered question may require a different observation interval. Access to weights permits re-encoding that interval; access only to existing vectors leaves the user dependent on the released description. The trade-off is between immediate reuse and the ability to revise what is represented.

4.3 Distribution Infrastructure

Access determines whether an analysis can use existing vectors, recover the corresponding observations, or generate embeddings for new inputs. Hosting platforms provide collections; spatial indexes connect vectors to footprints and imagery; product-specific software handles queries and decoding; model libraries support extraction and comparison. Table 5 distinguishes these functions. Their research value extends beyond download convenience: traceable links between vectors, observations, and encoder versions allow a result to be reproduced or an inadequate representation to be reconsidered. Common interfaces make comparisons easier, while source descriptions are still needed to decide whether the quantities being compared are equivalent.

Google Satellite Embedding can be analyzed server-side in Google Earth Engine or accessed as Cloud-Optimized GeoTIFF files in Google Cloud Storage (Google Earth Engine 2026b,a; Brown et al. 2025). The Copernicus Data Space Ecosystem publishes the Global Embeddings Dataset as GeoParquet files through EODATA S3 (Copernicus Data Space Ecosystem 2026). Hugging Face hosts Major TOM Core and embedding datasets (Czerkawski et al. 2024), while Source Cooperative provides catalog and object-storage access to LGND Clay Embeddings and Earth Index (Source Cooperative 2026; LGND.ai 2026; Earth Genome 2025).

Locating the appropriate vectors requires spatial organization and product-specific decoding as well as storage. Major TOM defines a geographic grid and metadata conventions for compatible observations and embeddings (Francis and Czerkawski 2024). Geo-Embeddings provides publication guidance and draft STAC and Zarr conventions for gridded and irregular collections (Geo-Embeddings 2026). In contrast, GeoTessera implements access specifically for TESSERA, including tile indexing, quantized arrays and scale factors, regional and point queries, and GeoTIFF export (Cambridge Centre for Earth Observation 2026; Feng et al. 2026a). These tools address different requirements: organizing compatible data does not automatically provide decoding or query support for every product.

Cross-product and cross-model libraries reduce repeated preparation, but differ in whether they retrieve vectors or generate them. TorchGeo provides dataset classes, spatial queries, and sampling for multiple embedding collections (Stewart et al. 2022; TorchGeo 2026). TerraTorch, maintained within the TorchGeo organization, builds on TorchGeo and PyTorch Lightning to load, adapt, and extract features from EO models rather than host global vectors (Gomes et al. 2025a). RS-Embed supports selected precomputed products and on-demand encoders through a common spatial and temporal query (Ye et al. 2026). GeoAI combines download and decoding of Google Satellite Embedding with access to supported foundation models through TerraTorch (Wu 2026). AiTLAS supplies model adapters and task execution, not a global embedding collection (Dimitrovski et al. 2023; Bias Variance Labs 2026). A common interface can simplify comparisons, while input preparation and representation support still need to match the analysis.

TorchSpatial implements 15 location encoders and LocBench in the same codebase (Wu et al. 2024). SRAI combines vector-data acquisition, regionalization, and regional embedding methods for sources such as OpenStreetMap and Overture Maps (Gramacki et al. 2023). The LGND API exposes hosted Clay embedding collections, similarity search, and creation of new embedding collections from user-supplied imagery (LGND AI 2026; Clay Foundation 2024). Catalog discovery, version tracking, spatial and temporal query, provenance, and cross-product composition remain divided among these interfaces.

4.4 Evaluation Benchmarks

Evaluation should explain what information is accessible, how readily it can be used, and under which conditions it remains useful. Intrinsic analyses inspect the representation through neighborhoods, clustering, attribute probes, or correspondence between sources. Extrinsic evaluation measures its use for a specified prediction or retrieval task. These categories describe the question rather than a fixed list of metrics: retrieval can probe cross-modal alignment or be the intended application itself. Spatial and temporal smoothness likewise need a reference interpretation, since a useful representation may preserve abrupt boundaries and disturbances rather than suppress them.

A benchmark that adapts an entire encoder tests a different capability from one that fits a predictor to fixed vectors. A simple probe examines information accessible with limited adaptation, whereas a more flexible predictor also tests how that information can be reorganized for the target. Comparing label budgets then asks whether prior learning reduces the measurements needed for a useful result (Fibaek et al. 2024; Marsocci et al.

Table 5 Infrastructure for publishing, accessing, and generating Earth embeddings.

Infrastructure	Type	Primary function	Access / format	Representative resources	Link
Google Earth Engine and Cloud Storage	Cloud analysis and storage	Server-side analysis and direct access to annual embedding files	Earth Engine API; GCS / COG	Google Satellite Embedding	
Copernicus Data Space Ecosystem	Data hosting	Hosting and direct distribution of embedding collections	EODATA S3 / GeoParquet	Global Embeddings Dataset	
Hugging Face Hub	Dataset repository	Versioned hosting and bulk distribution of EO datasets	Hub API / Parquet	Major TOM Core and embedding datasets	
Source Cooperative	Data publishing	Catalog and object access for public geospatial collections	HTTPS / S3; resource-specific formats	LGND Clay Embeddings; Earth Index	
LGND API	Hosted embedding service	Access, similarity search, and generation of embeddings from user imagery	REST API; bearer token; GeoParquet export	LGND Clay Embeddings and user-defined Clay collections	
Major TOM	Data specification and tools	Shared geographic grid and metadata for compatible EO datasets	Python tools; grid and metadata schema	Major TOM Core and derived embedding collections	
Geo-Embeddings	Conventions and registry	Guidance for storing, documenting, and publishing geospatial embeddings	Web documentation; draft STAC / Zarr conventions	Best practices, metadata templates, and implementation registry	
GeoTessera	Product client	Tile indexing, spatial query, dequantization, and export	Python / CLI; S3 / Zarr	TESSERA embeddings	
TorchGeo TerraTorch	Data and model toolkit	Geospatial data loading and sampling; foundation-model inference, embedding extraction, and adaptation	Python / PyPI; dataset API / CLI / YAML	Clay, Major TOM, Earth Index, TESSERA, Google Satellite Embedding, ESD, and EO foundation-model backbones	
RS-Embed	Embedding interface	Retrieval of precomputed vectors and on-demand encoder inference	Python / PyPI; Earth Engine / local inference	TESSERA, Google Satellite Embedding, Copernicus-Embed, and encoder adapters	
GeoAI	Embedding and model toolkit	Download, analysis, and export of embeddings; discovery and loading of EO foundation models	Python / PyPI; COG / GeoTIFF; TerraTorch	Google Satellite Embedding and registered EO foundation models	
TorchSpatial	Location-embedding library	Implementation and evaluation of coordinate encoders	Python / source; PyTorch	Fifteen location encoders and LocBench	
SRAI	Regional-embedding framework	Data acquisition, regionalization, and embedding of vector geospatial data	Python / PyPI; OSM / Overture / H3	Count-based, contextual, and neural regional embeddings	
AiTLAS	Model integration toolkit	Model adapters, configuration, and task pipelines	Python / PyPI	AnySat, Copernicus-FM, CROMA, Galileo, Panopticon, Presto, and TerraMind	

2026). Neither high probe accuracy nor a well-separated visualization establishes usefulness across regions or dates. Table 6 uses Cls, Seg, Reg, CD, OD, and IS for classification, semantic segmentation, regression, change detection, object detection, and instance segmentation, respectively; SDG denotes Sustainable Development Goal. The final "Sat. emb." column marks benchmarks designed specifically for fixed or precomputed satellite embeddings.

4.4.1 Task-Based Benchmarks

Task coverage defines which kinds of retained information a benchmark can assess. GEO-Bench (Lacoste et al. 2023) contains 6 classification and 6 semantic segmentation tasks with 20 baseline configurations; Prithvi-EO 2.0 reports an 8% improvement over its predecessor under this protocol (Szwarcman et al. 2026). This comparison addresses class and spatial discrimination, not regression or change detection. FoMo-Bench adds 15 multimodal forest monitoring datasets for classification, segmentation, and object detection (Bountos et al. 2025), broadening sensor and target coverage within a particular application domain.

Broader task coverage reveals that the value of pretraining depends on the information required and the adaptation allowed. PANGAEA evaluates 9 selected model entries, with SSL4EO-S12 represented by 4 variants, on 11 datasets for segmentation, change detection, and regression (Marsocci et al. 2026). Its comparisons with U-Net (Ronneberger et al. 2015) and a standard Vision Transformer (Dosovitskiy et al. 2021) show that supervised models remain competitive when labels are plentiful. GEO-Bench-2 covers 19

Table 6 Community benchmarks for geospatial foundation models and Earth observation embeddings.

Benchmark	Year	Venue	Scope	Sat. emb.
GEO-Bench	2023	NeurIPS	12 tasks: 6 Cls, 6 Seg	
PhilEO Bench	2024	IGARSS	Global Sentinel-2 data; Cls, Seg, Reg	
TorchSpatial / LocBench	2024	NeurIPS	17 data sets: 7 Cls, 10 Reg	
FoMo-Bench	2025	AAAI	15 data sets; Cls, Seg, OD	
PANGAEA	2026	GRSM	11 data sets; Seg, CD, Reg	
Copernicus-Bench	2025	ICCV	15 tasks using Sentinel-1, -2, -3, and -5P	
SustainFM	2025	arXiv	16 tasks corresponding to SDGs 1–16	
GEO-Bench-2	2026	TMLR	19 data sets; Cls, Seg, Reg, OD, IS	
Landsat-Bench	2025	ICMLW	3 Landsat benchmarks; Cls	
REOBench	2025	NeurIPS	6 tasks; 12 corruption types	
NeuCo-Bench	2026	CVPRW	5 data groups, 8 EO tasks; Cls, Reg	✓

datasets and 5 task types, with normalized scores within capability groups (Simumba et al. 2026). Through TerraTorch (Gomes et al. 2025a), it applies a common hyperparameter-search and repeated-seed protocol to 14 configurations. These include reconstruction-based models such as Clay and Prithvi (Clay Foundation 2024; Szwarcman et al. 2026), multisource models such as TerraMind, DOFA, and DeCUR (Jakubik et al. 2025; Xiong et al. 2024; Wang et al. 2025a), and features from SatlasPretrain and DINOv3 (Bastani et al. 2023; Siméoni et al. 2025). Natural-image ConvNeXt models remain competitive for high-resolution RGB imagery and object detection (Liu et al. 2022), while EO pretraining helps some multispectral and temporal tasks. Landsat-Bench isolates a narrower setting through 3 Landsat classification benchmarks with nearest-neighbor classification and linear probing (Corley et al. 2026b). These results support comparisons within a defined task and adaptation setting, rather than a ranking detached from the information each target requires.

Other protocols isolate sensor dependence, label requirements, efficiency, or robustness. Copernicus-Bench spans 15 tasks using Sentinel-1, Sentinel-2, Sentinel-3, and Sentinel-5P, organized into preprocessing, base applications, and specialized applications (Wang et al. 2025b). PhilEO Bench instead holds decoders and label budgets fixed on a 400 GB Sentinel-2 dataset for land-cover classification, road segmentation, and building-density regression (Fibaek et al. 2024). SustainFM extends comparison to transferability, operational impact, and energy efficiency through 16 tasks corresponding to Sustainable Development Goals 1–16 (Ghamisi et al. 2025); REOBench tests robustness across 6 tasks and 12 appearance-based or geometric corruptions (Li et al. 2025). These dimensions of evaluation are complementary: high average accuracy does not resolve sensitivity to missing labels, different sensors, or perturbed observations.

4.4.2 Evaluation of Fixed Embeddings

A benchmark for fixed embeddings evaluates precomputed satellite vectors rather than adapting the complete encoder. Using frozen features alone does not meet this definition. Landsat-Bench compares encoder outputs, and TorchSpatial / LocBench (Wu et al. 2024) evaluates 15 coordinate encoders on seven geo-aware image classification and ten image regression datasets. LocBench also introduces a Geo-Bias Score, but its inputs are locations rather than satellite embedding products.

Existing embedding benchmarks test compression, hidden tasks, and model selection. NeuCo-Bench (Vinge et al. 2026) organizes five data groups spanning eight EO tasks and evaluates fixed-size representations with one evaluation pipeline, hidden test labels, and a score that combines predictive quality with stability. Its hidden-task evaluation also addresses a central requirement of reuse: features should remain useful for questions not selected during their development. A subsequent study using NeuCo-Bench reports fixed representations more than 500× smaller than raw images and examines how pooling, normalization, and compression affect downstream performance (Gilch et al. 2026). Such comparisons quantify the predictive utility retained after compression.

Embed2Scale and the TESSERA v2 scaling study examine representation size in different ways. The Embed2Scale Challenge (Embed2Scale 2025) represents each image by a single 1,024-dimensional vector, reducing the number of scalar values by more than 7,000× relative to the source imagery; winning solutions fused features from several pretrained models (Kerekes et al. 2025; Xu et al. 2025). The TESSERA v2 study reports 395 training runs across 15 downstream tasks and finds that converged pretraining loss has a correlation below 0.2 in magnitude with aggregate downstream performance, while encoder capacity changes with training-data scale and projection-network size remains approximately fixed (Feng et al. 2026c). Downstream scores were more informative than pretraining loss within this model family; whether the result extends to other architectures, sensors, and objectives remains unknown.

4.4.3 Benchmark Results and Remaining Gaps

Benchmark results depend on the target and evaluation protocol. Temporal and multisensor representations such as AlphaEarth (Brown et al. 2025) and the TESSERA series (Feng et al. 2026a,c) encode seasonal variation and complementary sensor information for use across downstream tasks. Dimension counts are comparable only with matched spatial support, inputs, and adaptation protocols. PANGAEA (Marsocci et al. 2026) evaluates models with 10%, 50%, and 100% of the labeled training data and finds that supervised baselines remain competitive on several tasks, with the relative benefit of pretraining depending on the task and label budget. Benchmark reports should therefore state the adaptation method, amount of labeled training data, input data, and target.

Geographic and temporal transfer remain weakly measured. PANGAEA, SustainFM, and GEO-Bench-2 include more regions (Marsocci et al. 2026; Ghamisi et al. 2025; Simumba et al. 2026), but regional and environmental coverage remains uneven. A 2026 agricultural benchmark (Shang et al. 2026) evaluates Prithvi (Szwarcman et al. 2026), SpectralGPT (Hong et al. 2024), and SatMAE (Cong et al. 2022) on multitemporal crop segmentation and change detection across four U.S. states; region-separated splits report lower performance under geographic transfer. The result supports region-separated evaluation. Annual products also require tests across years and in regions undergoing rapid land-cover change. Cross-model scores are further confounded by differences in source imagery and preprocessing. Major TOM (Francis and Czerkawski 2024; Czerkawski et al. 2024) applies several encoders to the same tiles, while Earth Embeddings as Products (Fang et al. 2026) provides standardized TorchGeo loaders (Stewart et al. 2022). Geographic and temporal transfer should also be tested with identical source inputs.

Aggregate benchmark scores often rely on thousands of labeled pixels or patches, whereas many field studies have far fewer observations (Marsocci et al. 2026). Reporting performance across several labeled training-set sizes would characterize applications with limited labels more directly. Task composition introduces a second mismatch. Classification and segmentation dominate, while regression of biomass, canopy height, and yield, multi-year change detection, retrieval, and out-of-distribution generalization remain less common. Class separation does not guarantee preservation of continuous target variation. Year-to-year distances likewise require comparison with independent change records to distinguish environmental change from sensor or preprocessing effects. GEO-Bench-2 includes regression (Simumba et al. 2026), and Embed2Scale evaluates compression (Embed2Scale 2025); connecting these tests with temporal transfer and retrieval would clarify which properties remain useful beyond a familiar task.

Information gained and conditions of reuse. A useful comparison asks what an embedding adds to the information already available. Coordinates, raw observations, and expert-selected variables answer different baseline questions. Tests of the embedding alone and in combination with those inputs can distinguish substitution from complementarity. The pretraining sources also matter: recovering a variable related to a training target and predicting a previously unseen property test different forms of reuse. This does not make either task invalid, but it changes the interpretation of the result. Product comparisons should describe the information available to each model; controlled comparisons of learning methods should additionally hold source data and prediction conditions fixed. Access to a common benchmark is not by itself a guarantee that the evaluated representations began with equivalent information.

Reliability and resource requirements. Robustness tests should vary the conditions that can change the information available, including missing modalities, observation noise, acquisition timing, and spatial support. Image-corruption and distribution-shift evaluations provide examples (Li et al. 2025; Doerksen and Kerner 2026); their conclusions should be paired with uncertainty calibration and errors across target ranges or relevant populations. Resource comparisons should similarly separate representation size, extraction cost, access, and prediction cost. A precomputed product and a locally adapted encoder distribute those costs differently. Evaluation should identify representations suited to the available observations, labels, reliability requirements, and resources.

5 Experiments

The experiments examine complementary aspects of reuse: whether embeddings organize the same observations similarly, how effectively prediction models use them for selected targets, and how predictive performance changes after compression. Uniform Manifold Approximation and Projection (UMAP) (McInnes et al. 2018), linear centered kernel alignment (CKA) (Kornblith et al. 2019), and cosine-neighborhood overlap describe feature-space organization at geographically distributed samples. Classification and regression then evaluate target-related information under the specified prediction protocol. Finally, the dimension analysis varies PCA dimension after patch flattening, not the encoder's native output dimension. These comparisons relate

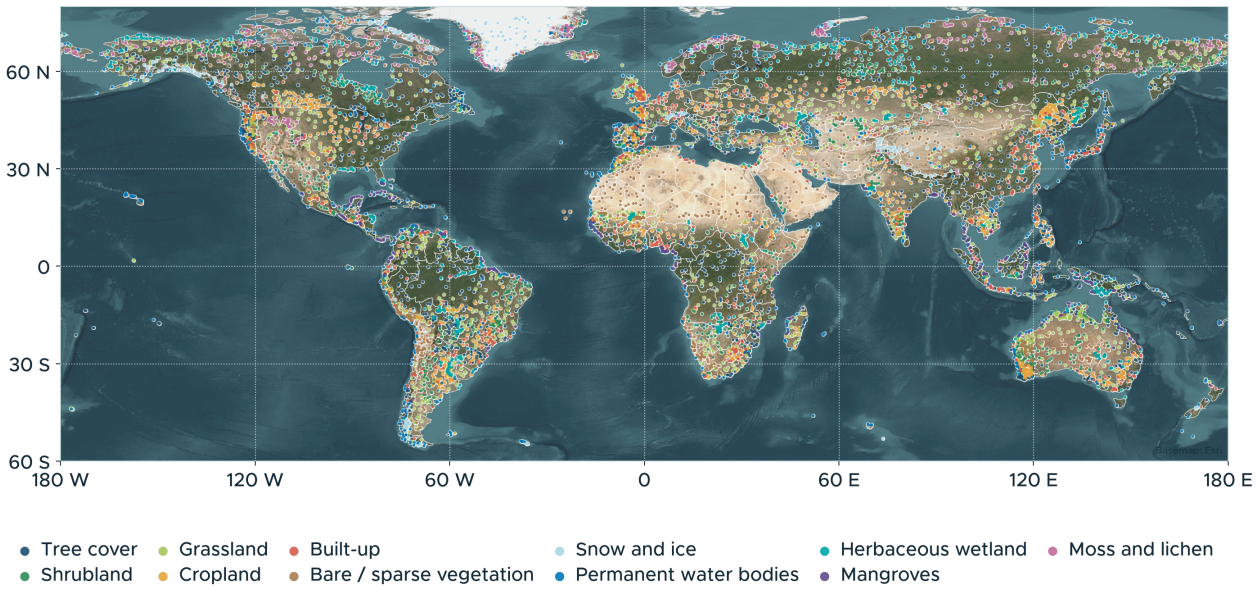


Fig. 7 Global distribution and WorldCover classes of the evaluation samples.

geometry to predictive use and storage choices for the evaluated land-surface inputs; they do not substitute for separate tests of temporal or regional transfer.

5.1 Data

Fig. 7 shows the 9,132 candidate locations distributed across terrestrial land areas. Each location defines a 640 m × 640 m patch and is associated with one of the 11 ESA WorldCover 2021 v200 reference classes (Zanaga et al. 2022); these labels color the sample map and UMAP projections, while WorldCover also provides one of the downstream classification targets.

The inputs comprise reflectance from 3 observation sources and 7 learned embeddings. The observation sources are Sentinel-2 (Drusch et al. 2012), Landsat, and MODIS. The learned inputs are ESD (Chen et al. 2026), Google Satellite Embedding (GSE) (Brown et al. 2025), AgriFM (Li et al. 2026b), Copernicus-FM (Wang et al. 2025b), TESSERA (Feng et al. 2026a), TerraMind (Jakubik et al. 2025), and WildSAT (Daroya et al. 2025). Representation-space and predictive comparisons use all 10 inputs, and the UMAP projection also includes their concatenation.

The classification targets are the Esri annual land-use and land-cover product at 10 m resolution (Esri 2022), FROM-GLC10 2017 (Gong et al. 2019), and ESA WorldCover 2021 v200 (Zanaga et al. 2022). The continuous targets are elevation from Copernicus GLO-30 (and 2022), above-ground biomass from the ESA Climate Change Initiative (Santoro and Cartus 2023), and Meta global canopy height (Tolan et al. 2024). These datasets cover discrete surface types and continuous variables with different units, spatial patterns, and class or value distributions.

5.2 Internal Representation Analysis

The internal comparison does not use a downstream target. UMAP provides a qualitative view of local organization, while linear CKA and neighborhood overlap measure global geometric similarity and local retrieval consistency. All inputs undergo the same preprocessing before comparison.

5.2.1 Low-Dimensional Structure

Let $X^{(s)} \in \mathbb{R}^{n \times d_s}$ denote the processed matrix for input s, where rows correspond to the same locations and d_s may differ across inputs. Spatial features were mean pooled, ℓ_2 normalized, winsorized at the 1$^{\text{st}}$ and 99$^{\text{th}}$ percentiles, and scaled by the median and interquartile range. Land-cover labels color the projected points but do not enter the UMAP fit, CKA, or neighborhood-overlap calculations.

In Fig. 8, the aligned locations have different local arrangements across sources. The three reflectance inputs form broad, continuous manifolds, although their shapes are not identical, and ESD (Chen et al. 2026) has a similarly diffuse organization. GSE (Brown et al. 2025), Copernicus-FM (Wang et al. 2025b), and TESSERA (Feng et al. 2026a) divide the samples into more fragmented local components, whereas

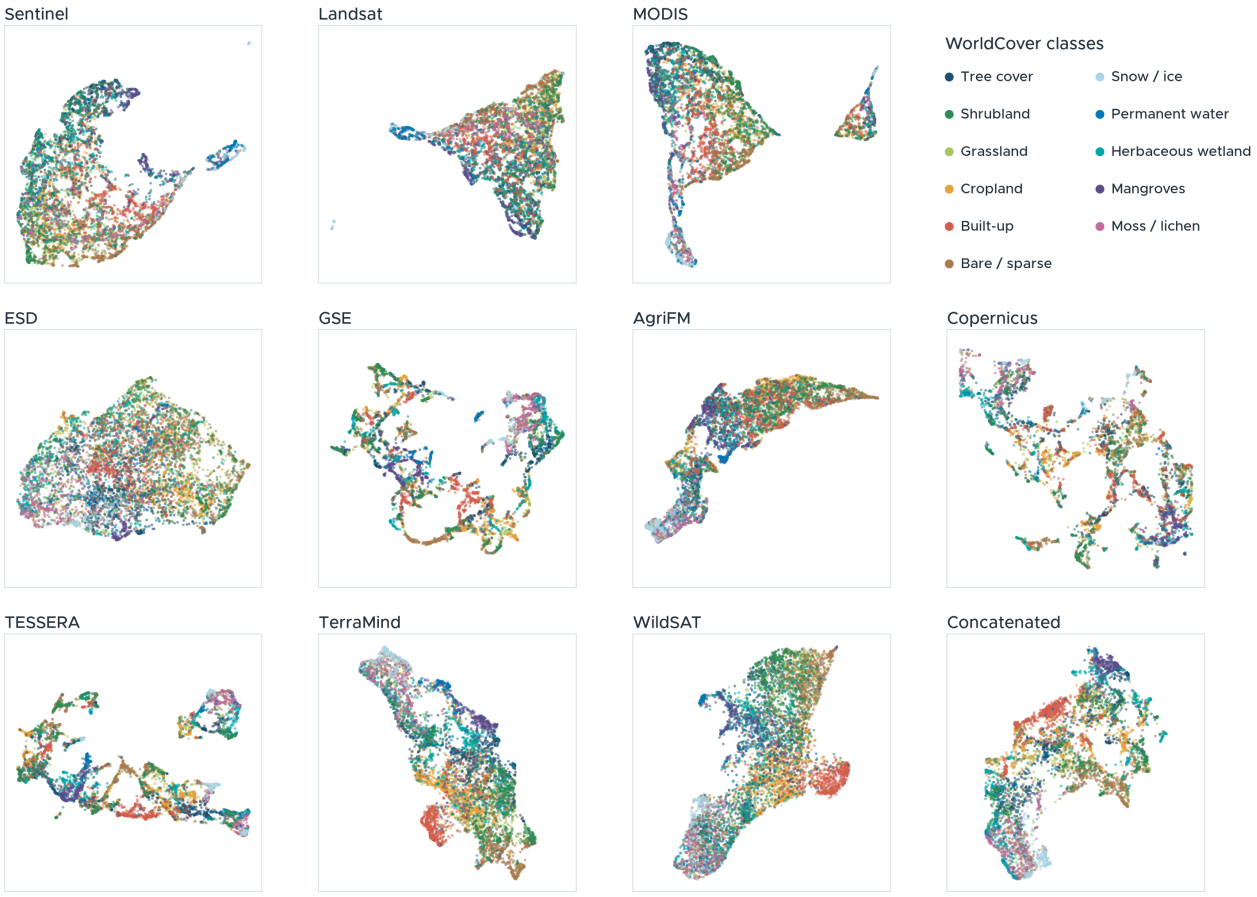


Fig. 8 UMAP projections of the aligned feature sources, colored by WorldCover class.

AgriFM (Li et al. 2026b), TerraMind (Jakubik et al. 2025), and WildSAT (Daroya et al. 2025) produce elongated structures with several class-dominated regions. The concatenated representation has a compact, multi-branch organization that does not reproduce any single input space, so concatenation changes the projected neighborhoods rather than merely enlarging one of the component manifolds.

No projection uniformly separates all land-cover classes. Some regions are dominated by a single class, but spectrally or structurally related surfaces still overlap. The UMAP panels are descriptive: coordinates, orientation, and distances are not comparable across independently fitted panels, and visual separation is not a quantitative clustering or prediction score. Linear CKA and neighborhood overlap provide pairwise comparisons of global geometry and local retrieval behavior.

5.2.2 Global Geometry and Local Neighborhoods

Linear CKA compares global representation geometry. For row-normalized and column-centered matrices X and Y, linear CKA is

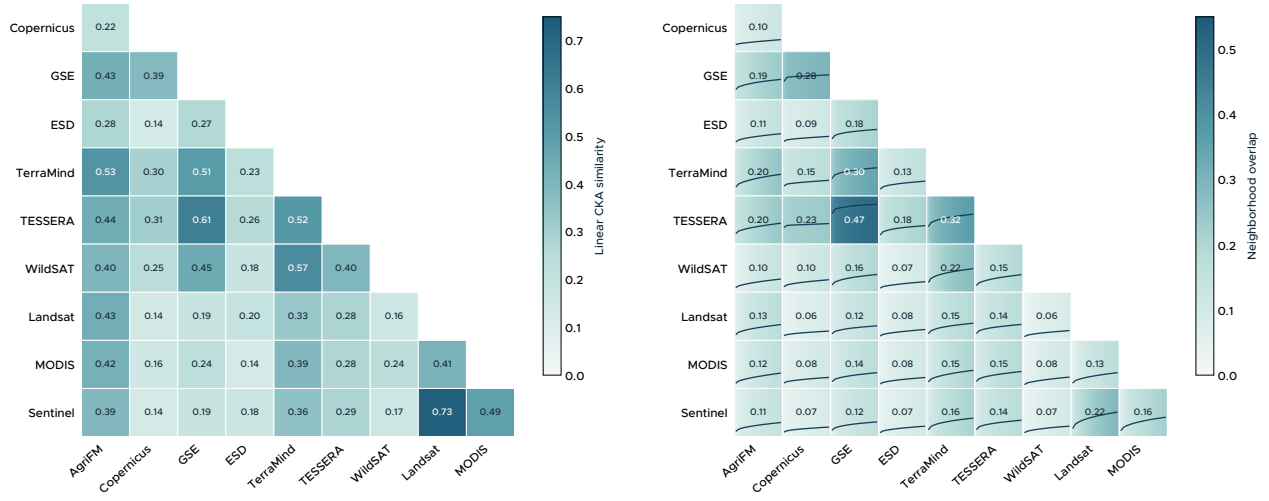
$$\mathrm{CKA}(X, Y) = \frac{\|X^\top Y\|_F^2}{\|X^\top X\|_F \, \|Y^\top Y\|_F}. \tag{9}$$

CKA is invariant to orthogonal transformations and isotropic rescaling, allowing sources with different feature dimensions to be compared. A high value indicates similar centered linear geometry, not identical vectors or identical nearest-neighbor rankings.

Local agreement is measured directly from cosine neighborhoods. Let $\mathcal{N}_k^X(i)$ be the k nearest neighbors of location i in representation X under cosine distance. The overlap between two representations is

$$O_k(X, Y) = \frac{1}{n} \sum_{i=1}^{n} \frac{\left|\mathcal{N}_k^X(i) \cap \mathcal{N}_k^Y(i)\right|}{k}. \tag{10}$$

The score lies between zero and one and measures whether the same locations would be retrieved locally in both spaces. We evaluate k from 5 to 200; the value printed in each matrix cell is the mean across these



(a) Linear CKA similarity.

(b) Cosine-neighborhood overlap.

Fig. 9 Pairwise similarity between feature spaces measured by linear CKA and cosine-neighborhood overlap.

neighborhood sizes. Both pairwise matrices are symmetric, so Fig. 9 shows only the lower triangle. Each neighborhood-overlap cell reports the change across the evaluated values of k on a common scale.

Fig. 9(a) shows two groups with relatively high global similarity. Among the reflectance inputs, Sentinel and Landsat are the closest pair (0.728), followed by Sentinel and MODIS (0.489), consistent with shared optical measurements but different spatial and temporal support. Among the learned representations, GSE (Brown et al. 2025) and TESSERA (Feng et al. 2026a) have the highest CKA (0.614). TerraMind (Jakubik et al. 2025) also has comparatively high CKA with WildSAT (Daroya et al. 2025) (0.566), AgriFM (Li et al. 2026b) (0.534), TESSERA (0.519), and GSE (0.507). By contrast, CKA between Copernicus-FM (Wang et al. 2025b) or ESD (Chen et al. 2026) and the reflectance inputs is only 0.135–0.203. These values describe linear geometry, not predictive quality or complementarity.

The local-overlap ranking in Fig. 9(b) is related but not identical. GSE and TESSERA again form the closest pair, with a mean overlap of 0.474 across the evaluated neighborhood sizes. TESSERA–TerraMind (0.318), GSE–TerraMind (0.303), and GSE–Copernicus-FM (0.281) form the next strongest learned-representation relations. For GSE and TESSERA, overlap rises from 0.381 at $k = 5$ to 0.503 at $k = 200$, so the pair shares both small and broader neighborhoods. The increase with k is partly mechanical because larger neighborhoods offer more opportunities for intersection; comparisons among pairs at the same k are more informative than the increase alone.

Global and local agreement are nevertheless not interchangeable. Sentinel and Landsat have the highest CKA, yet their mean neighborhood overlap is only 0.222 and increases from 0.076 at $k = 5$ to 0.294 at $k = 200$. Their representations therefore share strong large-scale linear structure while differing more substantially in the identities of the nearest locations. CKA and neighborhood overlap identify related spaces but do not measure task utility. The following classification and regression experiments compare the target information available to the evaluated prediction models.

5.3 Downstream Predictive Performance

The downstream experiments test which target properties can be recovered from each input under common data splits and prediction models. Comparing classification with regression distinguishes class separation from the recovery of continuous variation. Predictor and PCA-dimension comparisons then examine how the use and compression of the same features affect performance.

5.3.1 Experimental Design

Within each target, every input uses the same sampled locations and a fixed partition containing 70% training data and 30% held-out test data. Classification is stratified by class, whereas regression is split without target stratification. We evaluate 14 prediction models for each task. Linear and local methods comprise a learned linear head, k-nearest neighbors, a linear support vector classifier or regressor (Cortes and Vapnik 1995), logistic regression for classification, and ridge regression for regression. Tree ensembles comprise random

forest (Breiman 2001), gradient boosting and histogram gradient boosting (Friedman 2001), XGBoost (Chen and Guestrin 2016), LightGBM (Ke et al. 2017), and CatBoost (Prokhorenkova et al. 2018). The neural predictors are a multilayer perceptron (MLP), a convolutional neural network (CNN) (Lecun et al. 1998), a long short-term memory network (LSTM) (Hochreiter and Schmidhuber 1997), and a Vision Transformer (ViT) (Dosovitskiy et al. 2021). The MLP is the scikit-learn implementation (Pedregosa et al. 2011); the linear head, CNN, LSTM, and ViT are trained in PyTorch (Paszke et al. 2019).

Hyperparameters are selected by fivefold cross-validation within the training partition. Where supported by the predictor, classification uses class-balanced sample or loss weights; regression targets are standardized using training-partition statistics and transformed back before evaluation. For scikit-learn predictors (Pedregosa et al. 2011), each input is normalized per channel, flattened, and reduced by incremental principal component analysis (PCA) fitted only on the corresponding training fold. The PyTorch predictors (Paszke et al. 2019) instead use harmonized spatial tensors as input, preserving their channel and spatial organization. After hyperparameter selection, each predictor is refitted on the full training partition and evaluated on the held-out test partition.

5.3.2 Evaluation Measures

Let n be the number of test samples, C the number of classes, and $\mathbf{s}_i$ the class-score vector for sample i. Classification is summarized by accuracy, macro-F1, and top-3 accuracy:

$$\text{Accuracy} = \frac{1}{n}\sum_{i=1}^{n}\mathbb{I}(\hat{y}_i = y_i), \tag{11}$$

$$P_c = \frac{TP_c}{TP_c + FP_c}, \tag{12}$$

$$R_c = \frac{TP_c}{TP_c + FN_c}, \tag{13}$$

$$\text{MacroF1} = \frac{1}{C}\sum_{c=1}^{C}\frac{2P_cR_c}{P_c + R_c}, \tag{14}$$

$$\text{Top3} = \frac{1}{n}\sum_{i=1}^{n}\mathbb{I}(y_i \in \mathcal{T}_3(\mathbf{s}_i))\,. \tag{15}$$

where TP_c, FP_c, and FN_c are the true-positive, false-positive, and false-negative counts for class c, and $\mathcal{T}_3(\mathbf{s}_i)$ contains the three highest-scoring classes. Macro-F1 weights classes equally and is therefore the primary measure for imbalanced land-cover targets. Accuracy weights samples equally, while top-3 accuracy measures whether the reference class remains among the most plausible alternatives.

For continuous targets, we report the coefficient of determination (R^2) and root-mean-square error (RMSE) normalized by the test-target standard deviation. The latter is reported as normalized root-mean-square error (NRMSE):

$$\text{RMSE} = \sqrt{\frac{1}{n}\sum_{i=1}^{n}(y_i - \hat{y}_i)^2}, \tag{16}$$

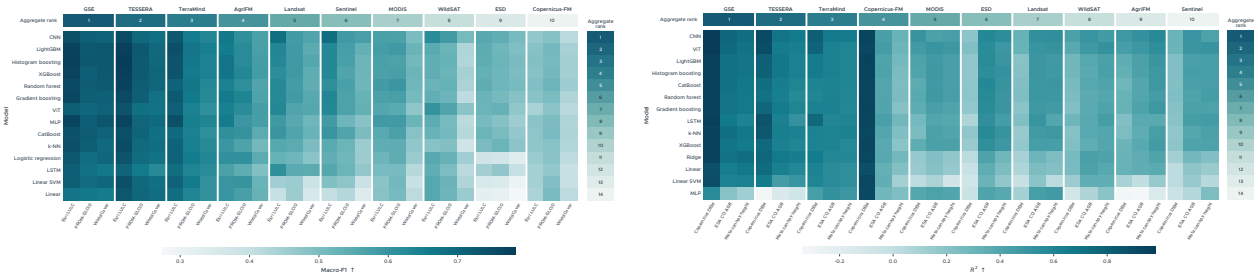
$$R^2 = 1 - \frac{\sum_{i=1}^{n}(y_i - \hat{y}_i)^2}{\sum_{i=1}^{n}(y_i - \bar{y})^2}, \tag{17}$$

$$\text{NRMSE} = \frac{\text{RMSE}}{\sigma}. \tag{18}$$

Higher values are better for the three classification measures and R^2; lower values are better for NRMSE. Here, $\bar{y}$ and σ are the mean and standard deviation of the test targets, respectively. Normalization by σ permits comparison across elevation, biomass, and canopy height without conflating predictive error with their physical scales. In the heatmaps, model ranks order mean scores across embeddings and datasets; embedding ranks order mean scores across prediction models and datasets.

5.3.3 Land-Cover Classification

Fig. 10a compares macro-F1 across prediction models and embeddings on Esri LULC, FROM-GLC10, and WorldCover. Mean values are 0.718 for GSE (Brown et al. 2025), 0.712 for TESSERA (Feng et al. 2026a), and



(a) Classification: Macro-F1. (b) Regression: R^2.

Fig. 10 Classification and regression performance across prediction models, embeddings, and datasets.

0.666 for TerraMind (Jakubik et al. 2025) across the evaluated models and datasets. TESSERA is strongest on Esri LULC, whereas GSE leads on FROM-GLC10 and WorldCover; TerraMind ranks third on each dataset. AgriFM (Li et al. 2026b) follows at 0.596, while the remaining learned inputs, WildSAT (Daroya et al. 2025), ESD (Chen et al. 2026), and Copernicus-FM (Wang et al. 2025b), obtain lower means. The ordering is broadly stable across predictors, but the size of the difference depends on the prediction model. Nonlinear and boosting methods often narrow the differences among inputs, whereas linear predictors produce larger separations.

Accuracy gives nearly the same embedding ordering but places less weight on minority-class performance. GSE averages 0.711, TESSERA 0.705, and TerraMind 0.664, compared with 0.588 for AgriFM. At the predictor level, XGBoost, LightGBM, histogram gradient boosting, and random forest form a close group, while the CNN attains the highest average macro-F1. Macro-F1 highlights differences in minority-class performance that accuracy can mask.

Top-3 accuracy is more compressed across embeddings. GSE, TESSERA, and TerraMind reach mean values of 0.958, 0.951, and 0.940, respectively, and AgriFM reaches 0.907. The observation inputs also yield higher scores under this less restrictive criterion. The correct class often remains among the top three predictions, but macro-F1 remains the main measure for imbalanced classification.

Class-specific recall and error rates are averaged equally across the 14 predictors, each selected by macro-F1 within the training folds. These averages describe individual-model performance rather than an ensemble.

For Esri LULC, GSE and TESSERA have the most balanced class recalls, averaging 77.1% and 77.7%, respectively; TerraMind follows at 73.4%. Their main errors concern flooded vegetation and bare ground being assigned to rangeland. The lower-scoring inputs show more class-dependent behavior: WildSAT is strong for crops and built areas but reaches only 30.7% for flooded vegetation, while the mean class recalls of Copernicus-FM and ESD are close to 52%. The observation inputs preserve water, trees, and snow more reliably than flooded vegetation or crops.

For FROM-GLC10, GSE, TESSERA, and TerraMind achieve mean class recalls of 72.7%, 72.2%, and 67.8%, respectively. Cropland is most often confused with grassland, and grassland with shrubland; snow and ice are frequently assigned to bare land. These directions recur across learned embeddings and observation inputs. The embeddings differ mainly in error rates, not confusion types.

WorldCover is more difficult for the lower-scoring embeddings. GSE and TESSERA maintain mean class recalls above 71%, and TerraMind reaches 66.4%, but shrubland and grassland remain difficult to separate. Moss and lichen have lower recall than spectrally distinctive classes such as built-up land and snow or ice. Wetlands are often assigned to tree cover by the observation inputs, while WildSAT also confuses mangroves with tree cover. The class-level results explain why similar overall accuracy can conceal different class-specific errors.

5.3.4 Continuous-Variable Regression

Fig. 10b reports R^2 for Copernicus DEM elevation, ESA Climate Change Initiative above-ground biomass, and Meta canopy height. Regression performance is more task-dependent than classification performance. Across the three targets, GSE (Brown et al. 2025) has the highest aggregate mean R^2 at 0.738, followed by TESSERA (Feng et al. 2026a) at 0.612, TerraMind (Jakubik et al. 2025) at 0.609, and Copernicus-FM (Wang et al. 2025b) at 0.519. The aggregate values conceal a marked target difference: Copernicus-FM records the highest mean for elevation (0.926), slightly above GSE (0.918), whereas GSE leads for biomass and canopy height. The high elevation score is expected because Copernicus-FM was pretrained on Copernicus GLO-30 DEM and the released Copernicus embedding therefore retains information derived from the same product used as the regression target (Wang et al. 2025b). TerraMind is second on both vegetation targets, while the

other inputs have aggregate means between 0.30 and 0.36. CNN and ViT provide the strongest predictor-level averages, consistent with nonlinear interactions being useful for the continuous targets.

NRMSE gives the same aggregate ordering on a standardized error scale. GSE obtains the lowest mean NRMSE (0.476), followed by TESSERA (0.601), TerraMind (0.623), and Copernicus-FM (0.640); the remaining inputs range from 0.796 to 0.832. NRMSE permits comparison across elevation, biomass, and canopy height despite their different physical scales.

Prediction errors are also examined across target ranges using models selected within the training folds. The following mean R^2 values average the scores of the 14 predictors rather than the predictions themselves.

Elevation shows the strongest separation among embeddings. Copernicus-FM and GSE predict elevations close to the observed values over most of the range and have mean R^2 values of 0.925 and 0.919, respectively. TESSERA reaches 0.706 and TerraMind 0.643, with both increasingly underestimating the highest elevations. Predictions from the other inputs respond weakly to increases above approximately 1,000 m, with underestimation recurring across predictors.

Above-ground biomass is less accurately recovered than elevation. GSE has the highest mean R^2 (0.658), followed by TerraMind (0.596), TESSERA (0.572), and ESD (Chen et al. 2026) (0.494). Predictions from all embeddings are closer to observed values at low biomass and increasingly underestimate high-biomass locations. Greater variation across predictors at high biomass indicates stronger dependence on predictor choice where observations are sparse and the target range is large.

The canopy-height results show a similar but weaker ordering. GSE, TerraMind, and TESSERA obtain mean R^2 values of 0.637, 0.578, and 0.547, respectively, while the other inputs range from 0.235 to 0.433. Model-averaged predictions are close to observed heights for low vegetation but increasingly underestimate taller canopies across all embeddings.

5.3.5 Dimensionality and Pareto Efficiency

Each input at a sampled location is represented as a tensor $\mathbf{X} \in \mathbb{R}^{H \times W \times C}$, where H and W are the spatial dimensions and C is the number of feature channels. For the dimensionality analysis, the normalized tensor is flattened and reduced by Incremental PCA to $d \in \{8, 16, 32, 64, 128, 256, 512, 1024\}$. Thus, d denotes the length of the reduced flattened vector, rather than the channel count of the original tensor. Figs. 11 and 12 compare predictive performance across all evaluated dimensions. For score $q_{r,p,d}$ obtained by representation r, predictor p, and dimension d, the mean scores across predictors and representations are

$$\bar{q}_{r,d} = \frac{1}{|\mathcal{P}_{r,d}|} \sum_{p \in \mathcal{P}_{r,d}} q_{r,p,d}, \tag{19}$$

$$\bar{q}_{p,d} = \frac{1}{|\mathcal{R}_{p,d}|} \sum_{r \in \mathcal{R}_{p,d}} q_{r,p,d}. \tag{20}$$

The first average compares representations over the evaluated predictors, and the second compares predictors over the evaluated representations. A point is Pareto efficient if no other point uses no more dimensions and performs no worse, with a strict improvement in at least one criterion; lower NRMSE indicates better performance.

The embedding profiles show that most gains occur at the lower end of the dimension sweep. Across the classification datasets, the best macro-F1, accuracy, and top-3 results occur between 32 and 128 dimensions. GSE (Brown et al. 2025) achieves the best mean performance in all but one of the 15 dataset–metric comparisons: TESSERA (Feng et al. 2026a) reaches the highest Esri-LULC macro-F1 (0.754) at 128 dimensions, while GSE leads the remaining classification metrics and all 6 regression comparisons. Elevation and above-ground biomass peak at 64 dimensions for GSE, with R^2 values of 0.942 and 0.686. Canopy height is the main exception to early saturation and improves to $R^2 = 0.665$ at 512 dimensions. Higher dimensions improve some tasks but not others.

The predictor profiles reach a similar conclusion. Most predictor-level optima occur at 32–128 dimensions, with 256 dimensions preferred for Esri accuracy and canopy-height regression. Histogram gradient boosting, LightGBM, and XGBoost account for most of the best-performing combinations, while random forest is optimal for FROM-GLC10 top-3 accuracy at 32 dimensions. Embedding rankings change with the predictor and dimension.

Performance Across Models and Embeddings. Across the 5 metrics, GSE (Brown et al. 2025), TESSERA (Feng et al. 2026a), and TerraMind (Jakubik et al. 2025) perform consistently well on the discrete and continuous targets evaluated here, but their ordering and the differences among other inputs vary by target and predictor. Copernicus-FM (Wang et al. 2025b) illustrates this task dependence by combining the

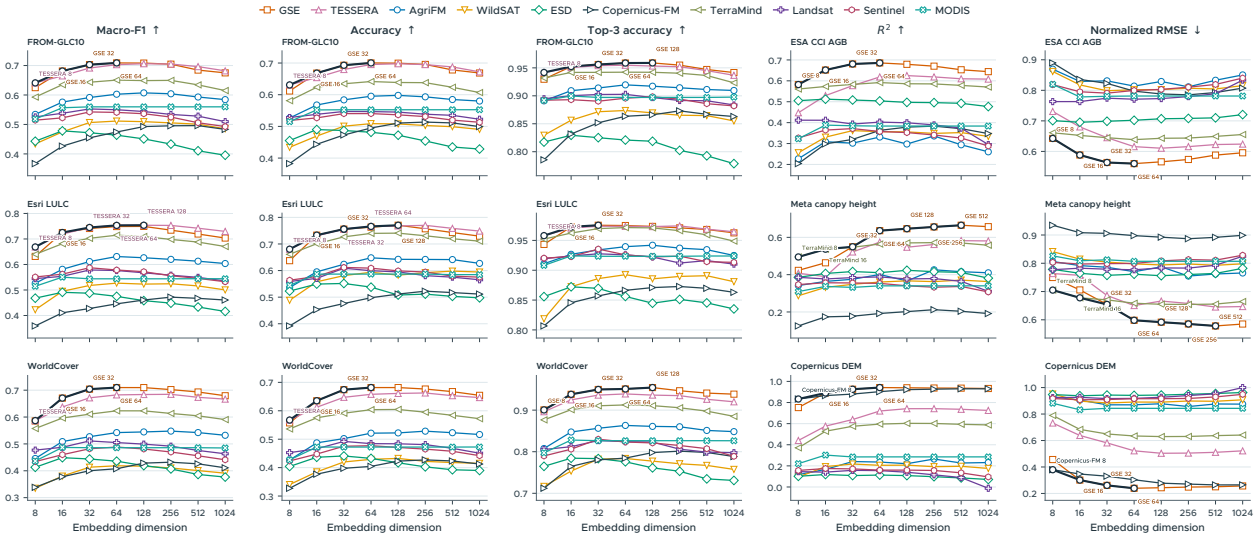


Fig. 11 Predictive performance across embeddings, PCA dimensions, and downstream datasets.

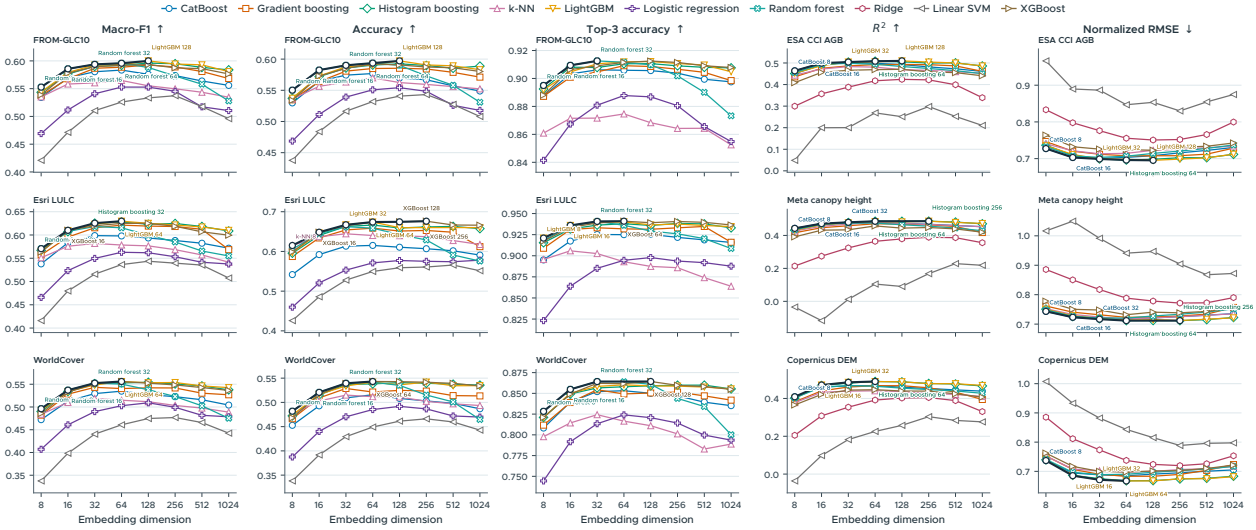


Fig. 12 Predictive performance across prediction models, PCA dimensions, and downstream datasets.

strongest elevation result with substantially lower classification, biomass, and canopy-height scores. Learned embeddings do not uniformly outperform the observation inputs: Landsat, Sentinel-2 (Drusch et al. 2012), and MODIS remain competitive with several learned embeddings, particularly for classification. Downstream rankings also differ from the pairwise geometric relations because CKA and neighborhood overlap measure similarity between feature spaces, whereas the predictive experiments measure task performance.

6 Applications

Applications reveal how broadly learned descriptions become informative for a specific question. The relevant comparison is not only whether an embedding predicts a target, but whether it replaces costly feature construction, complements existing measurements, or supplies context missing from a local dataset. Labels, measurement scales, observation dates, and downstream methods determine which role is tested. The examples on the right of Fig. 1 and the links in Fig. 13 show the range of uses. Within each domain below, studies are compared through the information required and the conditions under which that information remains useful.

Agriculture and Ecology. Representing vegetation requires distinguishing its identity from its condition and management. Crop mapping, tree-species classification, and biomass estimation test different aspects of this information (Zvonkov et al. 2025; Ball et al. 2026; Jin et al. 2026); soil-biodiversity prediction further relates remotely observed context to field measurements (Cerna et al. 2026). Comparisons must also distinguish frozen or pooled vectors from adapted encoders. Ecological evaluations of Prithvi-EO 2.0 and TerraMind

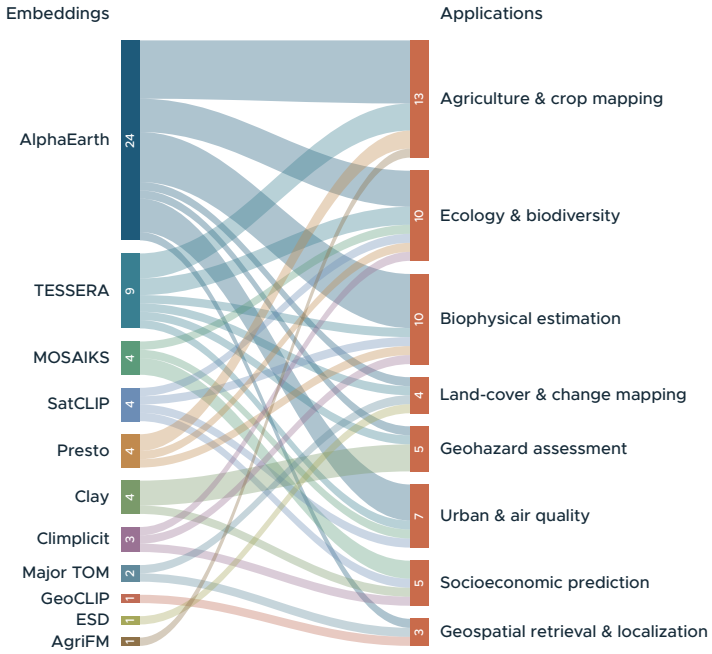


Fig. 13 Links between Earth embeddings and downstream applications.

span land-cover generation, forest functional traits, and peatland detection (Mahlasi et al. 2026), providing different tests of what the representations retain rather than interchangeable measures of ecological quality.

Several studies report gains when few labeled samples are available, but the best representation varies by region and target. Wang et al. (2026a) combined 64-dimensional AlphaEarth embeddings (Brown et al. 2025) with Sentinel-2 spectral, textural, and topographic variables in a random-forest classifier (Breiman 2001); the selected configuration reached 92.69% overall accuracy and a Kappa coefficient of 0.90 in Rizhao, China, and was applied without retraining in Qingdao. Because the model used a combined feature set, this result does not isolate the contribution of AlphaEarth. For 18 tree species and groups in Trentino, Ball et al. (2026) found that AlphaEarth (Brown et al. 2025) and TESSERA (Feng et al. 2026a) increased weighted F1 from 0.80 to 0.83 and macro F1 from 0.50 to 0.55 relative to conventional Sentinel-1/2 composites; performance approached saturation with 5% of the training parcels. Across 5 crop datasets on 5 continents, SSL4EO-S12 initialization (Wang et al. 2023) outperformed ImageNet initialization (Deng et al. 2009), whereas SatlasPretrain (Bastani et al. 2023) did not consistently improve performance. Training with data from other regions was most helpful when in-region labels were scarce (Chang et al. 2025).

Temporal alignment limits transfer even when local classification is accurate. In the Trentino experiment, cross-year weighted F1 decreased from 0.84 to 0.77 for TESSERA and from 0.85 to 0.73 for AlphaEarth (Ball et al. 2026). In Senegal's groundnut basin, TESSERA (Feng et al. 2026a) scored highest under the authors' performance, plausibility, transferability, and accessibility criteria; accuracy was 28% higher than the next-best method in one cross-year experiment (Lisaius et al. 2026; Brown et al. 2025). AlphaEarth was also competitive for locally trained crop-yield prediction and county-level tillage mapping in the United States, but it showed weaker spatial transfer, limited sensitivity to management timing, and lower interpretability (Ma et al. 2026). Annual summaries are therefore less suited to agricultural targets determined by within-season events.

Large-area crop mapping also exposes the difference between reusable encoders and precomputed products. AgriFM uses multisource temporal representations for crop mapping, but users must run the released encoder (Li et al. 2026b). Zvonkov et al. (2025) generated 128-dimensional Presto embeddings (Tseng et al. 2023) over all 56,785 km^2 of Togo in 16 hours at a reported cost of $313.40, producing a 128.8 GB embedding dataset. On CropHarvest, the resulting map reached 0.897 overall accuracy and an F1 score of 0.808, compared with 0.859 and 0.745 for the corresponding AlphaEarth map. WorldCereal likewise uses Presto in its crop-mapping workflow and fine-tunes it on the WorldCereal reference database (Butsko et al. 2025).

Vegetation studies distinguish identity, condition, and history, each of which places different demands on a common representation. Crop identity and cultivation are examined through complex cropping patterns in China, tomato systems in California, and paddy rice in India (Li and Yu 2026; Narimani et al. 2026; Biswanath Das et al. 2026). Biome and dominant-species prediction emphasize composition (Joseph et al. 2026; Strelnikov et al. 2025), whereas restoration and planted-mangrove mapping also require associations with past

interventions (Heiman 2026; Sun et al. 2026). Grouping these studies by the property inferred clarifies why success on one category does not settle another: similar current cover can have different management histories. Combining embeddings with hyperspectral observations for fish biodiversity or with language models for ecological assessment tests a further role, as complementary context rather than the complete source of target information (Qi et al. 2026; Yang et al. 2026b).

Field measurements test whether a learned description preserves variation within mapped categories. Forest-community, carbon, tree-crop, and plantation studies relate embeddings to composition and management (Gao et al. 2025; Paluba et al. 2026; Esteban Cava et al. 2026); inventory biomass and standing dead-tree fraction examine specific measured properties (Sohrabi 2026; Chowdhury et al. 2026). Grassland biomass extends this comparison beyond forests (Liu et al. 2026b). Together with forestry and multi-target environmental evaluations (Mura et al. 2026; Feng et al. 2026b), these studies connect broad pretraining to locally measured quantities. Their comparison should retain the measurement unit and target range: a representation can distinguish vegetation types while losing within-type variability needed to estimate a continuous property.

Spatial organization also affects what can be inferred from a fixed embedding. Pixel- versus object-based AlphaEarth evaluation, comparisons with Sentinel-2 and Landsat, and boosting-based classification examine the roles of the prediction unit, input, and classifier (Khan and Ahmad 2025; Mantey et al. 2025, 2026). Structure–semantic modulation studies how global embeddings support higher-resolution mapping (Lyu et al. 2026); cloud inpainting uses them as context for missing observations (Li et al. 2026a). These studies extend reuse beyond direct classification, while requiring distinct tests of class discrimination, boundary detail, or reconstruction quality.

Biophysical Estimation and Environmental Monitoring. An embedding may supply target-related information directly or complement variables selected from domain knowledge. Height, landslide, and air-quality studies examine these roles under different spatial and temporal conditions (Hamoudzadeh et al. 2026; Cheng et al. 2026; Alvarez et al. 2025); streamflow reconstruction combines satellite embeddings with existing discharge estimates (Lin et al. 2026). For Danish peatlands, AlphaEarth-only models had RMSE values 6% and 3% higher than expert-variable models for soil organic carbon and water-table depth, while combining embeddings with topography, water proximity, and synthetic wet and drained conditions improved spatial patterns (Koch et al. 2026; Brown et al. 2025). Predictor choice matters alongside covariates. Over approximately 8,000 km^2 of Nouvelle-Aquitaine, ridge regression, U-Net, and U-Net++ used the same AlphaEarth embeddings for surface height. Test R^2 was 0.38, 0.78 for U-Net (Ronneberger et al. 2015), and 0.84, respectively; U-Net++ had a test RMSE of 16.42 m (Hamoudzadeh et al. 2026). Thus, a score reflects both the available information and the predictor's ability to use its spatial organization.

Performance varies across target strata, regions, and forest types. Forest-biomass prediction from 89 plots at the Yunhe Forestry Station was weak when all plots were pooled ($R^2 = 0.06$), despite comparisons among random forest (Breiman 2001), support vector regression (Cortes and Vapnik 1995), a multilayer perceptron, and Gaussian-process regression. The best R^2 values differed by forest type: 0.33 for broad-leaved forest, 0.14 for mixed forest, and 0.48 for coniferous forest (Jin et al. 2026). For landslide susceptibility in Nantou County, Hong Kong, and Emilia-Romagna, CNN1D (Lecun et al. 1998), CNN2D, and Vision Transformer (Dosovitskiy et al. 2021) classifiers using the full 64-dimensional AlphaEarth representation improved F1 by approximately 4–15% and AUC by 0.04–0.11 over conventional conditioning factors; PCA-reduced embeddings (Jolliffe and Cadima 2016) were less accurate (Cheng et al. 2026).

Temporal aggregation further constrains environmental monitoring. Annual AlphaEarth embeddings paired with records of 5 air pollutants in Quito produced $R^2 = 0.71$ for nitrogen dioxide and sulfur dioxide under fivefold cross-validation, compared with 0.55 for particulate matter, 0.61 for carbon monoxide, and a negative value for ozone (Alvarez et al. 2025). Annual vectors can encode persistent land-use and urban-form correlates, but not all of the short-term chemistry and meteorology needed for atmospheric prediction.

Hazard studies clarify the difference between representing an event and its environmental setting. Mapping observed damage requires information aligned with the event, whereas susceptibility estimation can draw on persistent conditions. The Portugal burned-area study directly compares AlphaEarth and TESSERA; fire-severity and wildfire-exposure studies examine related questions across biomes and spatial scales (Silva and Gonçalves 2026; Mahato et al. 2026; Berg and Leyk 2026). Landslide change detection, susceptibility assessment, and positive–unlabeled learning use different targets and label assumptions (Leonardi et al. 2025; Liu et al. 2026a; Mingxuan Li et al. 2026), while Clay-CNN hybrids supply auxiliary context (Vu 2026). The event's timing and the role assigned to the embedding therefore matter more for comparison than the shared hazard name.

Physical-variable studies help distinguish a description of environmental setting from a representation of the process itself. Hydrological modeling and generalization examine catchment information (Qu et al. 2026; Ou and Zheng 2026), while groundwater-fluoride prediction and rock-glacier detection relate observed context

to different physical targets (Wei et al. 2025; Khajuria et al. 2026). Temperature recovery, evapotranspiration, and net ecosystem exchange test associations with energy and carbon exchange (Lee-Burkhart et al. 2026; Jiang et al. 2026; Du et al. 2026); comparisons with TROPOMI examine annual nitrogen-dioxide patterns (Alvarez et al. 2026). An embedding may describe persistent spatial differences while separate measurements specify current forcing or conditions. Its value can then be tested by adding it to an otherwise unchanged prediction method. This comparison tests the contribution of persistent spatial context to predictions of physical variables.

Geospatial Retrieval and Socioeconomic Applications. Retrieval uses distances between embeddings directly, whereas socioeconomic prediction adds labels, aggregation choices, and a downstream model. GeoCLIP (Vivanco Cepeda et al. 2023) evaluates worldwide image-to-coordinate retrieval, and Major TOM Embeddings (Czerkawski et al. 2024) supports similarity search over its released vectors. RANGE (Dhakal et al. 2025) augments coordinate embeddings with visual features retrieved from an auxiliary database and reports gains of up to 13.1% on classification and 0.145 in R^2 on regression relative to the evaluated location-embedding baselines. EarthEmbeddingExplorer provides an interactive interface for similarity retrieval over Sentinel-2 imagery (Zheng et al. 2026b). Dimension-level associations have also been used for retrieval with AlphaEarth (Rahman 2026), while FUSAR-GPT injects AlphaEarth spatiotemporal features into a SAR vision–language model for grounded interpretation (Zhang et al. 2026a).

Socioeconomic applications remain sensitive to the labels and spatial units used for prediction (Pettersson and Daoud 2025; Sherman et al. 2026). MOSAIKS (Rolf et al. 2021) used one precomputed feature set for forest cover, population density, road length, and housing value, and SatCLIP (Klemmer et al. 2025) evaluates coordinate embeddings on ecological and socioeconomic tasks. Sherman et al. (2026) combined MOSAIKS daytime features with nighttime imagery to estimate the Human Development Index for 61,530 municipalities and 819,309 grid cells. Pettersson and Daoud (2025) used AlphaEarth embeddings in a graph neural network across 37 Demographic and Health Survey datasets, where graph structure produced a small improvement over image-only baselines.

Aggregation changes the information presented to the downstream model. Corley et al. (2026a) compared 11 training-free and 2 parametric methods on 81,000 embedding GeoTIFFs from AlphaEarth, OlmoEarth (Herzog et al. 2026), and TESSERA. With mean pooling, accuracy fell by over 10 points for some embeddings when evaluation changed from random to geographic splits. Concatenated minimum, maximum, mean, and standard-deviation statistics improved average accuracy on geographic splits at four times the embedding size; covariance pooling achieved higher accuracy in some settings, whereas generalized mean pooling did not consistently outperform mean pooling. An evaluation using NeuCo-Bench also found mean pooling competitive, although the best layer and objective varied by task (Gilch et al. 2026).

Retrieval gives a direct test of what a learned relationship means. Multispectral retrieval and comparisons with general-purpose vision encoders evaluate image-based similarity (Blumenstiel et al. 2024; Park et al. 2026); joint-embedding prediction and crisis-response retrieval examine correspondence for other query settings (Choudhury et al. 2025; Walsh et al. 2026). Language-guided refinement and expert weather bulletins specify a desired match through text (Arefeen et al. 2026; Kim and Park 2026). Analyses of TESSERA land-use and topographic structure instead inspect organization without supervised prediction (Maffei et al. 2026). Together, these studies distinguish the geometry of a feature space from the relevance of its neighbors to an analytical question. Retrieval should be judged against that question's matching criterion, not vector distance alone.

Socioeconomic inference depends on how remotely observed conditions correspond to independently collected labels. Economic-activity estimation, urban-signal analysis, and AEF-Econ examine such associations (Yue et al. 2026; Gong et al. 2026; Hou et al. 2026), with cross-city noise modeling extending the comparison to environmental inequality (Zhang et al. 2026b). Health-related studies concern climate-sensitive diseases and postpartum-depression screening (Nazir et al. 2026; Frasch 2026); climate-risk work examines spatiotemporal associations (Pasupuleti 2023). In these settings, population coverage, label collection, and spatial aggregation are part of the inference, not incidental data choices. The embeddings provide environmental context, while an explanation of the outcome requires information about the processes that generated the labels.

What transfers across applications. The studies above support a conditional account of reuse. Features learned from extensive observations can reduce the burden on local labels, as illustrated by tea mapping, tree-species classification, and crop transfer (Wang et al. 2026a; Ball et al. 2026; Chang et al. 2025). Comparisons with expert variables and variation across target strata show why the benefit cannot be inferred from the extent of pretraining alone (Koch et al. 2026; Jin et al. 2026; Ma et al. 2026). A useful embedding supplies information that is missing, expensive to construct, or difficult to learn from the available target measurements. This explains both successful substitution for conventional features and cases where embeddings work better as an additional source.

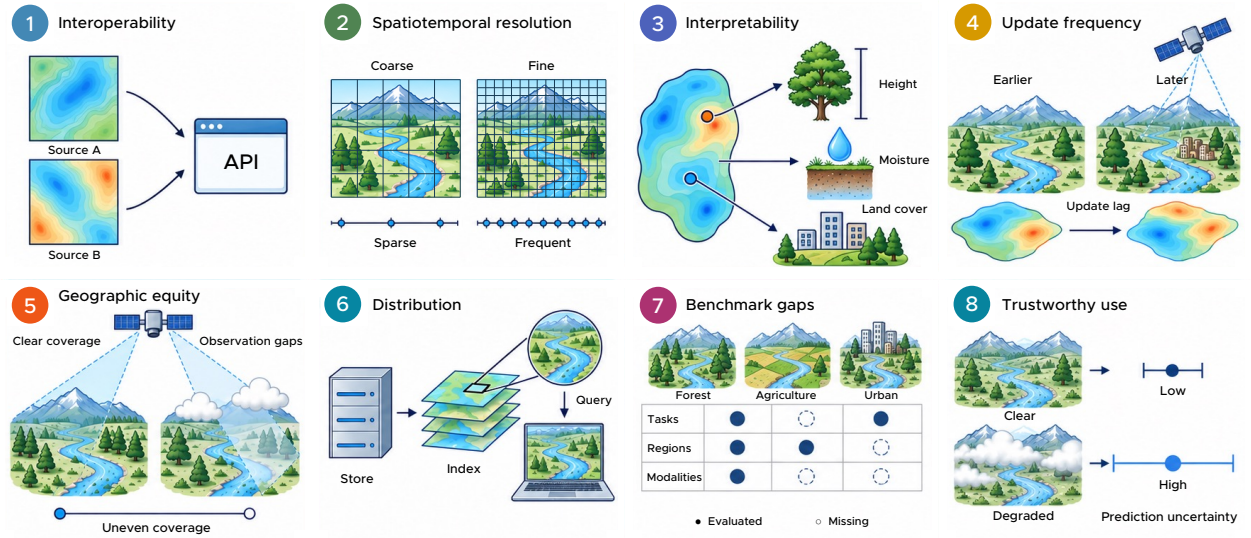


Fig. 14 Challenges and potential research directions for global Earth embedding products.

Temporal suitability depends on which changes must remain distinguishable. The Senegal crop-transfer results support the use of seasonal information (Lisaius et al. 2026), whereas management-timing and Quito pollution results expose limitations of annual summaries (Ma et al. 2026; Alvarez et al. 2025). Reusing an annual vector for a rapidly changing target may therefore require complementary observations rather than a more complex predictor alone. This connects temporal design to the information needed for inference, not simply to the number of dates used in pretraining.

Spatial resolution constrains downstream use. A 10 m embedding can provide contextual information for objects smaller than one pixel, but it cannot directly resolve the geometry of individual tree crowns, narrow roads, or small buildings. Pixel-, patch-, scene-, and coordinate-level embeddings should therefore be compared only after matching their support to the label geometry. Pooling experiments further show that converting pixel embeddings to parcel or patch features can alter geographic transfer performance (Corley et al. 2026a).

Transfer depends on whether the relationships learned from one population remain informative in another. Crop comparisons show benefits from other-region training when local labels are scarce (Chang et al. 2025), while agricultural-practice prediction remains sensitive to spatial transfer (Ma et al. 2026). Local validation therefore remains necessary even when vectors are globally available. Distribution coverage determines where embeddings can be queried; it does not determine where a predictor fitted to them remains accurate.

Reuse also changes where costs are incurred. The reported Presto computation for 56,785 km^2 of Togo cost \$313.40, approximately \$5.52 per 1,000 km^2 (Zvonkov et al. 2025). This is an encoding cost, not the full cost of producing and validating a map. Precomputed products move encoding to the producer, while access, storage, label collection, and validation remain part of downstream use. Practical value thus combines information retained with the resources needed to obtain a reliable result. When predictions inform sampling or resource allocation, a further question is how errors alter the proposed action. An accurate regional average can still be inadequate for identifying rare sites requiring attention. Such uses need target-specific assessment of missed cases, false alarms, and follow-up measurements rather than an assumption that improved average prediction guarantees better decisions.

7 Challenges and Future Perspectives

Broader reuse makes the consequences of representation choices more widely shared. The challenges below concern the information available at each location, its continuity through time, and the conditions under which it can support reliable analysis. The future perspectives then consider how addressing these problems could connect representation learning more closely with observation and scientific research.

7.1 Open Challenges

Reliable reuse requires accessible and interoperable data, sufficient detail to resolve the phenomenon of interest, and predictions that can be interpreted and evaluated across different conditions. Fig. 14 summarizes the associated challenges and potential research directions. These challenges interact: greater spatial and

temporal detail raises distribution costs, updates can alter learned relationships, and uneven coverage limits both evaluation and confidence in use.

7.1.1 Interoperability and Distribution

Interoperability concerns whether embeddings can be compared and combined, while distribution determines whether users can obtain the data needed for that analysis. Current products differ in spatial support, file format, temporal definition, and access method. Google Satellite Embedding is distributed as annual, pixel-wise Cloud-Optimized GeoTIFFs (Brown et al. 2025; Google Earth Engine 2026a); TESSERA uses quantized tiled arrays accessed through GeoTessera (Feng et al. 2026a); and Major TOM, the Copernicus Global Embeddings Dataset, and LGND Clay Embeddings use GeoParquet for patch- or scene-level vectors and their metadata (Czerkawski et al. 2024; Copernicus Data Space Ecosystem 2026; LGND.ai 2026). Earth Embeddings as Products and recent TorchGeo loaders expose several releases through similar query patterns (Fang et al. 2026; Stewart et al. 2022; TorchGeo 2026), but they do not remove differences in coordinate reference systems, tiling grids, temporal support, numeric precision, or source-data provenance. A minimal metadata specification should record the encoder and source-data versions, spatial footprint, valid time, numeric encoding, and processing history.

Storage remains a constraint even after inference has been centralized. A global land grid at 10 m resolution contains approximately 1.5×10^{12} cells. At 64 signed 8-bit values per cell, one uncompressed annual layer contains about 96 TB of numeric values before masking, file compression, tiling overhead, and metadata. At a fixed grid and precision, increasing the vector width from 64 to 1,024 multiplies value storage by sixteen, while changing from annual to monthly output multiplies it by twelve. These estimates describe uncompressed value storage; actual archive sizes also depend on coverage, masking, compression, and file overhead. Compression studies also address different costs. Across 6 remote sensing foundation models and 4 classification tasks, post-hoc slimming retained more than 71% of relative accuracy at 1% of the original floating-point operations (Hackel et al. 2026); this reduces encoder computation, not vector storage. TESSERA v2 instead reports that a 16-dimensional prefix retains approximately 92% of the aggregate performance of its 128-dimensional vector while using one eighth of the value storage (Feng et al. 2026c). Quantization (Jégou et al. 2011), ordered dimensions, and spatially coarser summaries may reduce distribution costs, but their effects should be tested separately for classification, continuous-variable regression, rare classes, and temporal change.

Precomputed layers reduce computation for users but do not eliminate the cost of training, global inference, hosting, and repeated updates. Current planetary releases depend on producers that can maintain large accelerator and object-storage resources (Brown et al. 2025; Feng et al. 2026a; Chen et al. 2026). Repeated use can spread these costs across analyses, but the saving depends on how often the collection is used, transferred, and regenerated. A storage reduction alone cannot establish an energy or emissions reduction; these require measurements across production and use. Lightweight encoders and selective access may be preferable when only a small area or a few dates are required.

Long-term reuse also requires continuity beyond a particular analysis. Google states that annual Satellite Embedding production will continue subject to source-data availability and that anticipated delivery changes will receive advance notice (Google Earth Engine 2026a). Comparable version, update, and deprecation policies are not yet documented consistently across the reviewed products. Stable archives and explicit maintenance responsibility, including community or public-sector mirrors, would protect reproducibility. More broadly, widespread reliance on the same representation could propagate common omissions across studies. Independent reference data and alternative descriptions can help identify such shared omissions.

7.1.2 Spatiotemporal Detail and Updating

Spatial resolution, temporal support, and update frequency jointly determine which conditions an embedding can describe. Aggregation over pixels or dates can suppress small features and brief events; more frequent publication cannot recover detail already lost during encoding. Temporal support differs substantially among released embeddings. Google Satellite Embedding and TESSERA provide annual summaries (Brown et al. 2025; Feng et al. 2026a); ESD retains within-year temporal information in each annual record (Chen et al. 2026); and Major TOM and the Copernicus Global Embeddings Dataset associate vectors with individual source acquisitions (Czerkawski et al. 2024; Copernicus Data Space Ecosystem 2026). The current public LGND Clay collection instead provides monthly aggregated chip-level embeddings beginning in 2017 (LGND.ai 2026). An annual release does not by itself establish how precisely within-year event timing can be recovered; acquisition-level collections retain individual observation dates but increase storage and processing costs. Evaluation should therefore test whether target features and changes remain detectable at the stated spatial and temporal support, and report the delay between observation and product availability. Generative models

such as DiffusionSat support temporal generation, multispectral super-resolution, and inpainting (Khanna et al. 2024). No reviewed product reports that generated observations improve embedding stability.

Encoder updates create a separate compatibility problem. Let f_{old} and f_{new} denote two encoder versions. Reusing a downstream predictor trained on the old representation requires a map from the new space to the old one, for example

$$f_{\text{old}}(\mathbf{x}) \approx \mathbf{A} f_{\text{new}}(\mathbf{x}). \tag{21}$$

If a linear map $\mathbf{A}$ is accurate on the relevant data, an existing predictor g_{old} can be evaluated as $g_{\text{old}}(\mathbf{A} f_{\text{new}}(\mathbf{x}))$. Orthogonal Procrustes analysis provides one way to estimate a linear alignment (Schönemann 1966), but it does not guarantee preservation of task-relevant information. A nonlinear adapter, regeneration of historical embeddings, or retraining of the downstream predictor may be needed when linear alignment is inadequate.

Version changes also affect longitudinal analysis. If adjacent annual layers are generated by different encoders, an observed difference can reflect either surface change or representation drift. Regenerating the complete historical archive holds the encoder fixed, but is costly and can change previously reported estimates; changes in observations and preprocessing still require examination. Each layer should record the encoder, source archive, preprocessing configuration, and inference date. Compatibility should be tested both for stable reference locations and for independently recorded changes. Preserving old predictions while losing sensitivity to new events would satisfy only part of the requirement for longitudinal use.

7.1.3 Interpretability and Trustworthy Use

Interpretability concerns what learned features describe; trustworthy use additionally requires knowing when their predictions are reliable. Distillation into interpretable Sentinel-1/2 proxies examines the connection to observable properties (Jing et al. 2026); reliability-aware models and latent stochastic regularization study prediction reliability and spatial uncertainty (Gonzalez-Calabuig et al. 2026; Johnson 2026). These approaches address distinct needs. Identifying an influential dimension can explain a predictor's dependence on its input, while relating that dimension to a physical process requires independent measurements and examination of observation and preprocessing effects.

The reviewed embedding layers do not provide calibrated, location-specific uncertainty estimates. Uncertainty can arise because observations are missing or noisy, compression removes relevant distinctions, target measurements are imprecise, or a predictor is used outside its fitted conditions. These sources require different responses: another observation may resolve missing information, whereas more labels may improve calibration of an otherwise adequate representation. Encoder ensembles measure disagreement, but require repeated inference and calibration against errors. Nearest-neighbor distance has been used for out-of-distribution detection (Sun et al. 2022); for Earth embeddings, distance from a reference collection could indicate an unfamiliar surface or simply sparse sampling. AlphaEarth's von Mises–Fisher bottleneck likewise does not supply per-location confidence because its concentration parameter is fixed during model construction (Brown et al. 2025). Useful uncertainty assessment connects a diagnostic to observed errors and to the decision it is intended to inform.

Task accuracy alone is insufficient for claims about reliable use. REOBench measures sensitivity to 12 image-corruption types across 6 tasks (Li et al. 2025), while EarthShift evaluates changes in geography, time, scale, sensor, and data source and reports average out-of-distribution degradation of 15–20% across 8 geospatial foundation models and 11 tasks (Doerksen and Kerner 2026). Although these studies evaluate model features, their protocols can also test released embeddings. Reliability claims also require documentation of data gaps, supported temporal and spatial scales, version history, and validation outside the regions used to fit downstream predictors.

Physical consistency introduces a related but distinct requirement. A latent coordinate need not have a physical unit for an embedding to be useful. When predictions concern a physical quantity, however, independently known bounds, conservation relations, or process behavior can provide tests beyond average accuracy (Reichstein et al. 2019). Such constraints must apply to the quantity and scale being modeled; they should not be imposed indiscriminately on similarity vectors. A physically plausible output can still be inaccurate, so consistency tests complement rather than replace measurement-based validation.

7.1.4 Geographic Coverage and Evaluation

Geographic equity and benchmark coverage are linked: where observations or reference labels are sparse, representation quality is harder both to improve and to assess. Planetary coverage does not imply uniform representation quality. Pretraining collections use different spatial sampling strategies: MMEarth balances 1.2 million locations across 14 biomes (Nedungadi et al. 2025), whereas SSL4EO-S12 samples approximately 250,000 locations around the world's 10,000 most populated cities and removes most patch overlap (Wang

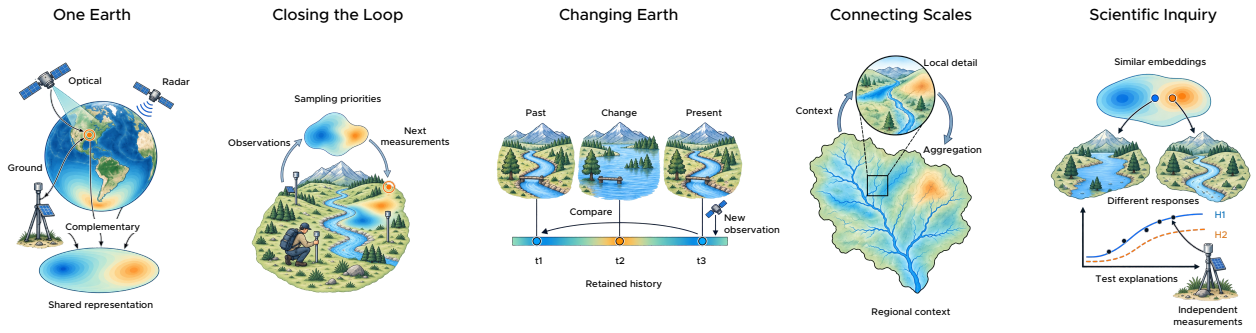


Fig. 15 Earth embeddings for observing and understanding a changing Earth.

et al. 2023). Kaur et al. (2026) report that the geographic and spectral composition of pretraining data affects downstream performance, with the preferred sampling strategy depending on the model and target distribution. Coverage maps and sample counts should therefore be accompanied by distributions over biome, sensor conditions, acquisition time, and relevant target populations.

Benchmark gaps concern the combinations of tasks, regions, and modalities that have been tested, not simply the total number of samples. MMEarth-Bench reports lower performance under geographic transfer across five environmental tasks and 12 modalities (Gordon et al. 2026). EarthShift finds that robustness varies by shift type, with relatively small temporal losses and larger losses under sensor and geographic shifts (Doerksen and Kerner 2026). Comparisons across climate, data availability, and socioeconomic conditions require the same tasks, spatially separated labels, identical downstream protocols, and enough observations in each group to separate representation quality from label noise and target prevalence. Reporting results for these combinations would distinguish low performance from missing evaluation and help prioritize new reference measurements.

Observation conditions also vary geographically. Persistent cloud, seasonal snow, illumination geometry, topographic shadow, and sensor revisit patterns alter which measurements are available at a location (Rolf et al. 2024). These factors can create distribution shifts, but their effect on embedding quality must be measured rather than inferred from geography alone. Multimodal products may reduce dependence on any single sensor, and a recent comparison found that combinations of AlphaEarth, TESSERA, GeoCLIP, and SatCLIP improved on the best individual embedding in four of six evaluated tasks; the gains remained task- and location-dependent (van der Plas et al. 2026). Regional evaluation should therefore report source availability and test both individual and combined embeddings under the same labels and splits.

Bias can enter through interpretation as well as coverage. A dense embedding layer may describe an area for which labels represent only accessible sites or particular populations. Missing reference data then limit the ability to establish who benefits from a prediction, not merely its average accuracy. Ethical concerns in satellite machine learning include the increased ease of monitoring activities and the consequences of applying models to affected communities (Rolf et al. 2024). For embeddings, privacy assessment is especially relevant when location-indexed features are linked with sensitive health, mobility, or household records. It should consider the linked data and intended inference, rather than assume that vector encoding anonymizes information. Humanitarian and environmental uses likewise require attention to who defines the target, whose errors are measured, and whether uncertain predictions can be reviewed before consequential action.

7.2 Future Perspectives

Beyond addressing the challenges above, we propose five future perspectives on how Earth embeddings could change the relationship between observation and analysis (Fig. 15). They consider shared descriptions of Earth, feedback to data collection, continuity through change, connections across scales, and scientific investigation.

7.2.1 One Earth

Earth observations measure different aspects of a common, evolving world. Their spatial support, timing, and physical sensitivity determine which properties are observable. This suggests learning descriptions of the underlying state that connect sensors while retaining complementary information. Multi-view representation learning provides a theoretical basis for identifying shared latent factors under explicit partial-observability assumptions (Yao et al. 2024). Current shared and modality-specific encodings offer practical approaches to this problem (Wang et al. 2025a), but agreement between sources does not settle which physical properties have been recovered. The open question is which properties can be estimated consistently across observations

and which remain source-dependent. Independent measurements, controlled removal of sources, and changes in spatial support could test that distinction. A useful shared description should retain correspondence where it is justified without suppressing informative disagreement.

7.2.2 Closing the Loop

Embeddings could help determine what should be observed next, reversing the usual direction from measurements to representations. Information-based sensor placement provides methods for selecting observations that reduce uncertainty at unmeasured locations (Krause et al. 2008). Active learning with Google satellite embeddings has also been studied for impervious-surface mapping through seed-driven grid adaptation (Zheng et al. 2026a), although sample selection is distinct from placing physical instruments. Combining embeddings with field measurements could produce a spatial field of expected observation value, from which sampling probabilities or sensor locations are chosen subject to cost, accessibility, and coverage. The aim would be to resolve uncertainty relevant to a research question, not simply sample the most unusual vectors. Selection should account for redundant candidate sites and allow observations outside the relationships already favored by the model. Otherwise, repeated sampling could reinforce an incomplete representation. Field trials at matched budgets, with independent evaluation data, could establish whether this feedback improves inference over spatially balanced or conventional sampling.

7.2.3 A Memory of a Changing Earth

A useful history must retain changes as well as allow past and present observations to be compared. Similar current conditions can follow different trajectories, so timing and sequence may matter beyond an annual summary. Backward-compatible learning addresses comparability during encoder updates, with existing demonstrations in visual retrieval (Shen et al. 2020); proposals such as emem address the traceability of analyses over stored embeddings (Kumari and Singh 2026). The unresolved question is how to retain persistent background, transient events, and their sequence while incorporating new observations. A history that preserves only stable attributes would miss disturbance; one that responds to every acquisition difference would confuse observation variation with change. Overlapping observations and stable references could distinguish genuine change from encoder drift, while dated event records could test whether historical detail survives an update. Selective updating could reduce computation, provided that the selection rule is also tested for missed changes in infrequently observed locations.

7.2.4 Connecting Scales

Connecting scales requires retaining how local properties are arranged, not only their average values. Averaging vectors can preserve composition while discarding adjacency and connectivity. Scale-aware pretraining addresses observations at different resolutions (Reed et al. 2023), and pooling studies show that aggregation affects downstream performance (Corley et al. 2026a). The next question is how local descriptions can preserve relationships important at a larger scale. A catchment depends on the organization of terrain and vegetation as well as their attributes; habitat connectivity similarly concerns arrangement, not only habitat quantity. Graph learning or geographically specified relations could connect local vectors through the relevant network, while semantic relations could specify how objects belong to larger units. Comparing directly encoded regions, simple aggregates, and relation-aware combinations against the same measurements would reveal when added structure improves inference. Tests under alternative boundaries would further distinguish dependence on an arbitrary partition from relationships that persist across scales.

7.2.5 Embeddings for Scientific Inquiry

Earth embeddings could contribute to the formation of scientific questions, not only to answering predefined ones. Learning jointly from diverse observations offers a way to capture patterns and interactions that may be difficult to identify from individual sources or preselected variables. Recurrent similarities, differences, and unexpected associations across these representations could suggest new hypotheses about the processes connecting observed conditions. For example, systematic embedding differences between regions with similar conventional environmental indicators could motivate investigation of omitted factors or their interactions. Studies relating embedding dimensions to environmental variables provide a starting point for examining such associations (Rahman 2026). Disentangled and physics-informed learning offer approaches to investigating latent factors and physical relationships, with assumptions that require justification (Higgins et al. 2017; Locatello et al. 2019; Raissi et al. 2019). Independent observations, targeted measurements, and process models could then test the resulting hypotheses; hybrid modeling provides a basis for connecting learned

information with process knowledge (Reichstein et al. 2019). The findings could, in turn, refine the hypotheses and identify additional observations or relationships to include in representation learning. This suggests a broader change in geospatial research: embeddings could participate in deciding what to investigate, rather than enter only after a question and its explanatory variables have been chosen. Moving between knowledge-led analysis and discoveries prompted by multisource representations could reshape how scientific hypotheses are proposed, tested, and revised.

8 Conclusion

Earth embeddings provide reusable representations that support a range of geospatial analyses. They can be obtained from reusable encoders, coordinate models, or precomputed collections (Jean et al. 2019; Klemmer et al. 2025; Brown et al. 2025). Information learned from extensive observations can then support questions with more limited target measurements. Its value nevertheless depends on the distinctions retained: stability can aid recurring estimation, while sensitivity to change is essential for events and evolving conditions. Benchmarks and applications show that usefulness varies with labels, region, task, and evaluation protocol (Marsocci et al. 2026; Ball et al. 2026; Ma et al. 2026). Our experiments similarly found that geometric similarity did not determine predictive accuracy and that retaining more PCA components of flattened patches did not consistently improve prediction. Clear specifications, continued access, and tests of transfer and update compatibility are therefore needed to connect the availability of vectors with reliable reuse (Fang et al. 2026; Doerksen and Kerner 2026; Gordon et al. 2026).

Through Represent, Relate, and Reason, this review connects representation design with relationships and inference. Comparing learning methods, models, products, access, benchmarks, and applications reveals why the source of supervision, the analysis unit, and the information available at use must be considered together. Fusion should retain useful differences as well as common content; evaluation should establish what an embedding adds to existing observations and knowledge; applications should identify when additional measurements remain necessary. This perspective supports choices based on the question and available information rather than model scale or vector width alone.

Open challenges concern uncertainty, comparability, equitable coverage, and the resources required for sustained use. Future research can build on shared descriptions of Earth while retaining source-specific information, use embeddings to guide new observations, preserve histories of change, and connect local properties through meaningful cross-scale relations. By revealing relationships across diverse observations, Earth embeddings could offer new perspectives on how scientific hypotheses are formulated and tested. We hope this review offers fresh perspectives and inspires further advances in Earth embedding research and geospatial analysis.

Statements and Declarations

Funding

This work was supported by the RGC Senior Research Fellow Scheme (SRFS) under Grant No. SRFS2627-7H02, and by the General Research Fund (GRF) from the Research Grants Council (RGC) of the Hong Kong Special Administrative Region, China under Grant No. 17617525.

Competing interests

The authors declare that they have no known competing financial interests or personal relationships that could have appeared to influence the work reported in this article.

Ethics approval

Not applicable.

Data and code availability

The data sources used in this review are described and cited in the article. Additional data and code supporting the comparative analyses are available from the corresponding author upon reasonable request.

Use of generative artificial intelligence

During the preparation of this work, the authors used GPT-6 solely to aid or polish writing and to generate graphical elements for schematic figures. After using this tool/service, the authors reviewed and edited the content as needed and take full responsibility for the content of the published article.

Author contributions

Yongchuan Cui: Conceptualization, Methodology, Investigation, Data curation, Formal analysis, Software, Visualization, Writing - Original draft. Keli Shi: Investigation, Validation, Writing - Review & Editing. Shunlin Liang: Conceptualization, Supervision, Validation, Writing - Review & Editing.

References

Aimar ES, Zhambulova G, Khan FS, et al (2025) Vlm2geovec: Toward universal multimodal embeddings for remote sensing. 10.48550/ARXIV.2512.11490, URL https://arxiv.org/abs/2512.11490

Alam MMT, Simic Milas A (2025) Dimensionality optimized machine learning retrieval of canopy chlorophyll, nitrogen, and phosphorus from google satellite embeddings. Smart Agricultural Technology 12:101601. 10.1016/j.atech.2025.101601, URL https://www.sciencedirect.com/science/article/pii/S2772375525008329

Allen M, Dorr F, Gallego-Mejia JA, et al (2023) Fewshot learning on global multimodal embeddings for earth observation tasks. 10.48550/ARXIV.2310.00119, URL https://arxiv.org/abs/2310.00119

Alvarez CI, Ulloa Vaca CA, Echeverria Llumipanta NA (2025) Machine learning for urban air quality prediction using google alphaearth foundations satellite embeddings: A case study of quito, ecuador. Remote Sensing 17(20):3472. 10.3390/rs17203472, URL http://dx.doi.org/10.3390/rs17203472

Alvarez CI, Schneider P, Wurm M (2026) Evaluating geospatial foundation-model embeddings for tropomi-based annual surface no2 estimation across europe 10.22541/essoar.15005949/v1, URL http://dx.doi.org/10.22541/essoar.15005949/v1

and (2022) Copernicus dem. 10.5270/esa-c5d3d65, URL http://dx.doi.org/10.5270/esa-c5d3d65

Arefeen MA, Debnath B, Rajendran RK, et al (2026) Open-sat: Llm-guided query embedding refinement for open-vocabulary object retrieval in satellite imagery. 10.48550/ARXIV.2605.05344, URL https://arxiv.org/abs/2605.05344

Assran M, Duval Q, Misra I, et al (2023) Self-supervised learning from images with a joint-embedding predictive architecture. In: Proceedings of the IEEE/CVF Conference on Computer Vision and Pattern Recognition (CVPR), pp 15619–15629

Astruc G, Gonthier N, Mallet C, et al (2025a) Anysat: One earth observation model for many resolutions, scales, and modalities. In: Proceedings of the Computer Vision and Pattern Recognition Conference (CVPR), pp 19530–19540

Astruc G, Gonthier N, Mallet C, et al (2025b) Omnisat: Self-supervised modality fusion for earth observation. In: Leonardis A, Ricci E, Roth S, et al (eds) Computer Vision – ECCV 2024. Springer Nature Switzerland, Cham, pp 409–427

Astruc G, Trulls E, Hosang J, et al (2026) Unigeoclip: Unified geospatial contrastive learning. In: Proceedings of the IEEE/CVF Conference on Computer Vision and Pattern Recognition (CVPR) Workshops, pp 7847–7856

Ayush K, Uzkent B, Meng C, et al (2021) Geography-aware self-supervised learning. In: Proceedings of the IEEE/CVF International Conference on Computer Vision (ICCV), pp 10181–10190

Bai L, Zhang X, Zhang S, et al (2025) Geolink: Empowering remote sensing foundation model with openstreetmap data. In: Advances in Neural Information Processing Systems 38. Neural Information Processing Systems Foundation, Inc. (NeurIPS), NeurIPS 2025, p 186757–186787, 10.52202/085713-5617, URL http://dx.doi.org/10.52202/085713-5617

Ball JG, Wicklein JA, Feng Z, et al (2026) Geospatial foundation models enable data-efficient tree species mapping in temperate mountain forests. Science of Remote Sensing 14:100466. 10.1016/j.srs.2026.100466, URL https://www.sciencedirect.com/science/article/pii/S2666017226001045

Bastani F, Wolters P, Gupta R, et al (2023) Satlaspretrain: A large-scale dataset for remote sensing image understanding. In: Proceedings of the IEEE/CVF International Conference on Computer Vision (ICCV), pp 16772–16782

Berg A, Leyk S (2026) Spatial scale effects in foundation model earth embeddings: A case study on predicting the exposure of structures to wildfire in colorado, usa 10.2139/ssrn.7026253, URL http://dx.doi.org/10.2139/ssrn.7026253

Betti L, Ricke S, Obadic I, et al (2026) What's in an earth embedding? an explainability analysis of location encoders. URL https://arxiv.org/abs/2606.24997, arXiv:2606.24997

Bi H, Feng Y, Tong B, et al (2026) Ringmoe: Mixture-of-modality-experts multi-modal foundation models for universal remote sensing image interpretation. IEEE Transactions on Pattern Analysis and Machine Intelligence 48(4):4388–4405. 10.1109/tpami.2025.3643453, URL http://dx.doi.org/10.1109/tpami.2025.3643453

Bias Variance Labs (2026) AiTLAS 2.0. GitHub repository, https://github.com/biasvariancelabs/aitlas, accessed: Jul. 30, 2026

Biswanath Das, Pranab Dhara, Vijender Kumar (2026) Identification of major kharif paddy growing areas in india- using msi data ,google satellite embedding and advanced machine learning 10.13140/RG.2.2.22893.96485, URL https://www.researchgate.net/doi/10.13140/RG.2.2.22893.96485

Blumenstiel B, Moor V, Kienzler R, et al (2024) Multi-spectral remote sensing image retrieval using geospatial foundation models. In: IGARSS 2024 - 2024 IEEE International Geoscience and Remote Sensing Symposium. IEEE, p 7286–7291, 10.1109/igarss53475.2024.10641903, URL http://dx.doi.org/10.1109/igarss53475.2024.10641903

Bodnar C, Bruinsma WP, Lucic A, et al (2025) A foundation model for the earth system. Nature 641(8065):1180–1187. 10.1038/s41586-025-09005-y, URL https://doi.org/10.1038/s41586-025-09005-y

Bountos NI, Ouaknine A, Papoutsis I, et al (2025) Fomo: Multi-modal, multi-scale and multi-task remote sensing foundation models for forest monitoring. Proceedings of the AAAI Conference on Artificial Intelligence 39(27):27858–27868. 10.1609/aaai.v39i27.35002, URL http://dx.doi.org/10.1609/aaai.v39i27.35002

Breiman L (2001) Random forests. Machine Learning 45(1):5–32. 10.1023/A:1010933404324, URL https://doi.org/10.1023/A:1010933404324

Brown CF, Kazmierski MR, Pasquarella VJ, et al (2025) Alphaearth foundations: An embedding field model for accurate and efficient global mapping from sparse label data. 10.48550/ARXIV.2507.22291, URL https://arxiv.org/abs/2507.22291

Butsko C, Tseng G, Van Tricht K, et al (2025) Deploying geospatial foundation models in the real world: Lessons from worldcereal. In: Audebert N, Azizpour H, Barrière V, et al (eds) Proceedings of The TerraBytes ICML Workshop: Towards global datasets and models for Earth Observation, Proceedings of Machine Learning Research, vol 292. PMLR, pp 13–31, URL https://proceedings.mlr.press/v292/butsko25a.html

C3S (2018) Era5 hourly data on single levels from 1940 to present. 10.24381/CDS.ADBB2D47, URL https://cds.climate.copernicus.eu/doi/10.24381/cds.adbb2d47

Cambridge Centre for Earth Observation (2026) GeoTessera. GitHub repository, https://github.com/ucam-eo/geotessera, accessed: Jul. 30, 2026

Caron M, Touvron H, Misra I, et al (2021) Emerging properties in self-supervised vision transformers. In: Proceedings of the IEEE/CVF International Conference on Computer Vision (ICCV), pp 9650–9660

Cerna S, Si-Moussi S, Calderón-Sanou I, et al (2026) Chapter two - limits and promises of earth observation foundation models in predicting multi-trophic soil biodiversity. In: Rusch A (ed) Advances in Ecological Research, Advances in Ecological Research, vol 74. Academic Press, p 31–64, 10.1016/bs.aecr.2026.02.005, URL https://www.sciencedirect.com/science/article/pii/S006525042600005X

Chang YC, Stewart AJ, Bastani F, et al (2025) On the generalizability of foundation models for crop type mapping. In: IGARSS 2025 - 2025 IEEE International Geoscience and Remote Sensing Symposium. IEEE, p 948–953, 10.1109/igarss55030.2025.11242260, URL http://dx.doi.org/10.1109/igarss55030.2025.11242260

Chen S, Wang J, Liu Q, et al (2024) Global 30 m seamless data cube (2000–2022) of land surface reflectance generated from landsat 5, 7, 8, and 9 and modis terra constellations. Earth System Science Data 16(11):5449–5475. 10.5194/essd-16-5449-2024, URL https://essd.copernicus.org/articles/16/5449/2024/

Chen S, Wang J, Yuan S, et al (2026) Democratizing planetary-scale analysis: an ultra-lightweight earth embedding database for accurate and flexible global land monitoring. Earth System Science Data 18(7):5375–5398. 10.5194/essd-18-5375-2026, URL https://essd.copernicus.org/articles/18/5375/2026/

Chen T, Guestrin C (2016) Xgboost: A scalable tree boosting system. In: Proceedings of the 22nd ACM SIGKDD International Conference on Knowledge Discovery and Data Mining. ACM, KDD '16, p 785–794, 10.1145/2939672.2939785, URL http://dx.doi.org/10.1145/2939672.2939785

Chen T, Kornblith S, Norouzi M, et al (2020) A simple framework for contrastive learning of visual representations. In: III HD, Singh A (eds) Proceedings of the 37th International Conference on Machine Learning, Proceedings of Machine Learning Research, vol 119. PMLR, pp 1597–1607, URL https://proceedings.mlr.press/v119/chen20j.html

Cheng G, Han J, Lu X (2017) Remote sensing image scene classification: Benchmark and state of the art. Proceedings of the IEEE 105(10):1865–1883. 10.1109/jproc.2017.2675998, URL http://dx.doi.org/10.1109/jproc.2017.2675998

Cheng Y, Zhu Q, Fan L (2026) From landslide conditioning factors to satellite embeddings: Evaluating the utilisation of google alphaearth for landslide susceptibility mapping using deep learning. 10.48550/ARXIV.2601.07268, URL https://arxiv.org/abs/2601.07268

Cher D, Iqbal H, Xing E, et al (2026) Tessellating the earth. In: Favaro P, Kukelova Z, Maki A, et al (eds) Computer Vision – ECCV 2026. Springer Nature Switzerland, Cham, pp 443–459

Choudhury S, Salunkhe Y, Mehrotra S, et al (2025) Rejepa: A novel joint-embedding predictive architecture for efficient remote sensing image retrieval. In: 2025 IEEE/CVF Conference on Computer Vision and Pattern Recognition Workshops (CVPRW). IEEE, p 2364–2373, 10.1109/cvprw67362.2025.00223, URL http://dx.doi.org/10.1109/cvprw67362.2025.00223

Choudhury S, Suvarna C, Tsogsuren I, et al (2026) S2vec: Self-supervised geospatial embeddings for the built environment. ACM Transactions on Spatial Algorithms and Systems 12(3):1–21. 10.1145/3787217, URL http://dx.doi.org/10.1145/3787217

Chowdhury AI, Ahishali M, Vastaranta M, et al (2026) Satellite embeddings as complementary predictors of standing dead-tree volume fraction in boreal forests 10.2139/ssrn.6922442, URL http://dx.doi.org/10.2139/ssrn.6922442

Clay Foundation (2024) Pretrained model release v1.5. https://clay-foundation.github.io/model/release-notes/specification.html

Cole E, Horn GV, Lange C, et al (2023) Spatial implicit neural representations for global-scale species mapping. In: Krause A, Brunskill E, Cho K, et al (eds) Proceedings of the 40th International Conference on Machine Learning, Proceedings of Machine Learning Research, vol 202. PMLR, pp 6320–6342, URL https://proceedings.mlr.press/v202/cole23a.html

Cong Y, Khanna S, Meng C, et al (2022) Satmae: Pre-training transformers for temporal and multi-spectral satellite imagery. In: Koyejo S, Mohamed S, Agarwal A, et al (eds) Advances in Neural Information Processing Systems, vol 35. Curran Associates, Inc., pp 197–211, 10.52202/068431-0015, URL https://proceedings.neurips.cc/paper_files/paper/2022/file/01c561df365429f33fcd7a7faa44c985-Paper-Conference.pdf

Copernicus Data Space Ecosystem (2025) Global embedding dataset now available on CDSE. https://dataspace.copernicus.eu/news/2025-11-14-global-embedding-dataset-now-available-cdse, accessed: Jul. 30, 2026

Copernicus Data Space Ecosystem (2026) Global embeddings dataset. Official documentation, https://documentation.dataspace.copernicus.eu/Data/ComplementaryData/Embeddings.html, accessed: Jul. 30, 2026

Corley I, Robinson C, Ferres JML, et al (2026a) From pixels to patches: Pooling strategies for earth embeddings. In: 4th ICLR Workshop on Machine Learning for Remote Sensing (Main Track), URL https://openreview.net/forum?id=oPfOVLFIrU

Corley I, Sharma L, Crasto R (2026b) Landsat-bench: Datasets and benchmarks for landsat foundation models. In: TerraBytes - ICML 2025 workshop, URL https://openreview.net/forum?id=ab70e2WB19

Cortes C, Vapnik V (1995) Support-vector networks. Machine Learning 20(3):273–297. 10.1007/BF00994018, URL https://doi.org/10.1007/BF00994018

Czerkawski M, Kluczek M, Bojanowski JS (2024) Global and dense embeddings of earth: Major tom floating in the latent space. 10.48550/ARXIV.2412.05600, URL https://arxiv.org/abs/2412.05600

Dalei DK, Shrivastava S, Panigrahi N (2025) Geographic places to semantic spaces: Analysis of geospatial embeddings. ISPRS Annals of the Photogrammetry, Remote Sensing and Spatial Information Sciences X-5/W2-2025:131–135. 10.5194/isprs-annals-X-5-W2-2025-131-2025, URL https://isprs-annals.copernicus.org/articles/X-5-W2-2025/131/2025/

Danish MS, Munir MA, Shah S, et al (2026) Terrafm: A scalable foundation model for unified multisensor earth observation. In: Vondrick C, Hariharan B, Raffel C, et al (eds) International Conference on Learning Representations, pp 12787–12809, URL https://proceedings.iclr.cc/paper_files/paper/2026/file/159511050630689045bf5593e74b13cc-Paper-Conference.pdf

Daroya R, Cole E, Mac Aodha O, et al (2025) Wildsat: Learning satellite image representations from wildlife observations. In: Proceedings of the IEEE/CVF International Conference on Computer Vision (ICCV), pp 6143–6154

Deng J, Dong W, Socher R, et al (2009) Imagenet: A large-scale hierarchical image database. In: 2009 IEEE Conference on Computer Vision and Pattern Recognition. IEEE, p 248–255, 10.1109/cvpr.2009.5206848, URL http://dx.doi.org/10.1109/cvpr.2009.5206848

Dhakal A, Ahmad A, Khanal S, et al (2024) Sat2cap: Mapping fine-grained textual descriptions from satellite images. In: 2024 IEEE/CVF Conference on Computer Vision and Pattern Recognition Workshops (CVPRW). IEEE, p 533–542, 10.1109/cvprw63382.2024.00058, URL http://dx.doi.org/10.1109/cvprw63382.2024.00058

Dhakal A, Sastry S, Khanal S, et al (2025) Range: Retrieval augmented neural fields for multi-resolution geo-embeddings. In: Proceedings of the Computer Vision and Pattern Recognition Conference (CVPR), pp 24680–24689

Díaz-Ireland G, Gülçin D, López-Sánchez A, et al (2026) Comparative evaluation of alphaearth annual embeddings vs. seasonal remote sensing layers with u-net segmentation for california crop and land-use mapping 10.2139/ssrn.6667132, URL http://dx.doi.org/10.2139/ssrn.6667132

Dimitrovski I, Kitanovski I, Panov P, et al (2023) Aitlas: Artificial intelligence toolbox for earth observation. Remote Sensing 15(9):2343. 10.3390/rs15092343, URL http://dx.doi.org/10.3390/rs15092343

Do MK, Han K, Lai P, et al (2025) Robsense: A robust multi-modal foundation model for remote sensing with static, temporal, and incomplete data adaptability. In: Proceedings of the Computer Vision and Pattern Recognition Conference (CVPR), pp 7427–7436

Doerksen K, Kerner H (2026) Earthshift: a benchmark for measuring robustness to real-world distribution shifts in earth observation. 10.48550/ARXIV.2605.29330, URL https://arxiv.org/abs/2605.29330

Dollinger J, Robert D, Plekhanova E, et al (2026) Climplicit: Climatic implicit embeddings for global ecological tasks. URL https://arxiv.org/abs/2504.05089, arXiv:2504.05089

Dosovitskiy A, Beyer L, Kolesnikov A, et al (2021) An image is worth 16x16 words: Transformers for image recognition at scale. URL https://arxiv.org/abs/2010.11929, arXiv:2010.11929

Drusch M, Del Bello U, Carlier S, et al (2012) Sentinel-2: Esa's optical high-resolution mission for gmes operational services. Remote Sensing of Environment 120:25–36. 10.1016/j.rse.2011.11.026, URL https://www.sciencedirect.com/science/article/pii/S0034425712000636, the Sentinel Missions - New Opportunities for Science

Du P, Cui L, Lian Y, et al (2026) Global inversion of terrestrial net ecosystem exchange: Integrating explicit multi-source predictors and high-dimensional remote-sensing embeddings. Remote Sensing 18(9):1390. 10.3390/rs18091390, URL http://dx.doi.org/10.3390/rs18091390

Dubayah R, Blair JB, Goetz S, et al (2020) The global ecosystem dynamics investigation: High-resolution laser ranging of the earth's forests and topography. Science of Remote Sensing 1:100002. 10.1016/j.srs.2020.100002, URL https://www.sciencedirect.com/science/article/pii/S2666017220300018

Dumeur I, Valero S, Inglada J (2025) Paving the way toward foundation models for irregular and unaligned satellite image time series. IEEE Transactions on Geoscience and Remote Sensing 63:1–21. 10.1109/tgrs.2025.3589013, URL http://dx.doi.org/10.1109/tgrs.2025.3589013

Earth Genome (2025) Earth Index Embeddings. Source Cooperative, URL https://source.coop/earthgenome/earthindexembeddings

Earth Resources Observation and Science (EROS) Center (2020) Landsat 8-9 operational land imager / thermal infrared sensor level-1, collection 2. 10.5066/P975CC9B, URL https://www.usgs.gov/centers/eros/science/usgs-eros-archive-landsat-archives-landsat-8-9-operational-land-imager-and

Embed2Scale (2025) Embed2scale challenge. 2025 CVPR EarthVision Data Challenge, EvalAI, URL https://eval.ai/web/challenges/challenge-page/2465/overview

Esri (2022) Esri releases updated land-cover map with new sets of global data. https://www.esri.com/about/newsroom/announcements/esri-releases-updated-land-cover-map-with-new-sets-of-global-data, accessed: 2026-07-31

Esri (2026) Global Location Encoder (Sentinel-2): Introduction to the model. ArcGIS AI Models documentation, URL https://doc.arcgis.com/en/pretrained-models/latest/vector/introduction-to-global-location-encoder-sentinel-2-.htm

Esteban Cava J, Navarro JA, Tomé Morán JL, et al (2026) Aplicaciones de google satellite embeddings en la cartografía de plantaciones forestales en uganda. Congresos UEx, actas de Congresos (2). 10.17398/3101-7177.2.201, URL http://dx.doi.org/10.17398/3101-7177.2.201

Fang H, Stewart AJ, Corley I, et al (2026) Earth embeddings as products: Taxonomy, ecosystem, and standardized access. 10.48550/ARXIV.2601.13134, URL https://arxiv.org/abs/2601.13134

Fayad I, Zimmer M, Schwartz M, et al (2025) DUNIA: Pixel-sized embeddings via cross-modal alignment for earth observation applications. In: Singh A, Fazel M, Hsu D, et al (eds) Proceedings of the 42nd International Conference on Machine Learning, Proceedings of Machine Learning Research, vol 267. PMLR, pp 16375–16406, URL https://proceedings.mlr.press/v267/fayad25a.html

Feng Z, Atzberger C, Jaffer S, et al (2026a) Tessera: Temporal embeddings of surface spectra for earth representation and analysis. In: Proceedings of the IEEE/CVF Conference on Computer Vision and Pattern Recognition (CVPR), pp 34818–34831

Feng Z, Atzberger C, Jaffer S, et al (2026b) Applications of the tessera geospatial foundation model to diverse environmental mapping tasks 10.2139/ssrn.6142416, URL http://dx.doi.org/10.2139/ssrn.6142416

Feng Z, Jaffer S, Shokar I, et al (2026c) Tessera v2: Scaling pixel-wise earth foundation models. 10.48550/ARXIV.2607.03949, URL https://arxiv.org/abs/2607.03949

Fibaek C, Camilleri L, Luyts A, et al (2024) Phileo bench: Evaluating geo-spatial foundation models. In: IGARSS 2024 - 2024 IEEE International Geoscience and Remote Sensing Symposium. IEEE, p 2739–2744, 10.1109/igarss53475.2024.10642780, URL http://dx.doi.org/10.1109/igarss53475.2024.10642780

Francis A, Czerkawski M (2024) Major tom: Expandable datasets for earth observation. In: IGARSS 2024 - 2024 IEEE International Geoscience and Remote Sensing Symposium. IEEE, p 2935–2940, 10.1109/igarss53475.2024.10640760, URL http://dx.doi.org/10.1109/igarss53475.2024.10640760

Frasch MG (2026) Reducing intersectional disparities in postpartum depression screening through geospatial foundation model embeddings: A cross-sectional study of 209,872 us women 10.2139/ssrn.6311855, URL http://dx.doi.org/10.2139/ssrn.6311855

Friedman JH (2001) Greedy function approximation: A gradient boosting machine. The Annals of Statistics 29(5). 10.1214/aos/1013203451, URL http://dx.doi.org/10.1214/aos/1013203451

Fuller A, Millard K, Green J (2023) Croma: Remote sensing representations with contrastive radar-optical masked autoencoders. In: Oh A, Naumann T, Globerson A, et al (eds) Advances in Neural Information Processing Systems, vol 36. Curran Associates, Inc., pp 5506–5538, 10.52202/075280-0241, URL https://proceedings.neurips.cc/paper_files/paper/2023/file/11822e84689e631615199db3b75cd0e4-Paper-Conference.pdf

Gao X, Pasquarella V, Laflower D, et al (2025) Mapping forest communities, including species composition, structure, and carbon, at 10-m resolution using geospatial embeddings 10.2139/ssrn.5936862, URL http://dx.doi.org/10.2139/ssrn.5936862

Gbodjo YJE, Ienco D (2026) Assessing the generalization of geospatial embeddings for temporaltransfer in land cover classification 10.2139/ssrn.6890917, URL http://dx.doi.org/10.2139/ssrn.6890917

Geo-Embeddings (2026) Best practices | Geo-Embeddings. https://geoembeddings.org/bestpractices.html, accessed: 2026-08-02

Ghamisi P, Yu W, Zhang X, et al (2025) Geospatial foundation models to enable progress on sustainable development goals. 10.48550/ARXIV.2505.24528, URL https://arxiv.org/abs/2505.24528

Gilch L, Wittmann I, Nitsche M, et al (2026) How to embed matters: Evaluation of eo embedding design choices. In: Proceedings of the IEEE/CVF Conference on Computer Vision and Pattern Recognition (CVPR) Workshops, pp 7909–7918

Gislason PO, Benediktsson JA, Sveinsson JR (2006) Random forests for land cover classification. Pattern Recognition Letters 27(4):294–300. 10.1016/j.patrec.2005.08.011, URL https://www.sciencedirect.com/science/article/pii/S0167865505002242, pattern Recognition in Remote Sensing (PRRS 2004)

Glaser Y, Stopa JE, Wolniewicz LM, et al (2025) Wv-net: A foundation model for sar ocean satellite imagery. Artificial Intelligence for the Earth Systems 4(4). 10.1175/aies-d-25-0003.1, URL http://dx.doi.org/10.1175

/aies-d-25-0003.1

Gomes C, Brunschwiler T (2024) Neural embedding compression for efficient multi-task earth observation modelling. In: IGARSS 2024 - 2024 IEEE International Geoscience and Remote Sensing Symposium. IEEE, p 8268–8273, 10.1109/igarss53475.2024.10642535, URL http://dx.doi.org/10.1109/igarss53475.2024.10642535

Gomes C, Blumenstiel B, De Sousa Almeida JL, et al (2025a) Terratorch: The geospatial foundation models toolkit. In: IGARSS 2025 - 2025 IEEE International Geoscience and Remote Sensing Symposium. IEEE, p 6364–6368, 10.1109/igarss55030.2025.11243570, URL http://dx.doi.org/10.1109/igarss55030.2025.11243570

Gomes C, Wittmann I, Robert D, et al (2025b) Lossy neural compression for geospatial analytics: A review. IEEE Geoscience and Remote Sensing Magazine 13(3):97–135. 10.1109/mgrs.2025.3546527, URL http://dx.doi.org/10.1109/mgrs.2025.3546527

Gong P, Liu H, Zhang M, et al (2019) Stable classification with limited sample: transferring a 30-m resolution sample set collected in 2015 to mapping 10-m resolution global land cover in 2017. Science Bulletin 64(6):370–373. 10.1016/j.scib.2019.03.002, URL https://www.sciencedirect.com/science/article/pii/S2095927319301380

Gong W, Srivastava U, Wang Y, et al (2026) Earth embeddings reveal diverse urban signals from space. 10.48550/ARXIV.2604.03456, URL https://arxiv.org/abs/2604.03456

Gonzalez-Calabuig M, Cohrs KH, Nedungadi V, et al (2026) Shrug-fm: Reliability-aware foundation models for earth observation. In: Proceedings of the IEEE/CVF Conference on Computer Vision and Pattern Recognition (CVPR) Workshops, pp 7919–7928

Google Earth Engine (2026a) AlphaEarth Foundations GCS data. Official documentation, https://developers.google.com/earth-engine/guides/aef_on_gcs_readme, accessed: Jul. 30, 2026

Google Earth Engine (2026b) Satellite embedding V1. Earth Engine Data Catalog, https://developers.google.com/earth-engine/datasets/catalog/GOOGLE_SATELLITE_EMBEDDING_V1_ANNUAL, accessed: Jul. 30, 2026

Gordon L, Belongie S, Igel C, et al (2026) Mmearth-bench: Global model adaptation via multimodal test-time training. 10.48550/ARXIV.2602.06285, URL https://arxiv.org/abs/2602.06285

Gramacki P, Leśniara K, Raczycki K, et al (2023) Srai: Towards standardization of geospatial ai. In: Proceedings of the 6th ACM SIGSPATIAL International Workshop on AI for Geographic Knowledge Discovery. ACM, SIGSPATIAL '23, p 43–52, 10.1145/3615886.3627740, URL http://dx.doi.org/10.1145/3615886.3627740

Guo X, Lao J, Dang B, et al (2024) Skysense: A multi-modal remote sensing foundation model towards universal interpretation for earth observation imagery. In: Proceedings of the IEEE/CVF Conference on Computer Vision and Pattern Recognition (CVPR), pp 27672–27683

Hackel L, Burgert T, Demir B (2026) How much of a model do we need? redundancy and slimmability in remote sensing foundation models. 10.48550/ARXIV.2601.22841, URL https://arxiv.org/abs/2601.22841

Hall DK, Riggs GA, Salomonson VV, et al (2002) Modis snow-cover products. Remote Sensing of Environment 83(1):181–194. 10.1016/S0034-4257(02)00095-0, URL https://www.sciencedirect.com/science/article/pii/S0034425702000950, the Moderate Resolution Imaging Spectroradiometer (MODIS): a new generation of Land Surface Monitoring

Hamoudzadeh A, Belloni V, Ravanelli R (2026) Inferring height from earth embeddings: First insights using google alphaearth. 10.48550/ARXIV.2602.17250, URL https://arxiv.org/abs/2602.17250

Han B, Zhang S, Shi X, et al (2024) Bridging remote sensors with multisensor geospatial foundation models. In: Proceedings of the IEEE/CVF Conference on Computer Vision and Pattern Recognition (CVPR), pp 27852–27862

Han J, Zhang B, Sun X, et al (2026) Fusionrs: A large-scale rgb-infrared remote sensing dataset for dual-modal vision-language foundation models. URL https://arxiv.org/abs/2606.17020, arXiv:2606.17020

Han T, Chen H, Wang C, et al (2025) Towards a new era of geo-foundation models: Expert-guided multimodal alignment and geospatial context awareness. In: Proceedings of the 33rd ACM International Conference on Advances in Geographic Information Systems. ACM, SIGSPATIAL '25, p 454–465, 10.1145/3748636.3762756, URL http://dx.doi.org/10.1145/3748636.3762756

Hao X, Chen W, Zou X, et al (2025) Nature makes no leaps: Building continuous location embeddings with satellite imagery from the web. In: Proceedings of the ACM on Web Conference 2025. ACM, WWW '25, p 2799–2812, 10.1145/3696410.3714629, URL http://dx.doi.org/10.1145/3696410.3714629

Haralick RM, Shanmugam K, Dinstein I (1973) Textural features for image classification. IEEE Transactions on Systems, Man, and Cybernetics SMC-3(6):610–621. 10.1109/tsmc.1973.4309314, URL http://dx.doi.org/10.1109/tsmc.1973.4309314

He K, Zhang X, Ren S, et al (2016) Deep residual learning for image recognition. In: Proceedings of the IEEE Conference on Computer Vision and Pattern Recognition (CVPR)

He K, Fan H, Wu Y, et al (2020) Momentum contrast for unsupervised visual representation learning. In: 2020 IEEE/CVF Conference on Computer Vision and Pattern Recognition (CVPR). IEEE, p 9726–9735, 10.1109/cvpr42600.2020.00975, URL http://dx.doi.org/10.1109/cvpr42600.2020.00975

He K, Chen X, Xie S, et al (2022) Masked autoencoders are scalable vision learners. In: Proceedings of the IEEE/CVF Conference on Computer Vision and Pattern Recognition (CVPR), pp 16000–16009

Hecht J, Arzoumanidis L, Li Z, et al (2026) Multi-modal contrastive learning for implicit earth embeddings via location tying. 10.48550/ARXIV.2606.20167, URL https://arxiv.org/abs/2606.20167

Heidler K, Mou L, Hu D, et al (2023) Self-supervised audiovisual representation learning for remote sensing data. International Journal of Applied Earth Observation and Geoinformation 116:103130. 10.1016/j.jag.2022.103130, URL https://www.sciencedirect.com/science/article/pii/S1569843222003181

Heiman A (2026) Characterizing brazilian atlantic forest restoration outcomes with geospatial alphaearth embeddings. 10.48550/ARXIV.2605.05547, URL https://arxiv.org/abs/2605.05547

Herzog H, Bastani F, Zhang Y, et al (2026) Olmoearth: Stable latent image modeling for multimodal earth observation. In: Proceedings of the IEEE/CVF Conference on Computer Vision and Pattern Recognition (CVPR), pp 34806–34817

Higgins I, Matthey L, Pal A, et al (2017) beta-vae: Learning basic visual concepts with a constrained variational framework. In: 5th International Conference on Learning Representations, ICLR 2017, Toulon, France, April 24-26, 2017, Conference Track Proceedings. OpenReview.net, URL https://openreview.net/forum?id=Sy2fzU9gl

Hochreiter S, Schmidhuber J (1997) Long short-term memory. Neural Computation 9(8):1735–1780. 10.1162/neco.1997.9.8.1735, URL http://dx.doi.org/10.1162/neco.1997.9.8.1735

Hong D, Zhang B, Li X, et al (2024) Spectralgpt: Spectral remote sensing foundation model. IEEE Transactions on Pattern Analysis and Machine Intelligence 46(8):5227–5244. 10.1109/tpami.2024.3362475, URL http://dx.doi.org/10.1109/tpami.2024.3362475

Hossain MA, Patel AV, Dube N, et al (2026a) Cr-jepa: Cross-modal joint-embedding predictive learning for remote sensing image retrieval. 10.48550/ARXIV.2606.00706, URL https://arxiv.org/abs/2606.00706

Hossain MA, Patel AV, Singh SK, et al (2026b) Hq-jepa: Hybrid quantum joint-embedding predictive architecture for cross-modal remote sensing representation learning. 10.48550/ARXIV.2605.31068, URL https://arxiv.org/abs/2605.31068

Hou S, Liu Z, Jiao H, et al (2026) Aef-econ: Toward plug-and-play socioeconomic foundation embeddings from alphaearth for urban remote sensing. 10.48550/ARXIV.2606.20697, URL https://arxiv.org/abs/2606.20697

Irvin J, Tao L, Zhou J, et al (2023) Usat: A unified self-supervised encoder for multi-sensor satellite imagery. 10.48550/ARXIV.2312.02199, URL https://arxiv.org/abs/2312.02199

Jakubik J, Yang F, Blumenstiel B, et al (2025) Terramind: Large-scale generative multimodality for earth observation. In: Proceedings of the IEEE/CVF International Conference on Computer Vision (ICCV), pp 7383–7394

Jean N, Wang S, Samar A, et al (2019) Tile2vec: Unsupervised representation learning for spatially distributed data. Proceedings of the AAAI Conference on Artificial Intelligence 33(01):3967–3974. 10.1609/aaai.v33i01.33013967, URL http://dx.doi.org/10.1609/aaai.v33i01.33013967

Jégou H, Douze M, Schmid C (2011) Product quantization for nearest neighbor search. IEEE Transactions on Pattern Analysis and Machine Intelligence 33(1):117–128. 10.1109/tpami.2010.57, URL http://dx.doi.org/10.1109/tpami.2010.57

Jha A, Singha M, Bhattacharya A, et al (2025) Rs3lip: Consistency for remote sensing image classification on part embeddings using self-supervised learning and clip. Computer Vision and Image Understanding 251:104254. 10.1016/j.cviu.2024.104254, URL https://www.sciencedirect.com/science/article/pii/S1077314224003357

Ji R, Wang X, Niu C, et al (2026) Specaware: a spectral-content aware foundation model for unifying multi-sensor learning in hyperspectral remote sensing mapping. ISPRS Journal of Photogrammetry and Remote Sensing 234:242–260. 10.1016/j.isprsjprs.2026.02.024, URL https://www.sciencedirect.com/science/article/pii/S0924271626000754

Jiang J, Zhao W, Yan C, et al (2026) Transformer-based mapping of 10 m spatiotemporally seamless daily urban evapotranspiration using geospatial foundation embeddings 10.2139/ssrn.6539464, URL http://dx.doi.org/10.2139/ssrn.6539464

Jin C, Jiang X, Wen L, et al (2026) Assessing the utility of satellite embedding features for biomass prediction in subtropical forests with machine learning. Remote Sensing 18(3):436. 10.3390/rs18030436, URL http://dx.doi.org/10.3390/rs18030436

Jing K, Zhang M, Wu B, et al (2026) Distilling geospatial foundation model semantics into interpretable sentinel-1/2 proxies for few-shot and cross-year crop type classification. Big Earth Data p 1–30. 10.1080/20964471.2026.2691477, URL http://dx.doi.org/10.1080/20964471.2026.2691477

Jing L, Vincent P, LeCun Y, et al (2022) Understanding dimensional collapse in contrastive self-supervised learning. In: The Tenth International Conference on Learning Representations, ICLR 2022, Virtual Event, April 25-29, 2022. OpenReview.net, URL https://openreview.net/forum?id=YevsQ05DEN7

Johnson DP (2026) Calibrated spatial uncertainty for earth observation foundation models via matérn-motivated latent stochastic regularization. Remote Sensing of Environment 346:115610. 10.1016/j.rse.2026.115610, URL https://www.sciencedirect.com/science/article/pii/S0034425726003809

Jolliffe IT, Cadima J (2016) Principal component analysis: a review and recent developments. Philosophical Transactions of the Royal Society A: Mathematical, Physical and Engineering Sciences 374(2065):20150202. 10.1098/rsta.2015.0202, URL http://dx.doi.org/10.1098/rsta.2015.0202

Joseph MB, Mendes FDS, Nguyen DMT, et al (2026) Continuous biome representations from earth observation embeddings. 10.48550/ARXIV.2606.11510, URL https://arxiv.org/abs/2606.11510

Ju J, Zhou Q, Freitag B, et al (2025) The harmonized landsat and sentinel-2 version 2.0 surface reflectance dataset. Remote Sensing of Environment 324:114723. 10.1016/j.rse.2025.114723, URL http://dx.doi.org/10.1016/j.rse.2025.114723

Kaur A, Purohit M, Muhawenayo G, et al (2026) Pretrain where? investigating how pretraining data diversity impacts geospatial foundation model performance. URL https://arxiv.org/abs/2604.21104, arXiv:2604.21104

Ke G, Meng Q, Finley T, et al (2017) Lightgbm: A highly efficient gradient boosting decision tree. In: Guyon I, Luxburg UV, Bengio S, et al (eds) Advances in Neural Information Processing Systems, vol 30. Curran Associates, Inc., URL https://proceedings.neurips.cc/paper_files/paper/2017/file/6449f44a102fde848669bdd9eb6b76fa-Paper.pdf

Kerekes D, Wittmann I, Brune E, et al (2025) Fused foundation model embeddings for earth observation compression: A winning solution to the Embed2Scale challenge. In: Workshop on Advances in Representation Learning for Earth Observation (REO) at EurIPS, URL https://github.com/REO-workshop/2025-EurIPS-REO-workshop/blob/main/papers/Fused_Kerekes.pdf

Khajuria V, Singh S, Paro L, et al (2026) Rock glacier detection using satellite embeddings and machine learning on google earth engine. Earth Systems and Environment 10(8):10299–10321. 10.1007/s41748-026-01139-x, URL https://doi.org/10.1007/s41748-026-01139-x

Khan H, Ahmad A (2025) Evaluating alphaearth foundation embeddings for pixel- and object-based land cover classification in google earth engine 10.20944/preprints202511.2172.v1, URL http://dx.doi.org/10.20944/preprints202511.2172.v1

Khanna S, Liu P, Zhou L, et al (2024) Diffusionsat: A generative foundation model for satellite imagery. In: Kim B, Yue Y, Chaudhuri S, et al (eds) International Conference on Learning Representations, pp 5586–5604, URL https://proceedings.iclr.cc/paper_files/paper/2024/file/16c3c941409d0581286eff49b180930f-Paper-Conference.pdf

Kim MH, Park HM (2026) Cosmo: Contrastive satellite image embedding techniques reflecting expert weather bulletins. IEEE Access 14:92385–92398. 10.1109/access.2026.3702845, URL http://dx.doi.org/10.1109/access.2026.3702845

Klemmer K, Rolf E, Robinson C, et al (2025) Satclip: Global, general-purpose location embeddings with satellite imagery. Proceedings of the AAAI Conference on Artificial Intelligence 39(4):4347–4355. 10.1609/aaai.v39i4.32457, URL http://dx.doi.org/10.1609/aaai.v39i4.32457

Klemmer K, Rolf E, Russwurm M, et al (2026) Earth embeddings: Toward artificial intelligence-centric representations of our planet. IEEE Geoscience and Remote Sensing Magazine p 2–15. 10.1109/mgrs.2026.3710416, URL http://dx.doi.org/10.1109/mgrs.2026.3710416

Knoblauch S, Li H, Mai G, et al (2026) Spatial representation learning beyond pixels: Unifying raster data and vector semantics for human-centric geospatial foundation models. 10.48550/ARXIV.2606.02374, URL https://arxiv.org/abs/2606.02374

Koch J, Denager T, Stisen S, et al (2026) Modelling carbon and groundwater in peatlands using alphaearth embeddings 10.22541/essoar.177135853.32181864/v1, URL http://dx.doi.org/10.22541/essoar.177135853.32181864/v1

Kornblith S, Norouzi M, Lee H, et al (2019) Similarity of neural network representations revisited. In: Chaudhuri K, Salakhutdinov R (eds) Proceedings of the 36th International Conference on Machine Learning, Proceedings of Machine Learning Research, vol 97. PMLR, pp 3519–3529, URL https://proceedings.mlr.press/v97/kornblith19a.html

Krause A, Singh A, Guestrin C (2008) Near-optimal sensor placements in gaussian processes: Theory, efficient algorithms and empirical studies. Journal of Machine Learning Research 9(8):235–284. URL http://jmlr.org/papers/v9/krause08a.html

Kumari J, Singh AS (2026) emem: A research on content-addressed, verifiable earth-memory protocol for ai agents over foundation-model embeddings 10.5281/ZENODO.20706893, URL https://zenodo.org/doi/10.5281/zenodo.20706893

Lacoste A, Lehmann N, Rodriguez P, et al (2023) Geo-bench: Toward foundation models for earth monitoring. In: Oh A, Naumann T, Globerson A, et al (eds) Advances in Neural Information Processing Systems, vol 36. Curran Associates, Inc., pp 51080–51093, 10.52202/075280-2223, URL https://proceedings.neurips.cc/paper_files/paper/2023/file/a0644215d9cff6646fa334dfa5d29c5a-Paper-Datasets_and_Benchmarks.pdf

Lecun Y, Bottou L, Bengio Y, et al (1998) Gradient-based learning applied to document recognition. Proceedings of the IEEE 86(11):2278–2324. 10.1109/5.726791, URL http://dx.doi.org/10.1109/5.726791

Lee-Burkhart K, Hatanaka Y, Sadowski P, et al (2026) Geospatial foundation model embeddings improve land surface temperature recovery in the hawaiian islands 10.2139/ssrn.6462445, URL http://dx.doi.org/10.2139/ssrn.6462445

Leonardi JA, Marsocci V, Yordanov V, et al (2025) Integration of geospatial foundation models in unsupervised change detection workflows for landslide identification. International Journal of Digital Earth 18(1). 10.1080/17538947.2025.2547292, URL http://dx.doi.org/10.1080/17538947.2025.2547292

LGND AI (2026) LGND developer documentation: Getting started guide. https://lgnd.ai/lgnd-docs, accessed: 2026-08-02

LGND.ai (2026) LGND embeddings. Source Cooperative, https://source.coop/clay/lgnd-embeddings, accessed: Jul. 30, 2026

Li S, He Y, Yang D, et al (2026a) Incorporating learned geospatial embeddings to deep image prior for inpainting cloud areas in remotely sensed images. Science of Remote Sensing 13:100404. 10.1016/j.srs.2026.100404, URL https://www.sciencedirect.com/science/article/pii/S2666017226000428

Li W, Liang S, Chen K, et al (2026b) Agrifm: A multi-source temporal remote sensing foundation model for agriculture mapping. Remote Sensing of Environment 334:115234. 10.1016/j.rse.2026.115234, URL https://www.sciencedirect.com/science/article/pii/S0034425726000040

Li X, Yu L (2026) Mapping complex cropping patterns in china (2018–2021) at 10 m resolution: a data-driven framework based on multi-product integration and google satellite embedding. Earth System Science Data 18(7):5601–5626. 10.5194/essd-18-5601-2026, URL https://essd.copernicus.org/articles/18/5601/2026/

Li X, Tao Y, Zhang S, et al (2025) REOBench: Benchmarking Robustness of Earth Observation Foundation Models. In: Advances in Neural Information Processing Systems, URL https://mlanthology.org/neurips/2025/li2025neurips-reobench/

Li X, Li C, Vivone G, et al (2026c) Seamo: A season-aware multimodal foundation model for remote sensing. Information Fusion 125:103334. 10.1016/j.inffus.2025.103334, URL https://www.sciencedirect.com/science/article/pii/S1566253525004075

Liang VW, Zhang Y, Kwon Y, et al (2022) Mind the gap: Understanding the modality gap in multi-modal contrastive representation learning. In: Advances in Neural Information Processing Systems 35. Neural Information Processing Systems Foundation, Inc. (NeurIPS), NeurIPS 2022, p 17612–17625, 10.52202/068

431-1280, URL http://dx.doi.org/10.52202/068431-1280

Lin H, Lin P, Zhang F, et al (2026) Fusing satellite embeddings to improve streamflow reconstruction across river networks. EGUsphere 2026:1–26. 10.5194/egusphere-2026-1834, URL https://egusphere.copernicus.org/preprints/2026/egusphere-2026-1834/

Lisaius MC, Keshav S, Blake A, et al (2026) Embedding -based crop type classification in the groundnut basin of senegal. 10.48550/ARXIV.2601.16900, URL https://arxiv.org/abs/2601.16900

Liu F, Chen D, Guan Z, et al (2024) Remoteclip: A vision language foundation model for remote sensing. IEEE Transactions on Geoscience and Remote Sensing 62:1–16. 10.1109/tgrs.2024.3390838, URL http://dx.doi.org/10.1109/tgrs.2024.3390838

Liu W, Li S, Shi C, et al (2026a) Landslide mapping and susceptibility assessment in the middle and lower reaches of the nujiang river (2017–2025) using satellite embedding and multidimensional environmental factors. Remote Sensing 18(11):1854. 10.3390/rs18111854, URL http://dx.doi.org/10.3390/rs18111854

Liu W, Shu Q, Zhang H, et al (2026b) Satellite embedding features for grassland aboveground biomass estimation in complex mountainous terrain: A case study of the three parallel rivers region, china. Remote Sensing 18(14):2348. 10.3390/rs18142348, URL http://dx.doi.org/10.3390/rs18142348

Liu Z, Mao H, Wu CY, et al (2022) A convnet for the 2020s. In: 2022 IEEE/CVF Conference on Computer Vision and Pattern Recognition (CVPR). IEEE, p 11966–11976, 10.1109/cvpr52688.2022.01167, URL http://dx.doi.org/10.1109/cvpr52688.2022.01167

Liu Z, Lao N, Wang Z, et al (2026c) Gair: Location-aware self-supervised contrastive pre-training with geo-aligned implicit representations. ISPRS Journal of Photogrammetry and Remote Sensing 237:166–182. 10.1016/j.isprsjprs.2026.04.035, URL https://www.sciencedirect.com/science/article/pii/S092427162600208X

Locatello F, Bauer S, Lucic M, et al (2019) Challenging common assumptions in the unsupervised learning of disentangled representations. In: Chaudhuri K, Salakhutdinov R (eds) Proceedings of the 36th International Conference on Machine Learning, Proceedings of Machine Learning Research, vol 97. PMLR, pp 4114–4124, URL https://proceedings.mlr.press/v97/locatello19a.html

Lyu J, Yang M, Cai J, et al (2026) Structure-semantic decoupled modulation of global geospatial embeddings for high-resolution remote sensing mapping. 10.48550/ARXIV.2604.19591, URL https://arxiv.org/abs/2604.19591

Ma Y, Shen Y, Swatantran A, et al (2026) Harvesting alphaearth: Benchmarking the geospatial foundation model for agricultural downstream tasks. International Journal of Applied Earth Observation and Geoinformation 149:105258. 10.1016/j.jag.2026.105258, URL https://www.sciencedirect.com/science/article/pii/S1569843226001743

Mañas O, Lacoste A, Giró-i Nieto X, et al (2021) Seasonal contrast: Unsupervised pre-training from uncurated remote sensing data. In: Proceedings of the IEEE/CVF International Conference on Computer Vision (ICCV), pp 9414–9423

Maffei T, Moretto M, Franceschi P (2026) Exploring tessera earth embeddings latent space: a regional unsupervised openstreetmap's landuse classification and topographic characterization 10.2139/ssrn.6578542, URL http://dx.doi.org/10.2139/ssrn.6578542

Mahato T, Sarkar S, Parida BR, et al (2026) Beyond multispectral limits: Satellite embeddings for fire severity estimation across global biomes 10.21203/rs.3.rs-9849270/v1, URL http://dx.doi.org/10.21203/rs.3.rs-9849270/v1

Mahlasi C, Baloyi GS, Gaffoor Z, et al (2026) Ecological mapping with geospatial foundation models. 10.48550/ARXIV.2602.10720, URL https://arxiv.org/abs/2602.10720

Mai G, Janowicz K, Yan B, et al (2020) Multi-scale representation learning for spatial feature distributions using grid cells. In: The Eighth International Conference on Learning Representations, openreview

Mai G, Lao N, He Y, et al (2023a) CSP: Self-supervised contrastive spatial pre-training for geospatial-visual representations. In: Krause A, Brunskill E, Cho K, et al (eds) Proceedings of the 40th International Conference on Machine Learning, Proceedings of Machine Learning Research, vol 202. PMLR, pp 23498–23515, URL https://proceedings.mlr.press/v202/mai23a.html

Mai G, Xuan Y, Zuo W, et al (2023b) Sphere2vec: A general-purpose location representation learning over a spherical surface for large-scale geospatial predictions. ISPRS Journal of Photogrammetry and Remote Sensing 202:439–462. 10.1016/j.isprsjprs.2023.06.016, URL https://www.sciencedirect.com/science/article/pii/S0924271623001818

Mai G, Huang W, Sun J, et al (2024) On the opportunities and challenges of foundation models for geoai (vision paper). ACM Transactions on Spatial Algorithms and Systems 10(2):1–46. 10.1145/3653070, URL http://dx.doi.org/10.1145/3653070

Mall U, Hariharan B, Bala K (2023) Change-aware sampling and contrastive learning for satellite images. In: Proceedings of the IEEE/CVF Conference on Computer Vision and Pattern Recognition (CVPR), pp 5261–5270

Mall UK, Phoo CP, Liu M, et al (2024) Remote sensing vision-language foundation models without annotations via ground remote alignment. In: Kim B, Yue Y, Chaudhuri S, et al (eds) International Conference on Learning Representations, pp 49294–49314, URL https://proceedings.iclr.cc/paper_files/paper/2024/file/d6c53fe062716387ff0df73cc53de60c-Paper-Conference.pdf

Mantey S, Attipoe IS, Alhassan A (2025) A comparative analysis of satellite imagery for land cover classification: Evaluating google satellite embeddings, sentinel-2, and landsat-8 data with xgboost 10.21203/rs.3.rs-7961146/v1, URL http://dx.doi.org/10.21203/rs.3.rs-7961146/v1

Mantey S, Attipoe ISK, Lawerteh JK (2026) Boosting algorithm: An ensemble learning tool for land use land cover classification using google alpha earth foundations satellite embeddings. Advances in Remote Sensing 15(01):1–22. 10.4236/ars.2026.151001, URL http://dx.doi.org/10.4236/ars.2026.151001

Marsocci V, Jia Y, Bellier GL, et al (2026) Pangaea: Assessing geospatial foundation models capabilities through a global and inclusive benchmark. IEEE Geoscience and Remote Sensing Magazine 14(1):245–285. 10.1109/mgrs.2025.3628194, URL http://dx.doi.org/10.1109/mgrs.2025.3628194

McFEETERS SK (1996) The use of the normalized difference water index (ndwi) in the delineation of open water features. International Journal of Remote Sensing 17(7):1425–1432. 10.1080/01431169608948714, URL http://dx.doi.org/10.1080/01431169608948714

McInnes L, Healy J, Saul N, et al (2018) Umap: Uniform manifold approximation and projection. Journal of Open Source Software 3(29):861. 10.21105/joss.00861, URL https://doi.org/10.21105/joss.00861

Mentzer F, Minnen D, Agustsson E, et al (2024) Finite scalar quantization: Vq-vae made simple. In: Kim B, Yue Y, Chaudhuri S, et al (eds) International Conference on Learning Representations, pp 51772–51783, URL https://proceedings.iclr.cc/paper_files/paper/2024/file/e2dd53601de57c773343a7cdf09fae1c-Paper-Conference.pdf

Meraner A, Ebel P, Zhu XX, et al (2020) Cloud removal in sentinel-2 imagery using a deep residual neural network and sar-optical data fusion. ISPRS Journal of Photogrammetry and Remote Sensing 166:333–346. 10.1016/j.isprsjprs.2020.05.013, URL https://www.sciencedirect.com/science/article/pii/S0924271620301398

Michail D, Saka E, Giannopoulos I, et al (2026) Osmgraphclip: Learning global location representations from openstreetmap graphs. 10.48550/ARXIV.2606.08046, URL https://arxiv.org/abs/2606.08046

Mingxuan Li, Wenkai Li, Hongliang Liu, et al (2026) Leveraging geospatial foundation model embeddings for local-scale landslide susceptibility mapping via positive-unlabeled learning 10.13140/RG.2.2.18370.34244, URL https://www.researchgate.net/doi/10.13140/RG.2.2.18370.34244

Mura M, Mura M, Puletti N, et al (2026) Operational deployment of satellite embeddings for forestry: An evaluation 10.2139/ssrn.6362220, URL http://dx.doi.org/10.2139/ssrn.6362220

Narimani M, Pourreza A, Farajpoor P (2026) Mapping tomato cropping systems in california using alphaearth geospatial embeddings and deep learning analysis. 10.48550/ARXIV.2605.21804, URL https://arxiv.org/abs/2605.21804

NASA/METI/AIST/Japan Spacesystems and U.S./Japan ASTER Science Team (2019) Aster global digital elevation model v003. 10.5067/ASTER/ASTGTM.003, URL https://www.earthdata.nasa.gov/data/catalog/lpcloud-astgtm-003

Nazir U, Cheng IH, Khalid S (2026) Alphaearth satellite embeddings for modelling climate sensitive diseases towards global health resilience. 10.48550/ARXIV.2605.10949, URL https://arxiv.org/abs/2605.10949

Nedungadi V, Kariryaa A, Oehmcke S, et al (2025) Mmearth: Exploring multi-modal pretext tasks for geospatial representation learning. In: Leonardis A, Ricci E, Roth S, et al (eds) Computer Vision – ECCV 2024. Springer Nature Switzerland, Cham, pp 164–182

Neuenschwander A, Pitts K, Jelley B, et al (2025) Atlas/icesat-2 l3a land and vegetation height, version 7. 10.5067/ATLAS/ATL08.007, URL http://nsidc.org/data/ATL08/versions/7

Neumann M, Pinto AS, Zhai X, et al (2020) In-domain representation learning for remote sensing. In: AI for Earth Sciences Workshop at International Conference on Learning Representations (ICLR), pp 1–20, URL https://arxiv.org/abs/1911.06721

Ojala T, Pietikainen M, Maenpaa T (2002) Multiresolution gray-scale and rotation invariant texture classification with local binary patterns. IEEE Transactions on Pattern Analysis and Machine Intelligence 24(7):971–987. 10.1109/tpami.2002.1017623, URL http://dx.doi.org/10.1109/tpami.2002.1017623

Oord Avd, Li Y, Vinyals O (2018) Representation learning with contrastive predictive coding. 10.48550/ARXIV.1807.03748, URL https://arxiv.org/abs/1807.03748

Oquab M, Darcet T, Moutakanni T, et al (2024) Dinov2: Learning robust visual features without supervision. Trans Mach Learn Res 2024. URL https://openreview.net/forum?id=a68SUt6zFt

Ou Z, Zheng Y (2026) Foundation-scale satellite embeddings reframe hydrological generalization as a representation problem. Geophysical Research Letters 53(7). 10.1029/2025gl121604, URL http://dx.doi.org/10.1029/2025gl121604

Paluba D, Marsocci V, Onačillová K, et al (2026) Gem-forest: A global satellite embedding–based map of forests and tree crops for 2020 10.5194/egusphere-2026-1401-v1, URL http://dx.doi.org/10.5194/egusphere-2026-1401-v1

Park H, Seo M, Choi DG (2026) Rethinking electro-optical vision foundation models for remote sensing retrieval: A controlled comparison with generalist vfm. 10.48550/ARXIV.2605.02283, URL https://arxiv.org/abs/2605.02283

Pasupuleti MK (2023) Ai climate risk in arcgis: Foundation-model remote sensing and spatio-temporal causality. International Journal of Academic and Industrial Research Innovations(IJAIRI) 03(12):114–126. 10.62311/nesx/rp-301223-114-126, URL http://dx.doi.org/10.62311/nesx/rp-301223-114-126

Paszke A, Gross S, Massa F, et al (2019) Pytorch: An imperative style, high-performance deep learning library. In: Wallach H, Larochelle H, Beygelzimer A, et al (eds) Advances in Neural Information Processing Systems, vol 32. Curran Associates, Inc., URL https://proceedings.neurips.cc/paper_files/paper/2019/file/bdbca288fee7f92f2bfa9f7012727740-Paper.pdf

Pedregosa F, Varoquaux G, Gramfort A, et al (2011) Scikit-learn: Machine learning in python. Journal of Machine Learning Research 12(85):2825–2830. URL http://jmlr.org/papers/v12/pedregosa11a.html

Pettersson MB, Daoud A (2025) Leveraging compact satellite embeddings and graph neural networks for large-scale poverty mapping. 10.48550/ARXIV.2511.01408, URL https://arxiv.org/abs/2511.01408

van der Plas TL, Bakermans JJW, Athanasiadis IN (2025) NeurEO: dissecting Earth observation embeddings with computational neuroscience. In: Workshop on Advances in Representation Learning for Earth Observation (REO) at EurIPS, URL https://github.com/REO-workshop/2025-EurIPS-REO-workshop/blob/main/papers/NeurEO_Plas.pdf

van der Plas TL, Bakermans JJ, Nedungadi V, et al (2026) Better together: Evaluating the complementarity of earth embedding models. URL https://arxiv.org/abs/2605.18667, arXiv:2605.18667

Priem J, Piwowar H, Orr R (2022) Openalex: A fully-open index of scholarly works, authors, venues, institutions, and concepts 10.5281/ZENODO.6936227, URL https://zenodo.org/record/6936227

Prokhorenkova L, Gusev G, Vorobev A, et al (2018) Catboost: unbiased boosting with categorical features. In: Bengio S, Wallach H, Larochelle H, et al (eds) Advances in Neural Information Processing Systems, vol 31. Curran Associates, Inc., URL https://proceedings.neurips.cc/paper_files/paper/2018/file/14491b756b3a51daac41c24863285549-Paper.pdf

Puriy N, Jakubik J, Blumenstiel B, et al (2026) Terraflow: Multimodal, multitemporal representation learning for earth observation. 10.48550/ARXIV.2603.12762, URL https://arxiv.org/abs/2603.12762

Qi W, Yu L, Liu T, et al (2026) Integrating hyperspectral data and google satellite embedding features for aquatic fish biodiversity prediction. Journal of Remote Sensing 6. 10.34133/remotesensing.1069, URL http://dx.doi.org/10.34133/remotesensing.1069

Qin X, Wang D, Zhang J, et al (2025) Timo: Spatiotemporal foundation model for satellite image time series. 10.48550/ARXIV.2505.08723, URL https://arxiv.org/abs/2505.08723

Qu P, Ouyang W, Zhang C, et al (2026) Utilizing earth foundation models to enhance the simulation performance of hydrological models with alphaearth embeddings. 10.48550/ARXIV.2601.01558, URL https://arxiv.org/abs/2601.01558

Radford A, Kim JW, Hallacy C, et al (2021) Learning transferable visual models from natural language supervision. In: Meila M, Zhang T (eds) Proceedings of the 38th International Conference on Machine Learning, Proceedings of Machine Learning Research, vol 139. PMLR, pp 8748–8763, URL https://proceedings.mlr.press/v139/radford21a.html

Rahman M (2026) Physically interpretable alphaearth foundation model embeddings enable llm-based land surface intelligence. Remote Sensing Applications: Society and Environment 42:102045. 10.1016/j.rsase.2026.102045, URL https://www.sciencedirect.com/science/article/pii/S2352938526001783

Raissi M, Perdikaris P, Karniadakis G (2019) Physics-informed neural networks: A deep learning framework for solving forward and inverse problems involving nonlinear partial differential equations. Journal of Computational Physics 378:686–707. 10.1016/j.jcp.2018.10.045, URL https://www.sciencedirect.com/science/article/pii/S0021999118307125

Rao A, Crasto R, Ooms T, et al (2026a) Localized, high-resolution geographic representations with slepian functions. In: Forty-third International Conference on Machine Learning, URL https://openreview.net/forum?id=eWQQ0tO0kB

Rao A, Rußwurm M, Klemmer K, et al (2026b) Measuring the intrinsic dimension of earth representations. In: Vondrick C, Hariharan B, Raffel C, et al (eds) International Conference on Learning Representations, pp 113200–113224, URL https://proceedings.iclr.cc/paper_files/paper/2026/file/b7dc580d26f294d48d6cf77c706f1c0f-Paper-Conference.pdf

Ravirathinam P, Parthasarathy A, Khandelwal A, et al (2026) Towards knowledge guided pretraining approaches for multimodal foundation models: Applications in remote sensing. ACM Transactions on Spatial Algorithms and Systems 10.1145/3806229, URL http://dx.doi.org/10.1145/3806229

Reed CJ, Gupta R, Li S, et al (2023) Scale-mae: A scale-aware masked autoencoder for multiscale geospatial representation learning. In: Proceedings of the IEEE/CVF International Conference on Computer Vision (ICCV), pp 4088–4099

Reichstein M, Camps-Valls G, Stevens B, et al (2019) Deep learning and process understanding for data-driven earth system science. Nature 566(7743):195–204. 10.1038/s41586-019-0912-1, URL https://doi.org/10.1038/s41586-019-0912-1

Rolf E, Proctor J, Carleton T, et al (2021) A generalizable and accessible approach to machine learning with global satellite imagery. Nature Communications 12(1):4392. 10.1038/s41467-021-24638-z, URL https://doi.org/10.1038/s41467-021-24638-z

Rolf E, Klemmer K, Robinson C, et al (2024) Position: Mission critical – satellite data is a distinct modality in machine learning. In: Salakhutdinov R, Kolter Z, Heller K, et al (eds) Proceedings of the 41st International Conference on Machine Learning, Proceedings of Machine Learning Research, vol 235. PMLR, pp 42691–42706, URL https://proceedings.mlr.press/v235/rolf24a.html

Rolf E, Klemmer K, Rußwurm M (2025) Earth embeddings: Harnessing the information in earth observation data with machine learning. In: Proceedings of the Special Interest Group on Computer Graphics and Interactive Techniques Conference Frontiers. ACM, SIGGRAPH Frontiers '25, p 1–2, 10.1145/3736539.3754446, URL http://dx.doi.org/10.1145/3736539.3754446

Ronneberger O, Fischer P, Brox T (2015) U-net: Convolutional networks for biomedical image segmentation. In: Navab N, Hornegger J, Wells WM, et al (eds) Medical Image Computing and Computer-Assisted Intervention – MICCAI 2015. Springer International Publishing, Cham, pp 234–241

Rosenqvist A, Shimada M, Suzuki S, et al (2014) Operational performance of the alos global systematic acquisition strategy and observation plans for alos-2 palsar-2. Remote Sensing of Environment 155:3–12. 10.1016/j.rse.2014.04.011, URL https://www.sciencedirect.com/science/article/pii/S0034425714001497

Rußwurm M, Klemmer K, Rolf E, et al (2024) Geographic location encoding with spherical harmonics and sinusoidal representation networks. In: Kim B, Yue Y, Chaudhuri S, et al (eds) International Conference on Learning Representations, pp 1746–1759, URL https://proceedings.iclr.cc/paper_files/paper/2024/file/073c8584ef86bee26fe9d639ec648e28-Paper-Conference.pdf

Muñoz Sabater J, Dutra E, Agustí-Panareda A, et al (2021) Era5-land: a state-of-the-art global reanalysis dataset for land applications. Earth System Science Data 13(9):4349–4383. 10.5194/essd-13-4349-2021, URL https://essd.copernicus.org/articles/13/4349/2021/

Santoro M, Cartus O (2023) Esa biomass climate change initiative (biomass_cci): Global datasets of forest above-ground biomass for the years 2010, 2017, 2018, 2019 and 2020, v4. 10.5285/AF60720C1E404A9E9D

2C145D2B2EAD4E, URL https://catalogue.ceda.ac.uk/uuid/af60720c1e404a9e9d2c145d2b2ead4e

Schmitt M, Hughes LH, Qiu C, et al (2019) Sen12ms – a curated dataset of georeferenced multi-spectral sentinel-1/2 imagery for deep learning and data fusion. ISPRS Annals of the Photogrammetry, Remote Sensing and Spatial Information Sciences IV-2/W7:153–160. 10.5194/isprs-annals-IV-2-W7-153-2019, URL https://isprs-annals.copernicus.org/articles/IV-2-W7/153/2019/

Schönemann PH (1966) A generalized solution of the orthogonal procrustes problem. Psychometrika 31(1):1–10. 10.1007/BF02289451, URL https://doi.org/10.1007/BF02289451

Shang Z, Das S, Eldawy A (2026) Benchmarking geospatial foundation models for agriculture applications. 10.48550/ARXIV.2606.29664, URL https://arxiv.org/abs/2606.29664

Shen Y, Xiong Y, Xia W, et al (2020) Towards backward-compatible representation learning. In: 2020 IEEE/CVF Conference on Computer Vision and Pattern Recognition (CVPR). IEEE, p 6367–6376, 10.1109/cvpr42600.2020.00640, URL http://dx.doi.org/10.1109/cvpr42600.2020.00640

Sherman L, Proctor J, Druckenmiller H, et al (2026) Global high-resolution estimates of the un human development index using satellite imagery and machine learning. Nature Communications 17(1):1315. 10.1038/s41467-026-68805-6, URL https://doi.org/10.1038/s41467-026-68805-6

Silva L, Gonçalves J (2026) Evaluating alphaearth and tessera geospatial embeddings for machine learning-based burned area mapping in portugal. 10.5281/ZENODO.21252157, URL https://zenodo.org/doi/10.5281/zenodo.21252157

Sim S (2026) Embedding-only uplink for onboard retrieval under shift in remote sensing. IEEE Geoscience and Remote Sensing Letters 23:8500205–8500205. 10.1109/lgrs.2026.3718430, URL http://dx.doi.org/10.1109/lgrs.2026.3718430

Siméoni O, Vo HV, Seitzer M, et al (2025) Dinov3. URL https://arxiv.org/abs/2508.10104, arXiv:2508.10104

Simonyan K, Zisserman A (2015) Very deep convolutional networks for large-scale image recognition. In: International Conference on Learning Representations

Simumba N, Lehmann N, Fraccaro P, et al (2026) GEO-bench-2: From performance to capability, rethinking evaluation in geospatial AI. Transactions on Machine Learning Research URL https://openreview.net/forum?id=NPf175jnP1

Smith MJ, Fleming L, Geach J (2023) Earthpt: a foundation model for earth observation. In: NeurIPS 2023 Workshop on Tackling Climate Change with Machine Learning, URL https://www.climatechange.ai/papers/neurips2023/2

Sohrabi H (2026) Integrating satellite embeddings and national forest inventory data to map above-ground biomass of temperate deciduous old-growth forests. Advances in Space Research 77(12):11837–11850. 10.1016/j.asr.2026.04.018, URL https://www.sciencedirect.com/science/article/pii/S0273117726004874

Source Cooperative (2026) Source cooperative documentation. https://docs.source.coop/, accessed: Jul. 30, 2026

Stewart AJ, Robinson C, Corley IA, et al (2022) Torchgeo: deep learning with geospatial data. In: Proceedings of the 30th International Conference on Advances in Geographic Information Systems. ACM, SIGSPATIAL '22, p 1–12, 10.1145/3557915.3560953, URL http://dx.doi.org/10.1145/3557915.3560953

Stewart AJ, Fang H, Corley IA, et al (2026) Earth embeddings. 10.48550/ARXIV.2608.03410, URL https://arxiv.org/abs/2608.03410

Strelnikov I, Ostapko V, Ibatulina Y (2025) Testing the applicability of foundational satellite data embedding models for remote identification of dominant species in herbaceous communities 10.5281/ZENODO.17800714, URL https://zenodo.org/doi/10.5281/zenodo.17800714

Sun X, Wang P, Lu W, et al (2023) Ringmo: A remote sensing foundation model with masked image modeling. IEEE Transactions on Geoscience and Remote Sensing 61:1–22. 10.1109/tgrs.2022.3194732, URL http://dx.doi.org/10.1109/tgrs.2022.3194732

Sun Y, Ming Y, Zhu X, et al (2022) Out-of-distribution detection with deep nearest neighbors. In: Chaudhuri K, Jegelka S, Song L, et al (eds) Proceedings of the 39th International Conference on Machine Learning, Proceedings of Machine Learning Research, vol 162. PMLR, pp 20827–20840, URL https://proceedings.mlr.press/v162/sun22d.html

Sun Y, Xue Z, Wu H, et al (2026) The first map of planted mangrove forests in china derived from time-series landsat and google satellite embeddings. Remote Sensing of Environment 344:115541. 10.1016/j.rse.2026.1

15541, URL https://www.sciencedirect.com/science/article/pii/S0034425726003111

Szwarcman D, Roy S, Fraccaro P, et al (2026) Prithvi-eo-2.0: A versatile multitemporal foundation model for earth observation applications. IEEE Transactions on Geoscience and Remote Sensing 64:1–20. 10.1109/tgrs.2025.3642610, URL http://dx.doi.org/10.1109/tgrs.2025.3642610

Tarasiou M, Zafeiriou S (2022) Embedding earth: Self-supervised contrastive pre-training for dense land cover classification. 10.48550/ARXIV.2203.06041, URL https://arxiv.org/abs/2203.06041

Toker A, Kondmann L, Weber M, et al (2022) Dynamicearthnet: Daily multi-spectral satellite dataset for semantic change segmentation. In: Proceedings of the IEEE/CVF Conference on Computer Vision and Pattern Recognition (CVPR), pp 21158–21167

Tolan J, Yang HI, Nosarzewski B, et al (2024) Very high resolution canopy height maps from rgb imagery using self-supervised vision transformer and convolutional decoder trained on aerial lidar. Remote Sensing of Environment 300:113888. 10.1016/j.rse.2023.113888, URL http://dx.doi.org/10.1016/j.rse.2023.113888

Tom M, Jiang Y, Baltsavias E, et al (2022) Learning a joint embedding of multiple satellite sensors: A case study for lake ice monitoring. IEEE Transactions on Geoscience and Remote Sensing 60:1–15. 10.1109/tgrs.2022.3211184, URL http://dx.doi.org/10.1109/tgrs.2022.3211184

TorchGeo (2026) TorchGeo v0.9.0. GitHub release, https://github.com/torchgeo/torchgeo/releases/tag/v0.9.0, accessed: Jul. 30, 2026

Torres R, Snoeij P, Geudtner D, et al (2012) Gmes sentinel-1 mission. Remote Sensing of Environment 120:9–24. 10.1016/j.rse.2011.05.028, URL https://www.sciencedirect.com/science/article/pii/S0034425712000600, the Sentinel Missions - New Opportunities for Science

Tseng G, Cartuyvels R, Zvonkov I, et al (2023) Lightweight, pre-trained transformers for remote sensing timeseries. In: NeurIPS 2023 Workshop on Tackling Climate Change with Machine Learning, URL https://www.climatechange.ai/papers/neurips2023/58

Tseng G, Fuller A, Reil M, et al (2025) Galileo: Learning global & local features of many remote sensing modalities. In: Singh A, Fazel M, Hsu D, et al (eds) Proceedings of the 42nd International Conference on Machine Learning, Proceedings of Machine Learning Research, vol 267. PMLR, pp 60280–60300, URL https://proceedings.mlr.press/v267/tseng25a.html

Tucker CJ (1979) Red and photographic infrared linear combinations for monitoring vegetation. Remote Sensing of Environment 8(2):127–150. 10.1016/0034-4257(79)90013-0, URL http://dx.doi.org/10.1016/0034-4257(79)90013-0

Tuia D, Roscher R, Wegner JD, et al (2021) Toward a collective agenda on ai for earth science data analysis. IEEE Geoscience and Remote Sensing Magazine 9(2):88–104. 10.1109/mgrs.2020.3043504, URL http://dx.doi.org/10.1109/mgrs.2020.3043504

Van Etten A, Hogan D, Manso JM, et al (2021) The multi-temporal urban development spacenet dataset. In: Proceedings of the IEEE/CVF Conference on Computer Vision and Pattern Recognition (CVPR), pp 6398–6407

Vinge R, Wittmann I, Schneider J, et al (2026) Neuco-bench: A novel benchmark framework for neural embeddings in earth observation. In: Proceedings of the IEEE/CVF Conference on Computer Vision and Pattern Recognition (CVPR) Workshops, pp 8063–8074

Vivanco Cepeda V, Nayak GK, Shah M (2023) Geoclip: Clip-inspired alignment between locations and images for effective worldwide geo-localization. In: Oh A, Naumann T, Globerson A, et al (eds) Advances in Neural Information Processing Systems, vol 36. Curran Associates, Inc., pp 8690–8701, 10.52202/075280-0379, URL https://proceedings.neurips.cc/paper_files/paper/2023/file/1b57aaddf85ab01a2445a79c9edc1f4b-Paper-Conference.pdf

Volpi M, Tuia D (2017) Dense semantic labeling of subdecimeter resolution images with convolutional neural networks. IEEE Transactions on Geoscience and Remote Sensing 55(2):881–893. 10.1109/tgrs.2016.2616585, URL http://dx.doi.org/10.1109/tgrs.2016.2616585

Vu HB (2026) Clay-cnn hybrids: Leveraging geospatial foundation models as auxiliary context for landslide detection. 10.48550/ARXIV.2606.14081, URL https://arxiv.org/abs/2606.14081

Waldmann L, Shah A, Wang Y, et al (2025) Panopticon: Advancing any-sensor foundation models for earth observation. In: Proceedings of the IEEE/CVF Conference on Computer Vision and Pattern Recognition (CVPR) Workshops, pp 2229–2239

Walsh J, Fawcett W, Colvard G, et al (2026) Zero-shot satellite image retrieval through joint embeddings: Application to crisis response 10.56272/a2c9ee39, URL http://dx.doi.org/10.56272/a2c9ee39

Wang L (2026) Satellite embedding: A review 10.31223/x54r20, URL http://dx.doi.org/10.31223/x54r20

Wang T, Isola P (2020) Understanding contrastive representation learning through alignment and uniformity on the hypersphere. In: III HD, Singh A (eds) Proceedings of the 37th International Conference on Machine Learning, Proceedings of Machine Learning Research, vol 119. PMLR, pp 9929–9939, URL https://proceedings.mlr.press/v119/wang20k.html

Wang W, Guo H, He S, et al (2026a) Ai-driven precision mapping of tea plantations using alphaearth foundations: A scalable solution for smart agricultural monitoring. Agriculture 16(4):412. 10.3390/agriculture16040412, URL http://dx.doi.org/10.3390/agriculture16040412

Wang Y, Braham NAA, Xiong Z, et al (2023) Ssl4eo-s12: A large-scale multimodal, multitemporal dataset for self-supervised learning in earth observation [software and data sets]. IEEE Geoscience and Remote Sensing Magazine 11(3):98–106. 10.1109/mgrs.2023.3281651, URL http://dx.doi.org/10.1109/mgrs.2023.3281651

Wang Y, Albrecht CM, Zhu XX (2024a) Multilabel-guided soft contrastive learning for efficient earth observation pretraining. IEEE Transactions on Geoscience and Remote Sensing 62:1–16. 10.1109/tgrs.2024.3466896, URL http://dx.doi.org/10.1109/tgrs.2024.3466896

Wang Y, Albrecht CM, Braham NAA, et al (2025a) Decoupling common and unique representations for multimodal self-supervised learning. In: Leonardis A, Ricci E, Roth S, et al (eds) Computer Vision – ECCV 2024. Springer Nature Switzerland, Cham, pp 286–303

Wang Y, Xiong Z, Liu C, et al (2025b) Towards a unified copernicus foundation model for earth vision. In: 2025 IEEE/CVF International Conference on Computer Vision (ICCV). IEEE, p 9888–9899, 10.1109/iccv51701.2025.00922, URL http://dx.doi.org/10.1109/iccv51701.2025.00922

Wang Z, Prabha R, Huang T, et al (2024b) Skyscript: A large and semantically diverse vision-language dataset for remote sensing. Proceedings of the AAAI Conference on Artificial Intelligence 38(6):5805–5813. 10.1609/aaai.v38i6.28393, URL http://dx.doi.org/10.1609/aaai.v38i6.28393

Wang Z, Lane K, Cai L, et al (2026b) A proxy consistency loss for grounded fusion of earth observation and location encoders. URL https://arxiv.org/abs/2604.18881, arXiv:2604.18881

Watt MS, Holdaway A, Marchant JS, et al (2026) National-scale forest aboveground biomass mapping in guyana using stability-based feature selection and geospatial embeddings. Forests 17(6):725. 10.3390/f17060725, URL http://dx.doi.org/10.3390/f17060725

Wei Y, Zhong R, Yang Y (2025) Groundwater fluoride prediction for sustainable water management: A comparative evaluation of machine learning approaches enhanced by satellite embeddings. Sustainability 17(18):8505. 10.3390/su17188505, URL http://dx.doi.org/10.3390/su17188505

Wen Y, Cai J, Ma Q, et al (2026) Mora: Mobility as the backbone for geospatial representation learning at scale. In: Vondrick C, Hariharan B, Raffel C, et al (eds) International Conference on Learning Representations, pp 37647–37664, URL https://proceedings.iclr.cc/paper_files/paper/2026/file/3f3f2d552b22bf985f8d3f91caa0b610-Paper-Conference.pdf

Wu N, Cao Q, Wang Z, et al (2024) Torchspatial: A location encoding framework and benchmark for spatial representation learning. In: Globerson A, Mackey L, Belgrave D, et al (eds) Advances in Neural Information Processing Systems, vol 37. Curran Associates, Inc., pp 81437–81460, 10.52202/079017-2588, URL https://proceedings.neurips.cc/paper_files/paper/2024/file/9449c2d5b0cc8c9a445752f3ff195a1c-Paper-Datasets_and_Benchmarks_Track.pdf

Wu Q (2026) Geoai: A python package for integrating artificial intelligence with geospatial data analysis and visualization. Journal of Open Source Software 11(118):9605. 10.21105/joss.09605, URL https://doi.org/10.21105/joss.09605

Xiao A, Xuan W, Wang J, et al (2025) Foundation models for remote sensing and earth observation: A survey. IEEE Geoscience and Remote Sensing Magazine 13(4):297–324. 10.1109/mgrs.2025.3576766, URL http://dx.doi.org/10.1109/mgrs.2025.3576766

Xiong Z, Wang Y, Zhang F, et al (2024) Neural plasticity-inspired multimodal foundation model for earth observation. 10.48550/ARXIV.2403.15356, URL https://arxiv.org/abs/2403.15356

Xu Z, Tang R, Bianco M, et al (2025) Geospatial foundational embedder: Top-1 winning solution on earthvision embed2scale challenge (cvpr 2025). URL https://arxiv.org/abs/2509.06993, arXiv:2509.06993

Yang H, Xia J, Zhang J (2026a) Deep feature fusion of alphaearth foundations satellite embeddings and sentinel-2 imagery for urban water mapping: A case study of lingang special area. IEEE Access 14:73082–73095. 10.1109/access.2026.3691743, URL http://dx.doi.org/10.1109/access.2026.3691743

Yang L, Chen N, Yue J, et al (2025) Survey of multimodal geospatial foundation models: Techniques, applications, and challenges. 10.48550/ARXIV.2510.22964, URL https://arxiv.org/abs/2510.22964

Yang Y, Wang J, Wu P, et al (2026b) Combining large language models with satellite embedding to comprehensively evaluate the tibetan plateau's ecological quality. Remote Sensing 18(4):643. 10.3390/rs18040643, URL http://dx.doi.org/10.3390/rs18040643

Yao D, Xu D, Lachapelle S, et al (2024) Multi-view causal representation learning with partial observability. In: Kim B, Yue Y, Chaudhuri S, et al (eds) International Conference on Learning Representations, pp 34817–34848, URL https://proceedings.iclr.cc/paper_files/paper/2024/file/956e5427549a82a7472e02adc88360e9-Paper-Conference.pdf

Ye D, Kiv D, Hu W, et al (2026) Any model, any place, any time: Get remote sensing foundation model embeddings on demand. 10.48550/ARXIV.2602.23678, URL https://arxiv.org/abs/2602.23678

Yue X, Zhao Z, Hu K (2026) Estimating economic activity from satellite embeddings. Applied Sciences 16(2):582. 10.3390/app16020582, URL http://dx.doi.org/10.3390/app16020582

Zanaga D, Van De Kerchove R, Daems D, et al (2022) Esa worldcover 10 m 2021 v200. 10.5281/ZENODO.7254221, URL https://zenodo.org/record/7254221

Zbontar J, Jing L, Misra I, et al (2021) Barlow twins: Self-supervised learning via redundancy reduction. In: Meila M, Zhang T (eds) Proceedings of the 38th International Conference on Machine Learning, Proceedings of Machine Learning Research, vol 139. PMLR, pp 12310–12320, URL https://proceedings.mlr.press/v139/zbontar21a.html

Zha Y, Gao J, Ni S (2003) Use of normalized difference built-up index in automatically mapping urban areas from tm imagery. International Journal of Remote Sensing 24(3):583–594. 10.1080/01431160304987, URL http://dx.doi.org/10.1080/01431160304987

Zhai X, Mustafa B, Kolesnikov A, et al (2023) Sigmoid loss for language image pre-training. In: Proceedings of the IEEE/CVF International Conference on Computer Vision (ICCV), pp 11975–11986

Zhang Q, Wang D, Yu X (2025a) Rlita: A region-level image–text alignment method for remote sensing foundation model. Remote Sensing 17(10):1661. 10.3390/rs17101661, URL http://dx.doi.org/10.3390/rs17101661

Zhang X, Yang Y, Ye Z, et al (2026a) Fusar-gpt: A spatiotemporal feature-embedded and two-stage decoupled visual language model for sar imagery. In: Proceedings of the IEEE/CVF Conference on Computer Vision and Pattern Recognition (CVPR), pp 42158–42168

Zhang Y, Ru L, Wu K, et al (2025b) Skysense v2: A unified foundation model for multi-modal remote sensing. In: Proceedings of the IEEE/CVF International Conference on Computer Vision (ICCV), pp 9136–9146

Zhang Y, Qin Q, Nie H, et al (2026b) Cross-city traffic noise modeling and inequality analysis via alphaearth geospatial foundation models. Transportation Research Part D: Transport and Environment 156:105378. 10.1016/j.trd.2026.105378, URL https://www.sciencedirect.com/science/article/pii/S1361920926001719

Zhang Z, Zhao T, Guo Y, et al (2024) Rs5m and georsclip: A large-scale vision- language dataset and a large vision-language model for remote sensing. IEEE Transactions on Geoscience and Remote Sensing 62:1–23. 10.1109/tgrs.2024.3449154, URL http://dx.doi.org/10.1109/tgrs.2024.3449154

Zheng K, He G, Yin R, et al (2026a) Seed-driven grid adaptation method: A prior-guided active learning framework for impervious surface mapping on the qinghai–xizang plateau using google satellite embeddings. Remote Sensing 18(10):1596. 10.3390/rs18101596, URL http://dx.doi.org/10.3390/rs18101596

Zheng Y, Wu W, Wu B, et al (2026b) Sentinel-2 image retrieval with global, cross-modal embeddings 10.5194/egusphere-egu26-11672, URL http://dx.doi.org/10.5194/egusphere-egu26-11672

Zhu XX, Xiong Z, Wang Y, et al (2026) On the foundations of earth foundation models. Communications Earth & Environment 7(1):103. 10.1038/s43247-025-03127-x, URL https://doi.org/10.1038/s43247-025-03127-x

Zvonkov I, Tseng G, Becker-Reshef I, et al (2025) Cropland mapping using geospatial embeddings. 10.48550/ARXIV.2511.02923, URL https://arxiv.org/abs/2511.02923